Copyright Warning & Restrictions

The copyright law of the United States (Title 17, United States Code) governs the making of photocopies or other reproductions of copyrighted material.

Under certain conditions specified in the law, libraries and archives are authorized to furnish a photocopy or other reproduction. One of these specified conditions is that the photocopy or reproduction is not to be "used for any purpose other than private study, scholarship, or research." If a, user makes a request for, or later uses, a photocopy or reproduction for purposes in excess of "fair use" that user may be liable for copyright infringement,

This institution reserves the right to refuse to accept a copying order if, in its judgment, fulfillment of the order would involve violation of copyright law.

Please Note: The author retains the copyright while the New Jersey Institute of Technology reserves the right to distribute this thesis or dissertation

Printing note: If you do not wish to print this page, then select "Pages from: first page # to: last page #" on the print dialog screen

ABSTRACT

FORMULATION AND DISSOLUTION OF POLYMER STRIP FILMS FOR THE DELIVERY OF POORLY WATER-SOLUBLE DRUG NANOPARTICLES

by
Scott Matthew Krull

Polymer films have emerged as a promising platform for delivery of pharmaceutical products in recent years due to simplified processing, greater flexibility, and improved patient compliance over traditional solid dosage forms. However, the large majority of efforts have focused on incorporation of water-soluble drugs. The objective of this dissertation is to explore the robustness and versatility of the strip film platform for delivery of poorly water-soluble drug nanoparticles to ultimately develop a predictive model for drug release from such films.

The robustness of the polymer strip film platform to successfully deliver a variety of poorly water-soluble drug nanoparticles without the need for surfactant is demonstrated first. Drug nanoparticle-loaded films are prepared with and without surfactant for five distinct poorly water-soluble drugs. Fast release is achieved for films made with all five drugs despite differences in water solubility, even in the absence of surfactant, with minimal differences in film quality and properties. Next, various formulation aspects are investigated for their impact on film quality and performance. In one study, three plasticizers at three different concentrations are incorporated into drug nanoparticle-loaded polymer films. A depression in glass transition temperature is observed with increasing plasticizer concentration, along with a corresponding decrease in film tensile strength and increase in film elongation. However, the type and amount of plasticizer used has no significant impact on the dissolution rate of the films, suggesting

that film mechanical properties can be effectively manipulated by varying plasticizer concentration with minimal impact on drug release. In another study, three different film-forming polymer molecular weights at three different viscosity levels are used to prepare films containing poorly water-soluble drug nanoparticles. No statistical differences in film tensile strength or elongation at break are observed between films regardless of polymer molecular weight despite requiring up to double the time to achieve 100% drug release, suggesting that film-forming polymer molecular weight can be used to manipulate drug release with little impact on film mechanical properties. The maximum practical drug loading in films is also investigated to address the misconception that strip films are limited to very low dosages. Films made using two film-forming polymer molecular weights are prepared with different concentrations of poorly water-soluble drug nanoparticles by varying the drug loading in the nanosuspension from which the nanoparticles are taken and the polymer-to-nanosuspension mixing ratio. All films up to 50 wt% drug loading show good content uniformity and drug nanoparticle redispersibility, suggesting that high drug loading can indeed be achieved in polymer films, although films tend to become less elastic and more brittle as drug loading increases above 40 wt%. Finally, a mathematical model is developed to predict the rate of drug release from polymer films containing drug particles based on first principles.

In summary, various formulation aspects of the polymer strip film platform are investigated for delivery of poorly water-soluble drug nanoparticles and a mathematical model predicting the rate of drug release from such films is developed based on these studies.

FORMULATION AND DISSOLUTION OF POLYMER STRIP FILMS FOR THE DELIVERY OF POORLY WATER-SOLUBLE DRUG NANOPARTICLES

by
Scott Matthew Krull

A Dissertation
Submitted to the Faculty of
New Jersey Institute of Technology
in Partial Fulfillment of the Requirements for the Degree of
Doctor of Philosophy in Chemical Engineering

Otto H. York Department of
Chemical, Biological and Pharmaceutical Engineering

January 2017

APPROVAL PAGE

FORMULATION AND DISSOLUTION OF POLYMER STRIP FILMS FOR THE DELIVERY OF POORLY WATER-SOLUBLE DRUG NANOPARTICLES

Scott Matthew Krull

Dr. Rajesh N. Davé, Dissertation Advisor Date
Distinguished Professor of Chemical, Biological and Pharmaceutical Engineering, NJIT

Dr. Ecevit A. Bilgili, Committee Member Date
Associate Professor of Chemical, Biological and Pharmaceutical Engineering, NJIT

Dr. Norman W. Loney, Committee Member Date
Professor of Chemical, Biological and Pharmaceutical Engineering, NJIT

Dr. Robert B. Barat, Committee Member Date
Professor of Chemical, Biological and Pharmaceutical Engineering, NJIT

Dr. Zafar Iqbal, Committee Member Date
Research Professor of Chemistry and Environmental Science, NJIT

BIOGRAPHICAL SKETCH

Author: Scott Matthew Krull

Degree: Doctor of Philosophy

Date: January 2017

Undergraduate and Graduate Education:

- Doctor of Philosophy in Chemical Engineering,
  New Jersey Institute of Technology, Newark, NJ, 2017

- Bachelor of Engineering in Chemical Engineering,
  The Cooper Union for the Advancement of Science and Art, New York, NY, 2011

Major: Chemical Engineering

Presentations and Publications:

Journal Articles:

Krull, S.M., Davé, R.N. Dissolution model for polymer films loaded with poorly soluble API particles. In preparation.

Kevadiya, B.D., Barvaliya, M., Anovadiya, A., Zhang, L., Brahmbhatt, H., Paul, P., Tripathi, C., Iqbal, Z., Krull, S.M., Bilgili, E., Davé, R.N. Cholesterol reducing drug nanocrystals embedded in versatile fast dissolving oral strip films for bioavailability enhancement. In preparation.

Karry, K.M., Susarla, R., Krull, S.M., Li, M., Bilgili, E., Davé, R.N., Michniak-Kohn, B. Development of biorelevant in vitro dissolution protocols for oral transmucosal (transoral) polymer films containing naproxen nanoparticles. In preparation.

Krull, S.M., Moreno, J., Li, M., Bilgili, E., Davé, R.N. Critical material attributes (CMAs) of strip films loaded with poorly water-soluble drug nanoparticles: III. Impact of drug nanoparticle loading. International Journal of Pharmaceutics. Under review.

Krull, S.M., Ammirata, J., Bawa, S., Li, M., Bilgili, E., Davé, R.N. Critical material attributes of strip films loaded with poorly water-soluble drug nanoparticles: II. Impact of polymer molecular weight. Journal of Pharmaceutical Sciences. In press.

Krull, S.M., Patel, H.V., Li, M., Bilgili, E., Davé, R.N., 2016. Critical material attributes (CMAs) of strip films loaded with poorly water-soluble drug nanoparticles: I. Impact of plasticizer on film properties and dissolution. European Journal of Pharmaceutical Sciences 92, 146-155.

Krull, S.M., Ma, Z., Li, M., Davé, R.N., Bilgili, E., 2016. Preparation and characterization of fast dissolving pullulan films containing BCS class II drug nanoparticles for bioavailability enhancement. Drug Development and Industrial Pharmacy 42 (7), 1073-1085.

Krull, S.M., Li, M., Bilgili, E., Davé, R.N., 2015. Polymer strip films for delivery of poorly water-soluble drugs. American Pharmaceutical Review 18 (3), 48-52.

Krull, S.M., Susarla, R., Afolabi, A., Li, M., Ying, Y., Iqbal, Z., Bilgili, E., Davé, R.N., 2015. Polymer strip films as a robust, surfactant-free platform for delivery of BCS Class II drug nanoparticles. International Journal of Pharmaceutics 489 (1-2), 45-57.

Conference Proceedings:

Krull, S.M., Bilgili, E., Davé, R.N., Modeling Dissolution of Polymer Strip Films Loaded with Poorly Water-Soluble Drug Nanoparticles. AIChE Annual Meeting, San Francisco, CA, November 18, 2016.

Krull, S.M., Li, M., Bilgili, E., Davé, R.N., Maximizing Poorly Water-Soluble API Nanoparticle Loading in Polymer Strip Films. AIChE Annual Meeting, San Francisco, CA, November 13, 2016.

Krull, S.M., Patel, H., Li, M., Bilgili, E., Davé, R.N., Controlling Mechanical Properties and Dissolution Rate of Strip Films Loaded with Griseofulvin Nanoparticles. AIChE Annual Meeting, Salt Lake City, UT, November 10, 2015.

Krull, S., Susarla, R., Afolabi, A., Li, M., Bilgili, E., Davé, R.N., Polymer Strip Films As a Robust, Surfactant-Free Platform for Delivery of BCS Class II Drug Nanoparticles. IFPAC Annual Meeting, Washington DC, January 28, 2015.

Krull, S., Susarla, R., Afolabi, A., Li, M., Bilgili, E., Davé, R.N., Polymer Strip Films As a Robust, Surfactant-Free Platform for Delivery of BCS Class II Drug Nanoparticles. AIChE Annual Meeting, Atlanta, GA, November 18, 2014.

To my family

ACKNOWLEDGMENT

I would like to extend my sincere gratitude to my dissertation advisor, Dr. Rajesh N. Davé, for his continuous guidance, financial support, and encouragement throughout my research. I am truly grateful for the advice you have given me and for doing everything in your power to put me in a position to grow and succeed as a Ph.D. student and beyond.

I offer thanks to Dr. Ecevit A. Bilgili, Dr. Norman W. Loney, Dr. Robert B. Barat, and Dr. Zafar Iqbal for accepting to serve on my committee and offering helpful suggestions. I would also like to extend special thanks to Dr. Bilgili for facilitating collaboration with his milling group, which commonly provided suspension samples for the work outlined in this dissertation.

I am grateful for financial support from the National Science Foundation in part through the ERC (EEC-0540855) award and from the National Institute of Health NIH-U01 in part through award U01FD005521.

I would like to extend acknowledgment to the following members of our group for their direct involvement in my research: Dr. Afolawemi Afolabi, Dr. Bhavesh Kevadiya, Dr. Mohammad Azad, Meng Li, Lu Zhang, Jennifer Ammirata, Sonia Bawa, Brian Moshofsky, Angela Ramirez, Hardik Patel, Jacqueline Moreno, and Salome Legarda, as well as Dr. Krizia Karry of Rutgers University. I am especially grateful to Dr. Ramani Susarla for serving as my mentor during my first two years as a Ph.D. student and for helping me develop the skills necessary to succeed in my research. I also offer special thanks to Dr. Xiaoliang Deng, my officemate for nearly five years, for

his constant moral and intellectual support, and Dr. Zhonghui Huang for always pushing me to move forward.

Finally, I would like to express my deepest gratitude to my family. To my mother, Hildy, and my father, Martin, for their endless love and support at every stage of my life, my brother, Peter, for his unique support as we grew up together, and everyone else who has supported me throughout my life. I would not have been able to accomplish what I have without you, and I promise to continue to make you proud!

TABLE OF CONTENTS

Chapter			Page
1	INTRODUCTION		1
	1.1	Background Information	1
	1.2	Objective	4
	1.3	Dissertation Outline	4
2	EFFECT OF DRUG AND SURFACTANT		6
	2.1	Introduction	6
	2.2	Experimental Procedures	10
		2.2.1 Materials	10
		2.2.2 Preparation Methods	10
		2.2.3 Characterization Methods	12
	2.3	Results and Discussion	16
		2.3.1 Precursor Suspension Viscosity	16
		2.3.2 Drug Particle Size after Milling and Redispersed from Films	18
		2.3.3 Film Characterization	21
	2.4	Conclusions	38
3	EFFECT OF PLASTICIZER		40
	3.1	Introduction	40
	3.2	Experimental Procedures	42
		3.2.1 Materials	42
		3.2.2 Preparation Methods	42
		3.2.3 Characterization Methods	44

TABLE OF CONTENTS
(Continued)

Chapter			Page
	3.3	Results and Discussion	47
		3.3.1 Viscosity of Polymer Solutions and Precursor Suspensions	47
		3.3.2 GF Particle Size after Milling and Redispersed from Films	48
		3.3.3 Film Characterization	51
	3.4	Conclusions	63
4	EFFECT OF FILM-FORMING POLYMER MOLECULAR WEIGHT		65
	4.1	Introduction	65
	4.2	Experimental Procedures	67
		4.2.1 Materials	67
		4.2.2 Preparation Methods	68
		4.2.3 Characterization Methods	70
	4.3	Results and Discussion	73
		4.3.1 Viscosity of Polymer Solutions and Precursor Suspensions	73
		4.3.2 GF Particle Size after Milling and Redispersed from Films	74
		4.3.3 Film Characterization	75
	4.4	Conclusions	89
5	EFFECT OF DRUG LOADING		90
	5.1	Introduction	90
	5.2	Experimental Procedures	92
		5.2.1 Materials	92
		5.2.2 Preparation Methods	93

TABLE OF CONTENTS
(Continued)

Chapter **Page**

5.3 Results and Discussion 95

5.3.1 Viscosity of Polymer Solutions and Precursor Suspensions..... 95

5.3.2 Scanning Electron Microscopy (SEM) 96

5.3.3 GF Particle Size After Milling and Redispersed from Films..... 99

5.3.4 GF Content and Uniformity in Films..... 101

5.3.5 Film Mechanical Properties 102

5.3.6 Dissolution 104

5.3.7 Thermogravimetric Analysis (TGA)..... 106

5.3.8 Long-term Stability of Films..... 108

5.4 Conclusions..... 111

6 DISSOLUTION MODEL FOR DRUG PARTICLE-LADEN FILMS 113

6.1 Introduction..... 113

6.2 Mathematical Model 115

6.2.1 Model Assumptions 115

6.2.2 Mass Balances..... 116

6.2.3 Dimensionless Variables and Parameters 119

6.2.4 Numerical Procedure..... 120

6.3 Experimental Procedures 121

6.3.1 Materials 122

6.3.2 Methods..... 122

6.4 Results and Discussion 125

TABLE OF CONTENTS
(Continued)

Chapter **Page**

6.4.1 System Parameters and Film Properties 125

6.4.2 Influence of System Parameters 127

6.4.3 Comparison with Experimental Results 130

6.5 Conclusions 140

7 OVERALL CONCLUSIONS AND FUTURE WORK 142

7.1 Overall Conclusions 142

7.2 Future Work 144

7.2.1 Thick Films for Buccal Delivery and Composite Films for Controlled Delivery of Multiple Drugs 144

7.2.2 Dissolution Model Expansion to Account for Other Types of Polymers 144

7.2.3 Mathematical Model for Prediction of Drying Rate from Drug Particle-loaded Polymer Films 145

APPENDIX DISSOLUTION PROFILE COMPARISON 146

A.1 Effect of Plasticizer 146

A.2 Effect of Film-Forming Polymer Molecular Weight 150

A.3 Effect of Drug Loading 150

REFERENCES 153

LIST OF TABLES

Table		Page
2.1	Physicochemical Properties of Drugs Incorporated into Polymer Films	10
2.2	Composition of Film Precursor Suspensions Cast to Form Strip Films Loaded with Drug Nanoparticles	12
2.3	Low Shear (2.2 s^{-1}) Viscosity of FNB, GF, NPX, PB and AZD Film Precursor Suspensions at 25 ºC	17
2.4	Particle Size Distribution of Drug in Milled Suspension Prior to Shear Mixing with Polymer Solution (Susp) and Drug Redispersed from Dry FNB, GF, NPX, PB and AZD Films (Film)	19
2.5	Content Uniformity and Thickness Variation within Films Containing FNB, GF, NPX, PB and AZD Nanoparticles, Respectively	22
2.6	Mechanical Properties of FNB, GF, NPX, PB, AZD, and Placebo Films	23
3.1	Film-Forming Polymer Solution Formulations Prior to Mixing with GF Nanosuspension	44
3.2	Particle Size Distributions of Fresh GF Nanosuspension and Redispersed Film Samples Immediately after Film Preparation, after 3 Months of Storage at 40 ºC, 75% RH, and after 6 Months of Storage at 40 ºC, 75% RH	50
3.3	Content Uniformity of HPMC Films with Different Plasticizers and Content. Values are an Average of 10 samples ~0.7 cm^2 in Area	56
4.1	Composition of HPMC Polymer Solution Formulations and Low Shear (2.2 s^{-1}) Room Temperature Viscosity of Polymer Solutions and Film Precursor Suspensions. Viscosities are Mean ± SD, n = 7	69
4.2	Content Uniformity of HPMC Films with Different Polymer MWs and Concentrations. Values are an Average of 10 Samples ~0.7 cm^2 in Area	76
4.3	Mechanical Properties of Films with Different HPMC MWs and Concentrations Containing GF Nanoparticles. Values are Mean ± SD, n = 4	78
4.4	Fitting Parameters Generated by Fitting Dissolution Curves from GF Nanoparticle-loaded HPMC Films of Varying Polymer MW and Concentration to Various Dissolution Models	83

LIST OF TABLES
(Continued)

Table		Page
4.5	Adjusted R^2 Values Generated by Fitting Dissolution Curves from GF Nanoparticle-loaded HPMC Films of Varying Polymer MW and Concentration to Various Dissolution Models	83
5.1	Composition of Polymer Solutions and Film Precursor Suspensions	94
5.2	Content Uniformity of Films with Different GF Loadings	102
5.3	Mechanical Properties of Films with Different GF Loadings	103
6.1	Composition and Viscosity of Polymer Solutions and Film Precursor Suspensions	124
6.2	System Parameters	126
6.3	Properties of Individual Films Determined by Formulation or Experiment	126
6.4	Parameters from Molecular Weight Study Films Used for Predictive Model	136
6.5	Parameters from Drug Loading Study Films Used for Predictive Model	138
A.1	Similarity (f_2) and Difference (f_1) Factors for Comparison of Dissolution Profiles of Fresh Films Loaded with GF Nanoparticles	147
A.2	Similarity (f_2) and Difference (f_1) Factors for Comparison of Dissolution Profiles of Films Loaded with GF Nanoparticles Containing No Plasticizer Immediately after Film Preparation, after 3 Months of Storage at 40 ºC, 75% RH, and after 6 Months of Storage at 40 ºC, 75% RH	147
A.3	Similarity (f_2) and Difference (f_1) Factors for Comparison of Dissolution Profiles of 2.5% Glycerin Films Loaded with GF Nanoparticles Immediately after Film Preparation, after 3 Months of Storage at 40 ºC, 75% RH, and after 6 Months of Storage at 40 ºC, 75% RH	148
A.4	Similarity (f_2) and Difference (f_1) Factors for Comparison of Dissolution Profiles of 5.0% Glycerin Films Loaded with GF Nanoparticles Immediately after Film Preparation, after 3 Months of Storage at 40 ºC, 75% RH, and after 6 Months of Storage at 40 ºC, 75% RH	148

LIST OF TABLES
(Continued)

Table **Page**

A.5 Similarity (f_2) and Difference (f_1) Factors for Comparison of Dissolution Profiles of 2.5% Triacetin Films Loaded with GF Nanoparticles Immediately after Film Preparation, after 3 Months of Storage at 40 ºC, 75% RH, and after 6 Months of Storage at 40 ºC, 75% RH..... 148

A.6 Similarity (f_2) and Difference (f_1) Factors for Comparison of Dissolution Profiles of 5.0% Triacetin Films Loaded with GF Nanoparticles Immediately after Film Preparation, after 3 Months of Storage at 40 ºC, 75% RH, and after 6 Months of Storage at 40 ºC, 75% RH..... 149

A.7 Similarity (f_2) and Difference (f_1) Factors for Comparison of Dissolution Profiles of 2.5% PEG Films Loaded with GF Nanoparticles Immediately after Film Preparation, after 3 Months of Storage at 40 ºC, 75% RH, and after 6 Months of Storage at 40 ºC, 75% RH..... 149

A.8 Similarity (f_2) and Difference (f_1) Factors for Comparison of Dissolution Profiles of 5.0% PEG Films Loaded with GF Nanoparticles Immediately after Film Preparation, after 3 Months of Storage at 40 ºC, 75% RH, and after 6 Months of Storage at 40 ºC, 75% RH..... 149

A.9 Similarity (f_2) and Difference (f_1) Factors for Comparison of Dissolution Profiles of HPMC Films Loaded with GF Nanoparticles 150

A.10 Similarity (f_2) and Difference (f_1) Factors for Comparison of Dissolution Profiles of Fresh HPMC Films with Different GF Nanoparticle Loadings 151

A.11 Similarity (f_2) and Difference (f_1) Factors for Comparison of Dissolution Profiles of HPMC-E15 Films with Different GF Nanoparticle Loadings after 0, 3, and 6 Months of Storage at 40 ºC, 75% RH..... 152

A.12 Similarity (f_2) and Difference (f_1) Factors for Comparison of Dissolution Profiles of HPMC-E4M Films with Different GF Nanoparticle Loadings after 0, 3, and 6 Months of Storage at 40 ºC, 75% RH..... 152

LIST OF FIGURES

Figure **Page**

2.1 Cross-sectional SEM images of films containing (a,b) FNB, (c,d) GF, (e,f) NPX, (g,h) PB, and (i,j) AZD nanoparticles without SDS and with SDS, respectively. 27

2.2 SEM surface images of films (a) P1 [PB without SDS], and (b) A2 [AZD with SDS]. 27

2.3 Normalized TGA curves for films containing FNB, GF, NPX, PB, and AZD nanoparticles (a) without SDS and (b) with SDS. 29

2.4 FTIR spectra of pure drug and films containing (a) FNB, (b) GF, (c) NPX, (d) PB, and (e) AZD nanoparticles. 31

2.5 Raman spectra of pure drug and films containing (a) FNB, (b) GF, (c) NPX, (d) PB, and (e) AZD nanoparticles. 32

2.6 Comparison of release profiles from films containing (a) FNB, (b) GF, (c) NPX, (d) PB, and (e) AZD nanoparticles in SDS media. 35

2.7 Comparison of drug release profiles in SDS media from films containing FNB, GF, NPX, PB, and AZD nanoparticles (a) without SDS and (b) with SDS. 36

2.8 Comparison of release profiles from films containing (a) NPX, (b) PB, and (c) AZD nanoparticles in DI water media. 38

3.1 Low shear (2.2 s^{-1}) room temperature viscosity of polymer solutions and film precursor suspensions. Values are mean ± SD, n = 7. 48

3.2 (a) T_g and (b) full DSC traces of GF nanoparticle-laden HPMC films containing various amounts of plasticizer. 53

3.3 (a) Tensile strength, (b) yield strength, (c) Young's modulus, and (d) percent elongation at break of HPMC films with different plasticizers and content containing GF nanoparticles. Values are mean ± SD, n = 4. 55

3.4 Comparison of dissolution profiles between HPMC films loaded with GF nanoparticles containing different plasticizers and plasticizer content. Values are mean ± SD, n = 6. 57

3.5 Normalized TGA curves for HPMC films with different plasticizers and plasticizer content loaded with griseofulvin nanoparticles. 60

LIST OF FIGURES
(Continued)

Figure **Page**

3.6 Cross sectional SEM images of HPMC films loaded with griseofulvin nanoparticles made from polymer solutions containing (a) no plasticizer, (b) 2.5% glycerin, (c) 5.0% glycerin, (d) 2.5% triacetin, (e) 5.0% triacetin, (f) 2.5% PEG, and (g) 5.0% PEG. Scale bars are 1 μm for (a-f) and 2 μm for (g). 61

3.7 Comparison of dissolution profiles for all films immediately after film preparation, after 3 months of storage at 40 ºC, 75% RH, and after 6 months of storage at 40 ºC, 75% RH. Values are mean ± SD, n = 6. 63

4.1 SDI film sample holder schematic. 71

4.2 Particle size statistics of GF nanosuspension and redispersed film samples. 75

4.3 Comparison of dissolution profiles between films loaded with GF nanoparticles containing different HPMC MWs and concentrations. Values are mean ± SD, n = 6. 81

4.4 Surface dissolution snapshots of low viscosity film formulations. Blue indicates absence of drug while warmer colors indicate higher concentrations of drug (note: the semicircle at the top of the 60 min snapshot of E50-Low is an air bubble, not a part of the film sample). 84

4.5 TGA curves for films with different HPMC MWs and concentrations loaded with GF nanoparticles. 86

4.6 Cross-sectional SEM images of (a) E15-Low, (b) E15-Med, (c) E15-High, (d) E50-Low, (e) E50-Med, (f) E50-High, (g) E4M-Low, (h) E4M-Med, and (i) E4M-High films containing GF nanoparticles. Magnification of 50,000× was used for all images. Scale bars indicate 1 μm. 88

5.1 Low shear (2.2 s^{-1}) room temperature viscosity of polymer solutions and film precursor suspensions. 96

5.2 Cross sectional SEM images of the following HPMC films with various GF nanoparticle loadings: (a) DL1-15, (b) DL2-15, (c) DL3-15, (d) DL4-15, (e) DL5-15, (f) DL6-15, (g) DL1-4M, (h) DL2-4M, (i) DL3-4M, (j) DL4-4M, and (k) DL5-4M. 97

5.3 d_{10}, d_{50} and d_{90} of GF nanoparticles in suspension and redispersed from HPMC-E15 and E4M films of varying API loading after 0, 3, and 6 months' storage at 40 ºC and 75% RH. 100

LIST OF FIGURES
(Continued)

Figure **Page**

5.4 Dissolution profiles of HPMC (a) E15 and (b) E4M films with various GF nanoparticle loadings. 106

5.5 TGA curves for HPMC (a) E15 and (b) E4M films with various GF nanoparticle loadings. 108

5.6 Comparison of dissolution profiles for E15 films immediately after film preparation, after 3 months of storage at 40 °C, 75% RH, and after 6 months of storage at 40 °C, 75% RH. Values are mean ± SD, n = 6. 110

5.7 Comparison of dissolution profiles for E4M films immediately after film preparation, after 3 months of storage at 40 °C, 75% RH, and after 6 months of storage at 40 °C, 75% RH. Values are mean ± SD, n = 6. 111

6.1 Process schematic of drug nanoparticle release from film matrix. 115

6.2 Predicted impact of the following system parameters on release profiles of poorly water-soluble drug particle-laden polymer films based on the mathematical model: (a) C_S, (b) S_{d0}, (c) L_0, (d) D_{de}, (e) D_{we}, (f) C_{p0}, (g) C_{we}, (h) k_d, and (i) d_{50}. Bold lettered values in each legend are based on formulation A1-100. 128

6.3 Comparison of experimentally determined dissolution rates from HPMC-E15 formulations and numerically predicted dissolution profiles for the same formulations. $k_d = 2.91\times10^{-4}$ cm/s for A1 formulations, $k_d = 4.36\times10^{-3}$ cm/s for A2 formulations, and $k_d = 0.116$ cm/s for A3 formulations. 131

6.4 Comparison of experimentally determined dissolution rates from HPMC-E15/E4M mixture formulations and numerically predicted dissolution profiles for the same formulations. $k_d = 2.91\times10^{-4}$ cm/s for B1 formulations, $k_d = 4.36\times10^{-3}$ cm/s for B2-50, and $k_d = 0.116$ cm/s for B3-50. 132

6.5 Comparison of experimentally determined dissolution rates from HPMC-E4M formulations and numerically predicted dissolution profiles for the same formulations. $k_d = 2.91\times10^{-4}$ cm/s for C1-50, $k_d = 4.36\times10^{-3}$ cm/s for C2-50, and $k_d = 0.116$ cm/s for C3-50. 133

6.6 Comparison of experimentally determined dissolution rates from films loaded with GF nanoparticles containing different HPMC MWs and concentrations and numerically predicted dissolution profiles for the same formulations. k_d = (a,b,d,e,g,h) 2.9×10^{-4} cm/s, (c) 1.7×10^{-4} cm/s, and (f,i) 2.3×10^{-4} cm/s. 136

LIST OF FIGURES
(Continued)

Figure **Page**

6.7 Comparison of experimentally determined dissolution rates from HPMC-E15 formulations with varying GF loading and numerically predicted dissolution profiles for the same formulations. k_d = (a,b) 2.9×10^{-4} cm/s, (c) 1.9×10^{-4} cm/s, (d) 5.8×10^{-5} cm/s, (e) 6.5×10^{-5} cm/s, and (f) 2.9×10^{-5} cm/s..... 139

6.8 Comparison of experimentally determined dissolution rates from HPMC-E4M formulations with varying GF loading and numerically predicted dissolution profiles for the same formulations. k_d = (a) 1.3×10^{-4} cm/s, (b) 6.5×10^{-5} cm/s, (c) 4.8×10^{-5} cm/s, (d) 1.2×10^{-2} cm/s, and (e) 2.0×10^{-1} cm/s..... 140

LIST OF TERMS

ANOVA	Analysis of variance
ATR	Attenuated total reflectance
AZD	Azodicarbonamide
BCS	Biopharmaceutics Classification System
CMA	Critical material attribute
DI	Deionized
DSC	Differential scanning calorimetry
EB	Elongation at break (%)
FNB	Fenofibrate
FTIR	Fourier transform infrared
GF	Griseofulvin
HPMC	Hydroxypropyl methylcellulose
IR	Infrared
MW	Molecular weight
NPX	Naproxen
ODE	Ordinary differential equation
PB	Phenylbutazone
PDE	Partial differential equation
PEG	Polyethylene glycol
PIDS	Polarized intensity differential scattering
PSD	Particle size distribution
RH	Relative humidity (%)

LIST OF TERMS

RSD	Relative standard deviation (%)
SD	Standard deviation
SDI	Surface dissolution imager
SDS	Sodium dodecyl sulfate
SEM	Scanning electron microscopy
TGA	Thermogravimetric analysis
TS	Tensile strength (MPa)
USP	United States Pharmacopeia
UV	Ultraviolet
WSMM	Wet stirred media milling
wt%	Percentage by mass (%)
YM	Young's modulus (GPa)
YS	Yield strength (MPa)

LIST OF SYMBOLS

a	Surface area of a single drug particle (cm^2)
a_0	Initial surface area of a single drug particle (cm^2)
C_d	Dissolved drug concentration (g/cm^3)
$\overline{C_d}$	Dimensionless dissolved drug concentration (-)
C_{de}	Equilibrium dissolved drug concentration in fully swollen polymer (g/cm^3)
C_{p0}	Initial polymer concentration (g/cm^3)
C_w	Solvent concentration (g/cm^3)
$\overline{C_w}$	Dimensionless solvent concentration (-)
C_{we}	Equilibrium solvent concentration in fully swollen polymer (g/cm^3)
C_S	Drug solubility in solvent (g/cm^3)
d_{10}	10% passing particle size (nm)
d_{50}	50% passing (median) particle size (nm)
d_{90}	90% passing particle size (nm)
D_d	Diffusion coefficient of drug in polymer (cm^2/s)
$\overline{D_d}$	Dimensionless diffusion coefficient of drug in polymer (-)
D_{de}	Diffusion coefficient of drug in polymer in equilibrium swollen polymer state (cm^2/s)
D_w	Diffusion coefficient of solvent in polymer (cm^2/s)
$\overline{D_w}$	Dimensionless diffusion coefficient of solvent in polymer (-)
D_{we}	Diffusion coefficient of solvent in polymer in equilibrium swollen polymer state (cm^2/s)

LIST OF SYMBOLS

F	Percentage of drug dissolved at time t (% release)
H	Film height (cm)
i	Indicates film component, either drug or solvent (-)
k_0	Zero-order release constant (% release/min)
k_1	First-order release constant (% release/min)
k_d	Surface-specific drug dissolution rate constant (cm/s)
k_H	Higuchi equation constant (% release/min$^{1/2}$)
k_{HC}	Hixson–Crowell equation constant (% release/min)
k_{KP}	Korsmeyer–Peppas equation constant (% release/min^n)
K_p	Polymer dissolution rate constant (g/cm^2-s)
$\overline{K_p}$	Dimensionless polymer dissolution rate constant (-)
L	Film thickness (cm)
L_0	Initial film thickness (cm)
m	Mass of single drug particle (g)
n	Korsmeyer–Peppas equation release exponent in Equation (4.4) (-)
n	Number of drug particles per unit volume of film in Equation (6.1) (#/cm^3)
S_{d0}	Initial solid drug concentration (g/cm^3)
t	Time (min)
t_{80}	Time of 80% drug release (min)
T_g	Glass transition temperature (ºC)
V	Film volume (cm^3)
v	Volume of single drug particle (cm^3)

LIST OF SYMBOLS

W	Film width (cm)
x	Spatial coordinate (cm)
y	Dimensionless spatial coordinate (-)

Greek letters

α	Dimensionless surface area of a single drug particle (-)
β_d	Exponent for Fujita-type free volume model for drug diffusion (-)
β_w	Exponent for Fujita-type free volume model for solvent diffusion (-)
η	Dimensionless film thickness (-)
κ	Dimensionless drug dissolution rate constant (-)
ρ_d	Drug particle density (g/cm^3)
ρ_p	Polymer density (g/cm^3)
ρ_w	Solvent density (g/cm^3)
τ	Dimensionless time (-)

Indices

j	Spatial coordinate along film thickness (-)

CHAPTER 1

INTRODUCTION

1.1 Background Information

Polymer strip films have become an increasingly popular method of drug delivery in recent years. In addition to offering a larger surface area for faster disintegration and dissolution (Dixit and Puthli, 2009) as well as the ability to circumvent the first pass metabolism in buccal applications (Averineni et al., 2009), films also offer several formulation, manufacturing, and consumer-based advantages over more traditional solid dosage forms. Noteworthy manufacturing advantages include inherently continuous processing and flexible, cost-effective scale-up (Hoffmann et al., 2011; Zhang et al., 2014). Consumers, particularly pediatric, geriatric, and dysphagic patients, have demonstrated a higher degree of compliance for film-based pharmaceuticals (Dixit and Puthli, 2009). Commercial feasibility of thin films as a drug delivery platform has been established with the introduction of Gas-X® Thin Strips® (simethicone) from Novartis® for pain or discomfort caused by excessive gas, Zuplenz® (ondansetron) from MonoSol Rx® for nausea and vomiting caused by radiation therapy, RapidFilms® (donezepil) from Labtec® GmbH for treatment of dementia caused by Alzheimer's disease, and Suppress™ Cough Strips (dextromethorphan/menthol) from InnoZen® Inc. to suppresses coughing due to minor throat and bronchial irritation. Recent developments have also explored more versatile applications for drug-loaded polymer films, including the gastro retentive Accordian Pill™ from Intec Pharma Ltd., as well as rolled or compressed multi-layer film tablets (Trout et al.). However, one thing that the majority of these films have in

common is their use of water-soluble drugs, which are easiest to formulate with for fast dissolution and homogeneous drug distribution. Despite the growing number of poorly water-soluble drug candidates in the pharmaceutical industry in recent years (Lipinski, 2002), they have yet to appear on the market in the strip film format due to their limited dissolution and bioavailability.

While initial studies and commercial applications for pharmaceutical films focused on incorporation of water-soluble drugs (Borges et al., 2015a; Dave et al., 2014; Dixit and Puthli, 2009; Garsuch and Breitkreutz, 2010), recent studies have begun to explore the potential for incorporation of poorly water-soluble drugs into polymer strip films. Films are believed to be an ideal delivery form for the growing library of poorly water-soluble drugs in part because they offer larger available surface area, allowing for rapid disintegration and dissolution, even in the oral cavity, which cannot be matched in traditional dosage forms (Dixit and Puthli, 2009). Although this is commonly done via hot melt extrusion (Kumar et al., 2014; Visser et al., 2015) or organic solvent casting (Prodduturi et al., 2005), both may lead to drug instability and drug loading limitations in the resulting films (Kipp, 2004). In light of these issues, various particle engineering techniques have also been employed to improve poorly water-soluble drug dissolution rate for incorporation into strip films. These include wet stirred media milling (WSMM) (Davé et al., 2014; Krull et al., 2016b; Sievens-Figueroa et al., 2012a; Susarla et al., 2015; Susarla et al., 2013) and high pressure homogenization (Lai et al., 2015; Shen et al., 2013) to reduce drug particle size, as well as liquid antisolvent precipitation (Beck et al., 2013) and melt emulsification (Bhakay et al., 2016) to produce drug nanoparticles via bottom-up approach. The results from the above film studies indicate that incorporating

small crystalline drug particles into polymer films can eliminate the need for organic solvents, offer predictable form, size, and distribution of drug particles, and most importantly, result in fast release for BCS (Biopharmaceutics Classification System) class II drugs. In addition, these studies demonstrate that the improvement in dissolution rate from films is even more pronounced when compared to those of physical mixtures and compacts of identical composition. The fast and predictable release of poorly water-soluble drugs offered by the film format is expected to be crucial, as agglomeration of primary drug particles upon release may lead to slower dissolution and limited bioavailability (de Villiers, 1996). This issue has been identified in other nanoparticle-based dosage forms, where loss of large surface area was a major obstacle to achieving expected gains in dissolution enhancement (Bhakay et al., 2014a; Bhakay et al., 2014b; Bhakay et al., 2013).

With the groundwork in place for strip films as a stable and robust platform for poorly water-soluble drug delivery, attention has shifted from process development to intelligent formulation design. One of the most intriguing aspects of the strip film format resides in its versatility. Strip films benefit from access to a wide variety of usable excipients, including film-formers and plasticizers, which can be used to control various properties of the films without sacrificing the integrity of the format (Borges et al., 2015b; Dixit and Puthli, 2009). However, little is known about how these critical material attributes (CMAs) impact properties of drug particle-laden films, such as drug particle stability and dissolution rate.

1.2 Objective

Pharmaceutical strip films have garnered significant attention thanks to improved patient compliance, cost-effective scale-up and the potential for continuous manufacturing. The ability to stabilize and release drug nanoparticles makes strip films an ideal platform for the delivery of poorly water-soluble drugs. However, this capability has only been demonstrated for a select few BCS class II drugs in combination with specific excipients. Due to the novelty of the platform, scant information exists on how the components of the film, most notably drug and polymer, impact various film properties and performance of the final dosage. In light of this, it is the ultimate objective of this work to demonstrate the robustness and predictable properties of strip films loaded with poorly water-soluble drug nanoparticles such that the nanoparticles are physically stabilized and released in the absence of aggregation so that their enhanced bioavailability is maintained upon delivery.

1.3 Dissertation Outline

This dissertation work is presented in seven chapters. Chapter 1 begins with a review of relevant background concepts and literature, followed by the objective and outline of the dissertation. Chapter 2 examines the ability of the strip film format to effectively stabilize and deliver a variety of poorly water-soluble drug nanoparticles with and without the aid of a surfactant. Chapter 3 investigates the capability of manipulating the mechanical properties of poorly water-soluble drug nanoparticle-laden films by adjusting the type and amount of plasticizer used without significantly impacting the rate of drug release during dissolution. Chapter 4 explores the ability to adjust the release rate of poorly water-soluble drug nanoparticles from strip films using various molecular weights of

film-forming polymer with limited impact on film mechanical properties. Chapter 5 studies the potential for high loadings (40-50 wt%) of poorly water-soluble drug nanoparticles in strip films and the effect of high drug loading on film properties. Chapter 6 presents a numerical first principles model for the dissolution of polymer films loaded with poorly water-soluble drug particles, which incorporates drug particle dissolution and diffusion, solvent imbibition, film swelling, and polymer erosion. Chapter 7 provides an overall summary and conclusion of the current work and proposes direction for potential future work.

CHAPTER 2

EFFECT OF DRUG AND SURFACTANT

2.1 Introduction

Although previous studies have shown the potential of the strip film format, they were limited by a small selection of drugs, poor content uniformity, and reliance on surfactant. Sievens-Figueroa et al. (2012a) investigated three poorly water-soluble drugs and demonstrated the feasibility of using HPMC-based thin films for delivery of drug nanoparticles, but their work suffered from use of long drying times and relatively low film precursor viscosities, all of which are considered to adversely impact drug content uniformity, which was not reported in their work. Beck et al. (2013) considered liquid anti-solvent crystallization of only one poorly water-soluble drug and followed similar formulation and manufacuring protocols, also neglecting to discuss the important topic of drug content uniformity. Although Susarla et al. (2013) used only one poorly water-soluble drug, their work was the first to demonstrate that film drying via combined conduction and convection leads to commercially feasible faster drying times, and more importantly, showed that employing higher viscosity polymeric film precursors leads to improved content uniformity. Unfortunately, all of these studies were limited because content uniformity was only assessed for one drug, and more importantly, surfactants were used to achieve drug particle stability and fast release. Consequently, the previous studies did not demonstrate the robustness of the process for a wide variety of BCS class II drugs and polymer strip films as a surfactant-free drug delivery platform with very good drug content uniformity.

Poorly water-soluble drugs exhibit limited dissolution and bioavailability, both of which are known to be significantly enhanced by the introduction of surfactant through either micellar solubilization of the drug particles (Ghebremeskel et al., 2007; Jamzad and Fassihi, 2006; Jinno et al., 2000) or improvement of wettability–redispersion (Bhakay et al., 2014a). One of the most common techniques used to improve the dissolution and bioavailability of these drugs involves particle size reduction, which increases the surface area-to-volume ratio of the drug particles, significantly enhancing their ability to solubilize when exposed to aqueous media (Hu et al., 2004; Thorat and Dalvi, 2012). Surfactants serve a crucial role as stabilizers in many particle size reduction processes, including wet stirred media milling (WSMM), in which they act to prevent freshly milled nanoparticles from aggregating back together during the milling process and storage, particularly in combination with nonionic steric stabilizers (Bilgili and Afolabi, 2012; George and Ghosh, 2013; Kipp, 2004; Van Eerdenbrugh et al., 2009). Thus, in general, for certain drugs and applications, sufficient dissolution and bioavailability upon delivery is impossible without the use of surfactants or other solubilizers/dispersants. For example, it is well known that redispersibility of poorly water-soluble drugs from spray dried and fluid bed coated composites is drastically improved by incorporation of surfactant, without which the dissolution enhancement due to nanoparticles could be insignificant (Balakrishnan et al., 2004; Bhakay et al., 2014a; Wong et al., 2006). When surfactants are not used, other dispersants such as mannitol may be used. However, even sufficiently large amounts of mannitol, which reduce the drug loading of the dried composite powder, may not lead to dissolution enhancement

comparable to the use of surfactant (Azad et al., 2015; Bhakay et al., 2014b; Knieke et al., 2015).

Previous studies have shown that, without any additional dispersants, complete dissolution of poorly water-soluble drug nanoparticles from 100 µm-thick HPMC based films can be achieved within 20 min, but only when a surfactant-based dissolution medium was used (Sievens-Figueroa et al., 2012a; Susarla et al., 2013). Both studies also started with drug nanosuspensions stabilized by a surfactant, thus suggesting the need for surfactant for dissolution enhancement even from the strip film format, which uses a high polymer concentration or polymer-to-drug ratio. These studies failed to investigate this important feature of the strip film based dosage form, namely, the use of a relatively high concentration of polymers, leading to high viscosity (>> 1,000 cP) film precursor suspensions that ensure a flexible, uniform film matrix. This feature is unique to strip films and may not be easily provided by other nanocomposite dosage forms such as core-shell nanocomposites (Bhakay et al., 2013) or spray-dried nanocomposites (Azad et al., 2015). Hence, an important question arises whether or not the relatively high polymer concentration required for film formation is sufficient to stabilize the drug nanoparticles without the use of surfactant. If the answer is positive, it can also help negate several disadvantages of the use of surfactant. For example, use of surfactant in suspensions can promote physical instability and particle growth via Ostwald ripening, especially if the concentration of surfactant is above the critical micelle concentration (Cerdeira et al., 2010; Verma et al., 2011). In addition, surfactant is also known to cause gastric and pulmonary irritation (Oberle et al., 1995).

In addition to the role of surfactant, interaction between polymer and drug is known to significantly influence drug particle stability as well as release from solid dosage forms. Strong polymer–drug interaction in solid dispersions and suspensions has been shown to promote particle stability (Huang et al., 2008; Karavas et al., 2007). However, while these interactions have been shown to influence various film properties, such has only been classified in solvent cast films incorporating amorphous drug. Nair et al. (2001) observed hydrogen bonding between drug and polymer via Fourier transform infrared (FTIR) spectroscopy in polyvinylpyrrolidone films across multiple drugs. Puttipipatkhachorn et al. (2001) noted slower dissolution from salicylic acid films than theophylline films, likely due to greater interaction between salicylic acid and chitosan, the film-former, than was observed with theophylline. Wu and McGinity (1999) found that introducing ibuprofen and methylparaben to Eudragit RS 30 D films resulted in a plasticizing effect and Lin et al. (1995) observed a similar trend upon loading piroxicam into Eudragit E films, noting a shift in characteristic IR peaks for piroxicam indicative of interaction with Eudragit E. However, none of these studies addresses polymer interaction with drug nanoparticles, let alone the ability for these interactions to effectively prevent drug particle aggregation.

This chapter demonstrates that surfactant-free polymer strip films loaded with poorly water-soluble drug nanoparticles have excellent content uniformity and retain the same advantages as films containing surfactant-stabilized drug nanoparticles, including nanoparticle redispersibility and fast dissolution.

2.2 Experimental Procedures

2.2.1 Materials

Fenofibrate (FNB; Jai Radhe Sales, Ahmedabad, India), griseofulvin (GF; Letco Medical, Decatur, AL), naproxen (NPX; Medisca, Plattsburgh, NY), phenylbutazone (PB; Medisca, Plattsburgh, NY), and azodicarbonamide (AZD; Pfaltz & Bauer, Waterbury, CT) were selected as model BCS class II drugs. Physicochemical properties of the drugs are shown in Table 2.1 (Verschueren, 2001; Yalkowsky, 2003). Low molecular weight (MW) hydroxypropyl methylcellulose (HPMC; Methocel E15 Premium LV, MW ~ 14,000, The Dow Chemical Company, Midland, MI) was used as a stabilizer and film former. Sodium dodecyl sulfate (SDS; Fisher Scientific, Pittsburgh, PA) was also used as a stabilizer for formulations containing surfactant. Glycerin (Sigma-Aldrich, Saint Louis, MO) was used as a film plasticizer. Drug particle size was reduced via WSMM as described in Sub-section 2.2.2.1. All other materials were used without further processing.

Table 2.1 Physicochemical Properties of Drugs Incorporated into Polymer Films

Drug	Solubility in water at 25 ºC (µg/ml)	MW (g/mol)	Melting point (ºC)	log P
FNB	0.8	360.8	81	5.3
GF	8.6	352.8	220	2.2
NPX	15.9	230.3	153	3.2
PB	34.0	308.4	105	3.2
AZD	35.0	116.1	225	-1.7

2.2.2 Preparation Methods

2.2.2.1 Preparation of Drug Nanosuspensions. Surfactant-free drug nanosuspensions were produced via WSMM utilizing a Netzsch mill (Microcer, Fine particle technology

LLC, Exton, PA) according to previously established methods (Bilgili and Afolabi, 2012; Monteiro et al., 2013). HPMC-E15LV served as a stabilizer. All suspensions were milled for 120 min and consisted of 10% drug (on a w/w basis wrt water) dispersed in a stabilizer solution of 2.5% HPMC (on a w/w basis wrt water). 0.5% SDS (on a w/w basis wrt water) served as an additional stabilizer for the corresponding surfactant-containing formulations.

2.2.2.2 Preparation of Film Precursor Suspensions. HPMC polymer solutions were prepared according to Dow® protocol (Susarla et al., 2013). The starting polymer concentration was chosen to ensure the mixture of polymer solution and nanosuspension had sufficiently high viscosity (~8000 cP) to produce a uniform, good quality film (Susarla et al., 2013). Corresponding amounts of HPMC-E15LV and glycerin, selected for their ability to form quality films loaded with drug nanoparticles (Sievens-Figueroa et al., 2012a), were added to water at 90 ºC such that the composition of the polymer solution was 17% HPMC and 5% glycerin (on a w/w basis) and allowed to cool to room temperature under continuous stirring. The polymer solution was then shear mixed with the drug nanosuspensions in a 2:1 ratio by mass at approximately 120 rpm for 6-12 h using a motor driven dual-propeller mixer (McMaster-Carr, USA) (Susarla et al., 2013). In the case of placebo formulations X1 and X2, the appropriate drug-free stabilizer solution was used instead of the drug nanosuspension. The compositions of the resulting polymer–nanosuspension mixtures, hereafter referred to as film precursor suspensions, are listed in Table 2.2.

Table 2.2 Composition of Film Precursor Suspensions Cast to Form Strip Films Loaded with Drug Nanoparticles

Formulation	Drug	wt% drug	wt% HPMC	wt% glycerin	wt% SDS
F1	FNB	3.0	12.1	3.3	0.00
F2	FNB	3.0	12.1	3.3	0.15
G1	GF	3.0	12.1	3.3	0.00
G2	GF	3.0	12.1	3.3	0.15
N1	NPX	3.0	12.1	3.3	0.00
N2	NPX	3.0	12.1	3.3	0.15
P1	PB	3.0	12.1	3.3	0.00
P2	PB	3.0	12.1	3.3	0.15
A1	AZD	3.0	12.1	3.3	0.00
A2	AZD	3.0	12.1	3.3	0.15
X1	N/A	0.0	12.1	3.3	0.00
X2	N/A	0.0	12.1	3.3	0.15

2.2.2.3 Preparation of Polymer Films Containing Drug Nanoparticles. For each film, approximately 8-9 g of film precursor suspension was manually cast onto a stainless steel substrate at room temperature using a casting knife (Elcometer, MI). The casting thickness was fixed at 1,000 μm and the final dimensions of the films were approximately 8 cm × 9 cm. The wet films were then dried at 50 ºC in the third zone of a Lab-Cast Model TC-71LC Tape Caster (HED International, NJ) in batch mode under laminar air flow for a period of 1 h (Davé et al., 2014). The dry films were peeled from the substrate and stored in individual sealed plastic bags at room temperature for characterization within days of preparation.

2.2.3 Characterization Methods

2.2.3.1 Viscosity of Film Precursor Suspensions. The apparent shear viscosity of film precursor suspensions was measured using an R/S-CC+ Coaxial Cylinder Rheometer (Brookfield Engineering, Middleboro, MA) equipped with a shear rate

controlled coaxial cylinder (CC25) and Lauda Eco water jacket assembly (Lauda-Brinkmann LP, Delran, NJ) for temperature control. Film precursor suspensions were subjected to a low shear rate program (0-20 s^{-1}) at 25 ± 0.5 ºC to measure low shear viscosity. Raw data was analyzed using Rheo 3000 software (Brookfield Engineering, Middleboro MA). All experiments were performed a minimum of four times.

2.2.3.2 Drug Particle Size after Milling and Redispersed from Films. The size distribution of drug particles was measured both in suspension immediately after milling and redispersed from films using a Coulter LS 13320 Laser Diffraction Particle Size Analyzer (Beckman Coulter, Miami, FL). In order to measure particle size after milling, a 1.2 ml sample was removed from the holding tank of the mill, dispersed into 4 ml of the respective stabilizer solution via pipette and vortex mixed at 1500 rpm for 1 min prior to sizing.

The nanoparticle stabilization imparted by the films is assessed based on their ability to preserve drug particle size from the suspension through the process of film formation and subsequently upon redispersion in water. To assess drug nanoparticle redispersibility, samples of films, cut using circular punches of ~0.71 cm^2 in area, were vortex mixed in 3 ml of deionized (DI) water for 3-5 min. Additional punched film samples were required for drugs with higher solubility in order to prevent any significant fraction of drug particles from dissolving in the 110 ml of DI water in the sample cell prior to particle sizing (1 for FNB, 3 for GF, 7 for NPX, 10 for PB and AZD).

2.2.3.3 Determination of Drug Content and Uniformity in Films. Ten circular samples ~0.71 cm^2 in area were punched from each film and dissolved in 250 ml of 5.4 mg/ml SDS solution under continuous stirring for a minimum of 3 h. A Thermo

Scientific Evolution 300 UV-Vis spectrophotometer (Thermo Fisher Scientific Inc., MA) was used to measure the UV absorbance of each sample using the appropriate wavelength of maximum absorbance for each drug (290 nm for FNB, 291 nm for GF, 272 nm for NPX, 264 nm for PB, and 245 nm for AZD) and the concentration of each sample was calculated using a corresponding calibration curve. The average drug weight per unit area of the film, average weight percentage of the drug in the film, and relative standard deviation (RSD) of these two measures were calculated for each set of 10 samples.

2.2.3.4 Film Mechanical Properties. Film mechanical properties were measured using a TA-XT Plus Texture Analyzer (Stable Microsystems, UK). Rectangular film strips with dimensions of 50 mm × 15 mm were held between two grips and stretched at a constant speed of 1 mm/s until the point of tensile failure. Tensile strength (TS), yield strength (YS), Young's modulus (YM), and percent elongation at break (EB) were computed from the resulting stress vs. strain data. Data represents an average of four strips.

2.2.3.5 Scanning Electron Microscopy (SEM). A field emission scanning electron microscope (FESEM) LEO1530VP GEMINI (Carl Zeiss, Inc., Peabody, MA) was used to examine the composite structure in the film and to observe the presence of any drug aggregates within the films. A small sample of the film was placed on an aluminum stub using carbon tape and carbon coated using a sputter coater (Bal-Tec MED 020 HR, Leica Microsystems, Wetzlar, Germany) prior to imaging. The cross sectional image of all films and surface image of select films were recorded.

2.2.3.6 Thermogravimetric Analysis (TGA). Thermogravimetric analysis (TGA) was performed using a TGA/DSC1/SF Stare system (Mettler Toledo, Inc., Columbus, OH). A ~2 mg film sample was placed in a ceramic crucible and heated under nitrogen flow from 25 ºC to 150 ºC at a constant rate of 10 ºC/min, held at 150 ºC for 15 min, heated to 250 ºC at a rate of 10 ºC/min, and finally cooled back to 25 ºC at a rate of 10 ºC/min.

2.2.3.7 Fourier Transform Infrared (FTIR) Spectroscopy. FTIR spectra were measured for each film as well as pure as-received drug powders and placebo films containing no drug using a Fourier Transform Infrared Spectrometer (Nicolet 560 FTIR) with an attached Attenuated Total Reflectance (ATR) accessory and a single reflection ZnSe crystal (MIRacle, Pike Technologies). Samples were measured within the range from 600 to 4,000 cm^{-1}. The spectral resolution of FTIR spectra was set to 4 cm^{-1} and compared to the background interferogram. Reported final spectra are an average of 100 scans.

2.2.3.8 Raman Spectroscopy. Raman spectroscopy was carried out with an EZ Raman-L system (SN: LE-178155, Enwave Optronics, Inc.) equipped with a fiber optic probe (785 nm laser, 250 mW, working distance 6 mm). The spectral range was between 100 and 3,300 cm^{-1}. Raman spectra were taken for an average of 3 scans, each 10 s long and totaling 60 s in scanning time.

2.2.3.9 Flow-through Cell Dissolution (USP IV). A flow-through cell dissolution apparatus (USP IV; Sotax, Switzerland) with cells of 22.6 mm internal diameter and 0.2 µm Pall HT Tuffryn filters was employed for better discrimination of

nanoparticle-loaded polymer films (Sievens-Figueroa et al., 2012b). Previous work has shown that use of 0.1 µm filters instead of 0.2 µm filters had no significant impact on the release profiles of films containing drug nanoparticles with mean diameter as low as 160 ± 30 nm (Kakran et al., 2010; Sievens-Figueroa et al., 2012a; Sievens-Figueroa et al., 2012b). Circular film samples ~0.71 cm^2 in area were secured horizontally inside the cells within 5 g of 1 mm glass beads. Cell temperature was maintained at 37.0 ± 0.5 ºC and dissolution media was circulated at a flow rate of 16 ml/min. Two dissolution media were employed for comparison, each using 100 ml per cell: 5.4 mg/ml SDS solution (USP recommended for GF, for which these methods were established) (Sievens-Figueroa et al., 2012a; Sievens-Figueroa et al., 2012b; Susarla et al., 2013) and DI water as a surfactant-free medium (pH 6.7). The average drug release across six samples from each film was plotted as a function of time.

2.3 Results and Discussion

2.3.1 Precursor Suspension Viscosity

Viscosity of the film precursor suspension has been shown to have a significant impact on the content uniformity of the resulting dry film. Susarla et al. (2013) demonstrated that use of higher viscosity precursors generally led to more uniformly distributed drug nanoparticles in films. Table 2.3 shows the apparent shear viscosity of all film precursor suspensions at low shear rate (2.2 s^{-1}) to mimic conditions of film casting. With the exception of FNB, surfactant-free film precursor suspension viscosities ranged from about 9,000-11,000 cP while those of SDS formulations ranged from 11,000-13,000 cP. FNB showed the greatest increase in viscosity with the addition of surfactant (+43%),

followed by NPX (+28%), PB (+11%), and AZD (+8%), while GF (-3%) showed no statistical difference ($p > 0.05$).

Table 2.3 Low Shear (2.2 s^{-1}) Viscosity of FNB, GF, NPX, PB and AZD Film Precursor Suspensions at 25 ºC

Formulation	Viscosity (cP)
F1	7,470 ± 320
F2	10,340 ± 580
G1	11,010 ± 440
G2	10,640 ± 410
N1	10,020 ± 570
N2	12,840 ± 550
P1	10,030 ± 150
P2	11,180 ± 910
A1	12,010 ± 150
A2	12,920 ± 360

Viscosity increases with increasing surfactant concentration have also been reported in dilute polymer solutions. Brackman (1991) observed a general increase in viscosity and viscoelasticity of aqueous poly(ethylene oxide) solutions (< 30 cP) as SDS concentration was increased and Kulicke et al. (1998) observed a viscosity increase with increasing SDS concentration (up to 13 mM) for weakly hydrophobic 0.5% (w/w) HPMC solutions. Bilgili and Afolabi (2012) also showed that the viscosities of polymer (HPC) solutions and milled drug suspensions were higher in the presence of SDS than in its absence. This behavior is believed to be caused by the repulsion of adsorbed surfactant micelles between polymer chains which increases with the addition of surfactant until the polymer chains become saturated. The fact that a similar increase in viscosity with increasing surfactant concentration is also present under the viscous conditions required for film formation suggests that the same principle could apply to more viscous systems, as well (Bilgili and Afolabi, 2012). Fortunately, as will be shown in Sub-section 2.3.3.1,

the viscosity of all film precursors was sufficiently high enough so that the differences in precursor viscosity between formulations are unlikely to have appreciable influence on the RSD values describing the content uniformity of the resulting films.

2.3.2 Drug Particle Size after Milling and Redispersed from Films

Nano-milled BCS class II drugs have been shown to exhibit enhanced bioavailability owing to the increased specific surface area of the drug particles (Merisko-Liversidge et al., 2003), provided that the drug particles retain their small size upon incorporation into the final dosage form (Merisko-Liversidge and Liversidge, 2011). The ability of the film format to impart physical stability to the milled drug particles was investigated by redispersing the particles from the film in water, measuring their sizes, and comparing their sizes against those of the milled drug particles (Beck et al., 2013; Sievens-Figueroa et al., 2012a; Susarla et al., 2013). If the drug particles redispersed from the film are comparable in size to the drug particles in the milled suspension, it may be concluded that the embedded drug particles are stabilized within the film.

Particle size distribution data for drug particles in milled suspension prior to shear mixing with polymer solution and for drug particles redispersed from dry films is given in Table 2.4. Suspension size data suggests that WSMM allowed for preparation of drug nanosuspensions with median sizes < 400 nm (except G1). Despite being subjected to identical milling conditions and milling time, FNB, GF, and AZD all yielded suspensions with significantly smaller drug particle sizes (> 100 nm difference in median particle size) with surfactant than without, particularly GF which exhibited micron-size agglomerates in the absence of surfactant. This behavior was expected, as the addition of surfactant as a stabilizer for WSMM has been shown to have several synergistic

stabilizing effects when used in conjunction with nonionic polymer, generally yielding smaller particle sizes (Bhakay et al., 2014a; Bilgili and Afolabi, 2012). In addition, the significant fraction of particles between 1-2 μm in the AZD suspensions may be attributed to its hardness and higher solubility in water relative to the other drugs used in this study (Bhakay et al., 2011; Keck and Müller, 2006). However, the enhanced stabilization offered by surfactant for WSMM is not always as pronounced or even required, as demonstrated by the similar median particle sizes of the NPX and PB suspensions (141/136 nm and 156/176 nm without surfactant/with surfactant, respectively).

Table 2.4 Particle Size Distribution of Drug in Milled Suspension Prior to Shear Mixing with Polymer Solution (Susp) and Drug Redispersed from Dry FNB, GF, NPX, PB and AZD Films (Film)

Formulation	F1		F2		G1		G2		N1	
Source	Susp	Film	Susp	Film	Susp	Film	Susp	Film	Susp	Film
d_{10} (nm)	160	151	67	135	150	103	123	109	76	75
d_{50} (nm)	280	275	178	283	1,460	238	161	164	141	138
d_{90} (nm)	503	489	417	620	5,178	491	214	269	246	248
Formulation	N2		P1		P2		A1		A2	
Source	Susp	Film	Susp	Film	Susp	Film	Susp	Film	Susp	Film
d_{10} (nm)	70	68	102	100	113	94	235	229	181	222
d_{50} (nm)	136	134	156	5,496	176	184	370	366	278	352
d_{90} (nm)	313	359	254	63,004	282	430	1,719	1,744	1,831	1,685

Although the median particle size of the milled suspensions ranged from 130-370 nm across all formulations (except G1), it will be demonstrated in Sub-section 2.3.3.7 that particle size variation within this range has no significant impact on the dissolution rate of drug from the resulting films. Thus, the primary concern is to ensure that the drug nanoparticles do not experience any agglomeration during film production. The size of the drug particles redispersed from films containing FNB, NPX, and AZD was similar to

the size of the drug particles in the respective milled suspensions, all with median particle sizes below 400 nm (Table 2.4). This suggests that the drug nanoparticles in these films did not further agglomerate upon incorporation into films for both SDS and SDS-free formulations, demonstrating the ability of the polymer matrix of the film to stabilize these drug nanoparticles just as well without the aid of surfactant. This can be traced back to the additional polymer added during the preparation of the film precursor suspension, leading to a drug:polymer mass ratio of ~1:4 (Table 2.2). This extra polymer helps to preserve the drug particle size within the film while also enhancing the stabilization of the drug particles upon redispersion via adsorption (Bilgili and Afolabi, 2012; Knieke et al., 2013), allowing for recovery of the drug nanoparticles from films in redispersion. Redispersion from P1 (formulation without surfactant) yielded agglomerates, whereas redispersion from P2 yielded nanoparticles. However, as will be shown later, this had no impact on the film dissolution and may suggest that the redispersion protocols employed are conservative and may not necessarily assess the extent of reversible agglomeration. In other words, the redispersion test and dissolution test have different hydrodynamic conditions and they correspond to different measurement times, hence their results are expected to have some differences. Redispersion from both GF films yielded nanoparticles despite agglomeration in the surfactant-free suspension, implying that the GF agglomerates produced in the surfactant-free suspension are breakable upon redispersion, allowing for recovery of the primary nanoparticles. Analysis of SEM images of films was used to qualitatively supplement all drug particle redispersion results (Sub-section 2.3.3.3).

2.3.3 Film Characterization

2.3.3.1 Drug Content and Uniformity in Films. As with any pharmaceutical dosage form, content uniformity is essential to ensuring product quality. Although the capability of forming strip films containing uniformly dispersed GF nanoparticles has been demonstrated previously (Davé et al., 2014; Susarla et al., 2013), the same has not yet been shown for other BCS class II drugs. The average and relative standard deviation (RSD) for film thickness, drug mass per unit area of film and drug loading on a w/w basis for all formulations are shown in Table 2.5. It is emphasized that the film samples are very small, ~0.71 cm^2 and thus about $1/10^{th}$ of the expected dosage size, hence the final dosage RSD values are expected to be even lower/better than those reported here. It should be noted that some variability in drug mass per unit area is due to variability in film thickness, the optimization of which is beyond the scope of this study. This effect can be seen by comparing thickness and mass RSDs to that of drug loading (wt%), which is significantly less than the other two as a result of being inherently normalized by the mass of each sample measured. The variation in drug distribution throughout the films by mass per unit area was within 6% RSD, and most are < 3% RSD. Not only does this consistency demonstrate the robustness of the film manufacture process to produce films with good content uniformity for a wide variety of poorly water-soluble drugs, but it also emphasizes the capability of the strip film format as a whole to produce dosages with uniform drug content, even for doses as low as 1-2 mg, a significant challenge for other solid dosage forms.

Table 2.5 Content Uniformity and Thickness Variation within Films Containing FNB, GF, NPX, PB and AZD Nanoparticles, Respectively

Formulation	Thickness (μm)	RSD (%)	Drug mass per unit area (mg/cm^2)	RSD (%)	wt% drug	RSD (%)
F1	92.8	2.4%	1.71	2.8%	14.9	2.0%
F2	102.0	1.4%	2.08	4.2%	17.0	2.6%
G1	92.9	2.4%	1.95	1.8%	15.2	1.3%
G2	95.4	2.7%	1.93	3.5%	14.5	1.2%
N1	101.5	5.4%	1.53	5.0%	12.7	1.6%
N2	108.3	0.8%	1.84	3.1%	14.2	1.6%
P1	107.8	2.2%	1.65	6.5%	13.6	3.6%
P2	93.4	3.8%	1.90	4.4%	15.1	3.7%
A1	98.8	2.1%	1.97	3.1%	16.6	2.2%
A2	92.6	1.4%	2.00	2.7%	17.7	0.7%

While surfactant is known to improve the dispersibility of poorly water-soluble drugs and the average film precursor suspension with surfactant was 2000 cP more viscous than without, the presence of surfactant in the film did not have either significant or consistent effect on film content uniformity across all five drugs under investigation. NPX and PB films both exhibited 2% RSD less variation in drug distribution with SDS than without, while FNB, GF, and AZD films exhibited less significant differences in drug distribution RSD between films with and without SDS. While content uniformity improved for AZD films with the inclusion of SDS and declined for FNB and GF films with SDS, it is difficult to say whether or not a difference of 1% RSD was due to the formulation. When averaged together by SDS content, the variation in drug distribution of surfactant-free films was 3.8% RSD and thickness variation was 2.9% RSD, demonstrating the feasibility of producing uniform films loaded with drug nanoparticles without the need for surfactant. When averaged together, films containing surfactant exhibited comparable variation in drug distribution, 3.6% RSD and in thickness 2.0% RSD, suggesting that the amount of surfactant required to stabilize the drug nanoparticles

in suspension does not influence the content uniformity of films made from those suspensions, positively or negatively.

2.3.3.2 Film Mechanical Properties. In addition to the importance of having flexible films with sufficient mechanical strength, the mechanical properties of films may also influence dissolution kinetics, as will be discussed in Sub-section 2.3.3.7 (Mangwandi et al., 2014). The tensile strength (TS), yield strength (YS), Young's modulus (YM), and percent elongation at break (EB) for all film formulations are shown in Table 2.6. NPX, PB, and AZD films all exhibited TS around 30 MPa, YS around 25 MPa, YM around 2.0 GPa, and EB around 23%. GF and FNB exhibited significantly higher TS (~47 MPa), YS (~41 MPa), YM (~2.8 GPa), and lower EB (~16%) than the other three drugs. As will be shown in Sub-section 2.3.3.4, films containing less water-soluble drug nanoparticles also retained less water upon drying, which is known to contribute to increased tensile strength and decreased elasticity (Biliaderis et al., 1999).

Table 2.6 Mechanical Properties of FNB, GF, NPX, PB, AZD, and Placebo Films

Formulation	Tensile strength (MPa)	Yield strength (MPa)	Young's modulus (GPa)	Elongation at break (%)
F1	45.7 ± 2.0	41.8 ± 3.8	2.62 ± 0.19	14.2 ± 5.4
F2	49.0 ± 3.4	47.0 ± 1.8	3.02 ± 0.14	13.4 ± 2.3
G1	45.5 ± 2.4	37.0 ± 0.4	2.68 ± 0.17	20.5 ± 2.8
G2	50.4 ± 4.3	43.4 ± 2.8	2.79 ± 0.13	16.9 ± 2.5
N1	26.1 ± 3.5	22.0 ± 2.1	1.58 ± 0.17	23.2 ± 3.8
N2	32.7 ± 0.6	27.2 ± 0.9	1.96 ± 0.08	23.4 ± 2.0
P1	28.8 ± 0.9	25.4 ± 0.6	1.82 ± 0.07	20.4 ± 1.9
P2	33.0 ± 2.3	28.2 ± 0.5	2.20 ± 0.06	22.2 ± 1.3
A1	30.2 ± 0.2	22.4 ± 0.8	2.22 ± 0.10	25.4 ± 0.6
A2	29.7 ± 0.8	23.3 ± 0.0	2.28 ± 0.07	21.4 ± 2.1
X1	36.8 ± 0.8	25.3 ± 1.1	1.88 ± 0.08	27.6 ± 1.2
X2	26.1 ± 1.9	23.5 ± 2.0	1.72 ± 0.07	14.6 ± 3.6

Interesting outcomes are seen in terms of the impact of the SDS on film mechanical strength. Although placebo films exhibited an 11 MPa decrease in TS upon addition of SDS, an increase of ~5 MPa in TS was observed upon incorporation of SDS in films for all drugs except AZD, for which no significant difference was observed between films with and without SDS. While surfactant is known to exhibit a plasticizing effect in polymer films (Rodríguez et al., 2006), as is observed in the placebo films, it is hypothesized that the dominant role of SDS in the drug-loaded films is that of a nanoparticle stabilizer. Since the drug particles are milled along with the SDS and no additional SDS is added upon mixture with polymer solution, it follows that most of the SDS in the film precursor suspension and subsequent dry film should be adsorbed onto the surface of the drug nanoparticles. As a result, the ionic stabilization imparted to the drug nanoparticles by the SDS may allow for more favorable interaction with the HPMC, strengthening the polymer network. The opposite is true when drug nanoparticles are incorporated into films without any form of ionic stabilization, as the exposed hydrophobic surfaces may serve to weaken the polymer network.

2.3.3.3 Scanning Electron Microscopy (SEM). SEM images were taken to qualitatively confirm drug nanoparticle size and morphology within the polymer matrix of the dry films. Cross-sectional images for each film are shown in Figure 2.1 and surface images for select films are shown in Figure 2.2. The drug nanoparticles seem to be well-dispersed and encapsulated by the polymer owing to ~4:1 polymer-to-drug ratio to such an extent that depending on the cut surface, they may not even appear clearly (Figure 2.1). While these images may not be representative of the whole film, this encapsulation may help to explain the stabilization effect imparted by the additional

excess polymer added during the preparation of the film precursor suspension. With the exception of GF, no significant nanoparticle agglomeration was observed from the acquisition of the cross-sectional images. In agreement with suspension sizing data, G1 (Figure 2.1c) exhibited some agglomeration of nanoparticles in the film, whereas G2 (Figure 2.1d) did not, owing to the electrostatic stabilization provided by the surfactant in the nanosuspension. The ability to recover GF nanoparticles after redispersion from the surfactant-free film is indicative of reversible or soft agglomerates which are not expected to impact the dissolution rate as they break apart to reform the original nanoparticles under light mechanical forces or hydrodynamic stress. The largest observable PB particles in P1 surface images were 1-2 µm in size (Figure 2.2a), well below the 5.5 µm median size of the particles redispersed from the film. This suggests that the PB particles may have formed irreversible agglomerates of smaller aggregates of 1-2 µm that could not be completely redispersed from the P1 film as per the redispersion protocol. AZD film surface images revealed micron-size drug particles, as well (Figure 2.2b). Since these micron-size particles were also present in the original AZD nanosuspensions and were preserved as such upon incorporation into the film format, the presence of micron-size AZD particles in the film is likely a result of the difficulty of nano-milling AZD due to its hardness and relatively high solubility in water compared to the other drugs under investigation, as opposed to the film manufacture process. These findings corroborate the robustness of the film format to stabilize drug nanoparticles formed via WSMM with and without surfactant, as the drug particles observed in every film were qualitatively consistent with the size of the drug particles in the suspensions

from which they were taken, with the exception of P1 whose drug particles may not have been completely recovered during redispersion.

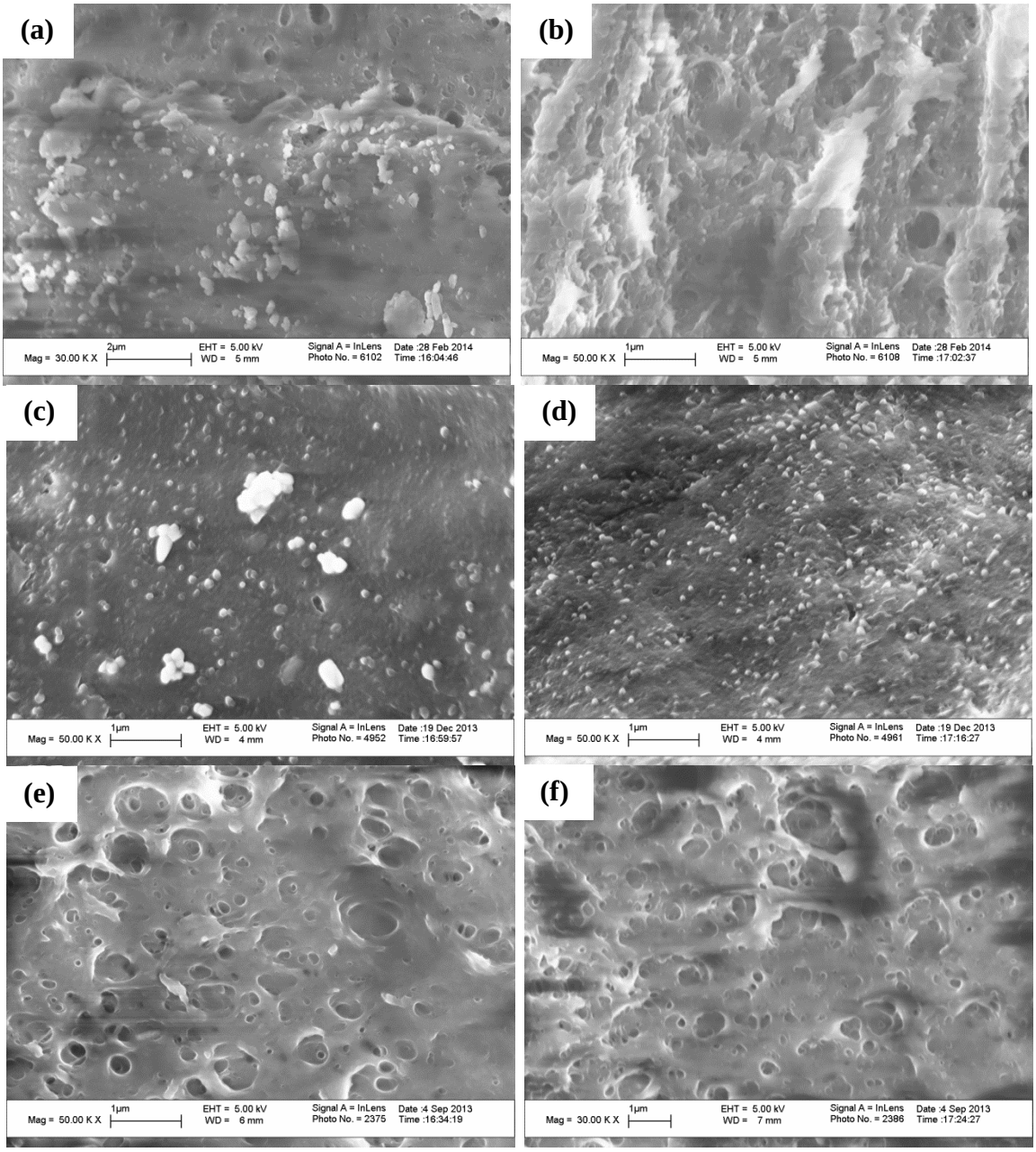

Figure 2.1 Cross-sectional SEM images of films containing (a,b) FNB, (c,d) GF, (e,f) NPX, (g,h) PB, and (i,j) AZD nanoparticles without SDS and with SDS, respectively. (Continued)

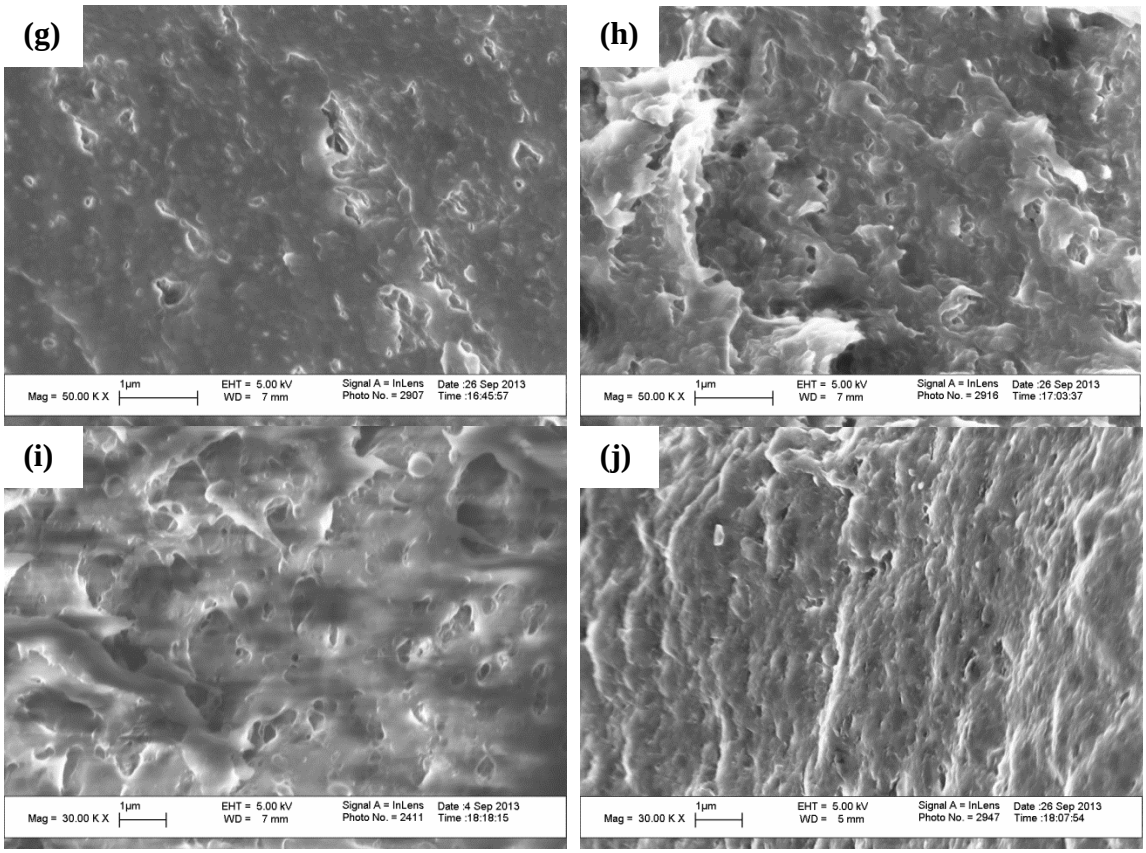

Figure 2.1 (Continued) Cross-sectional SEM images of films containing (a,b) FNB, (c,d) GF, (e,f) NPX, (g,h) PB, and (i,j) AZD nanoparticles without SDS and with SDS, respectively.

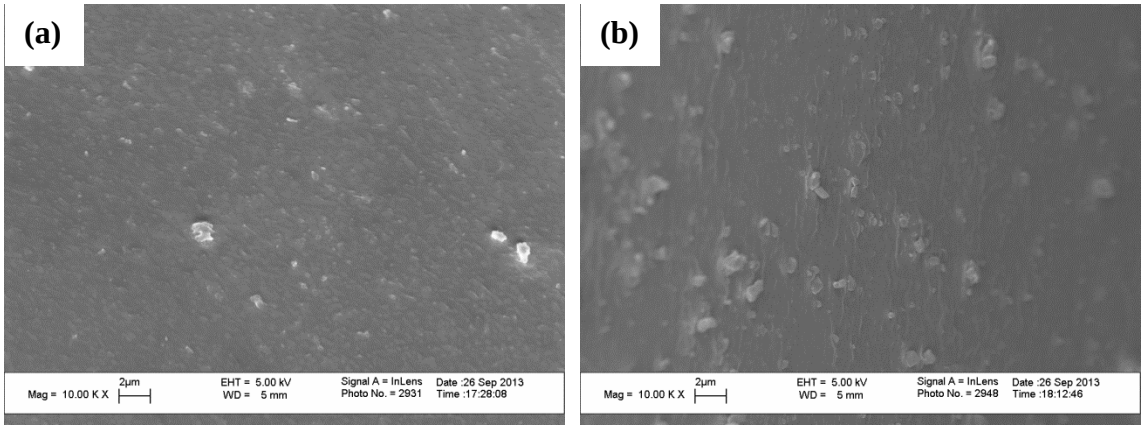

Figure 2.2 SEM surface images of films (a) P1 [PB without SDS], and (b) A2 [AZD with SDS].

2.3.3.4 Thermogravimetric Analysis (TGA). TGA analysis was done and curves were normalized to account for varying drug and SDS content between films (Figure 2.3). Weight loss up to 100 ºC was between 2-8 wt% for NPX, PB, and AZD films, primarily due to the loss of free or bound water. This percentage dropped to 1% for FNB and GF films, most likely due to the lower water solubility of the incorporated drug nanoparticles. This is in line with the increased mechanical strength and decreased elasticity exhibited by FNB and GF films, as films with less bound water are generally more brittle (Biliaderis et al., 1999). 15 min exposure to 150 ºC resulted in additional weight loss of 10-15 wt% for all films, mainly attributed to the loss of glycerin (Susarla et al., 2013).

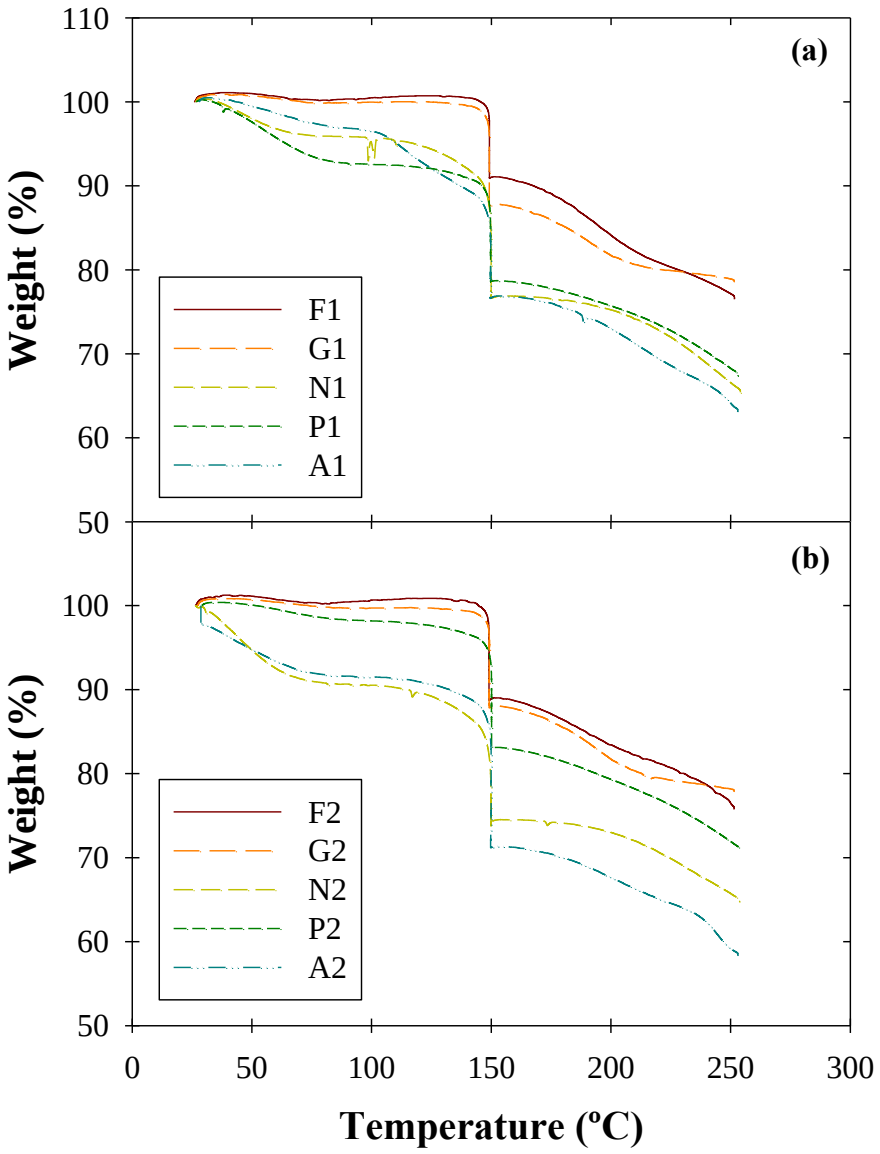

Figure 2.3 Normalized TGA curves for films containing FNB, GF, NPX, PB, and AZD nanoparticles (a) without SDS and (b) with SDS.

2.3.3.5 Fourier Transform Infrared (FTIR) Spectroscopy. To observe potential molecular interactions between components within the film, FTIR spectroscopy was performed on all film samples and pure drug powder (Figure 2.4). All drug-laden film samples exhibited a positive peak shift of 5-12 cm^{-1} for the C–O–C stretch and/or C–O ($R–CH_2–OH$) stretch in HPMC from their respective 1113 cm^{-1} and 1054 cm^{-1} peaks in

the drug-free placebo films, indicative of polymer–drug interaction. In addition, NPX and AZD spectra also revealed a shift in hydrogen bonding from drug–drug to polymer–drug within the film. The COOH dimer peak at 1684 cm^{-1} for NPX, indicative of drug–drug hydrogen bonding, disappears entirely from the film spectra while the COO^- peak at 1396 cm^{-1} splits to form a doublet peak with 1375 cm^{-1} (Figure 2.4c). Disappearance of the NPX dimer peak due to interaction with the polymer matrix was also observed in polyvinylpyrrolidone films by Nair et al. (2001). The C═O stretch peak for AZD at 1724 cm^{-1} splits to form a doublet peak with 1740 cm^{-1} in the film spectra (Figure 2.4e). In addition, the two peaks associated with the combination of NH_2 scissoring and C═O stretching for AZD at 1662 cm^{-1} and 1638 cm^{-1} shift to 1677 cm^{-1} and disappear entirely from the film spectra, respectively, suggesting preferred hydrogen bonding with the polymer than with other AZD molecules (Lee et al., 2008). This preferred hydrogen bonding between drug molecules and polymer suggests that the additional polymer required for the film format aids in physical stabilization of the drug nanoparticles at the molecular level.

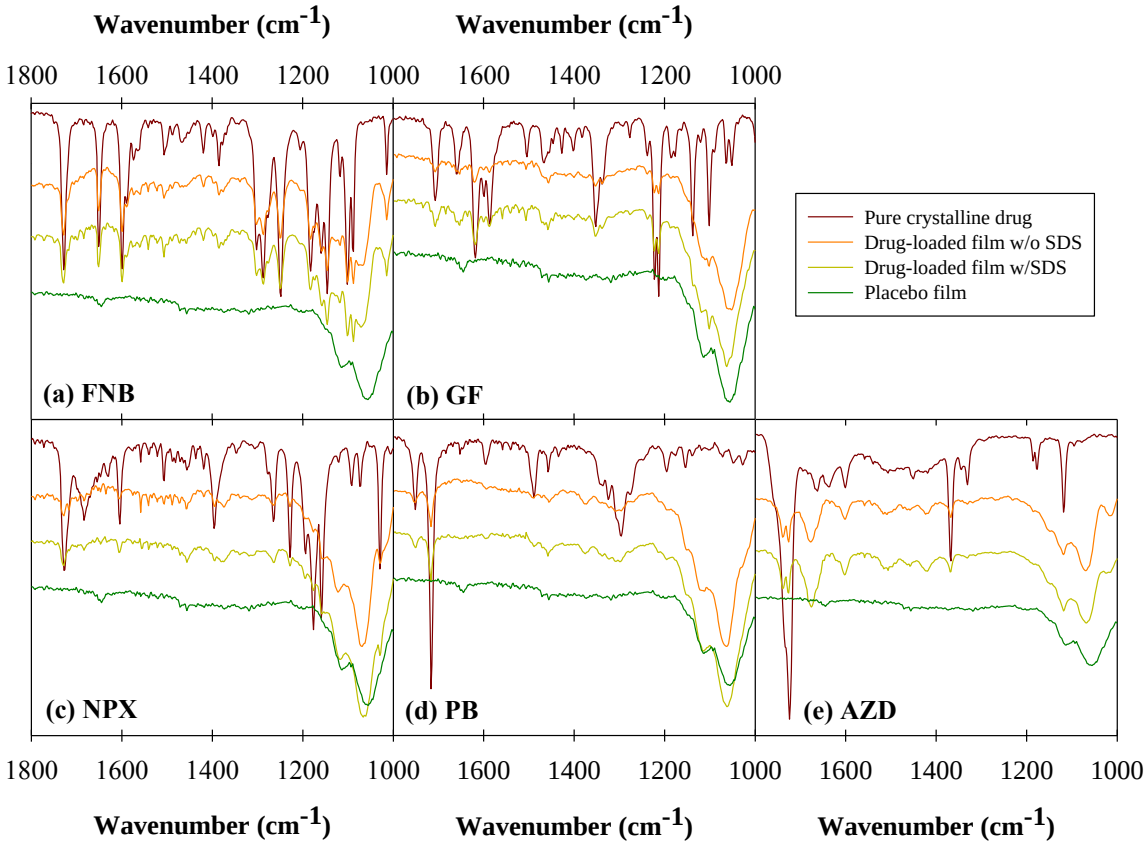

Figure 2.4 FTIR spectra of pure drug and films containing (a) FNB, (b) GF, (c) NPX, (d) PB, and (e) AZD nanoparticles.

2.3.3.6 Raman Spectroscopy. Raman spectroscopy was employed to investigate the crystallinity of the drug within the films. Raman spectra for pure amorphous drug, as-received pure crystalline drug powder, drug-loaded film without SDS, drug-loaded film with SDS, and placebo film are shown in Figure 2.5. Although some films exhibited stronger drug peaks than others, characteristic peaks for all drugs were evident in their respective film spectra.

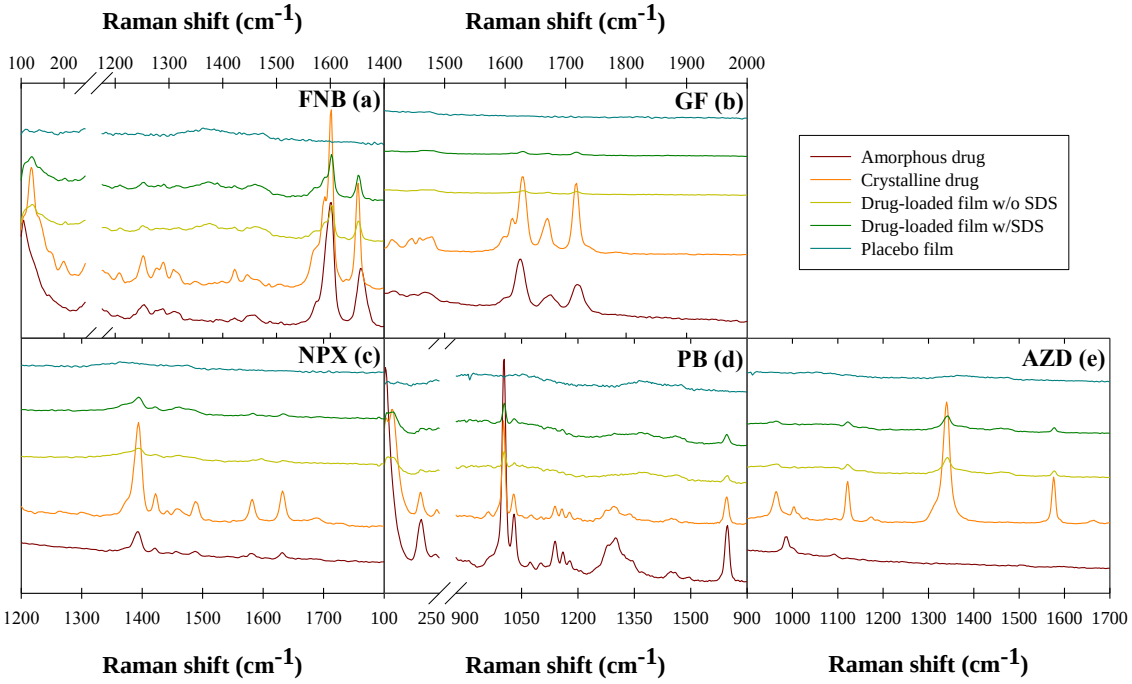

Figure 2.5 Raman spectra of pure drug and films containing (a) FNB, (b) GF, (c) NPX, (d) PB, and (e) AZD nanoparticles.

The most prominent peaks displayed in the FNB film spectra were at 1148, 1602, and 1652 cm^{-1} for C–O stretching, in-plane benzene ring stretching and C═O stretching, respectively (Heinz et al., 2009), which overlapped with the corresponding peaks of the pure drug powder spectrum (Figure 2.5a). FNB films also displayed a peak at 124 cm^{-1} which overlapped with the 124 cm^{-1} peak of the pure drug powder spectrum not present in the amorphous spectrum (any peaks at 104 cm^{-1}, such as that in the amorphous

spectrum, are likely artifacts caused by notch filter cutoff). GF films and pure GF powder shared a trio of peaks between 1600 and 1750 cm^{-1} corresponding to C═O stretching of the benzofuran ring (Figure 2.5b). Although the GF signal from the GF films was relatively weak, all three peaks in this trio exhibited a noticeable shift from the crystalline form to the amorphous form and the peaks visible in the film spectra aligned with those of the crystalline drug. The strongest peak present in the NPX film spectra occurred at 1394 cm^{-1} corresponding to the in-plane bend for the naphthalene ring of NPX, also present in the spectrum for pure crystalline NPX and clearly absent from the placebo film spectrum (Figure 2.5c). However, Raman was unable to distinguish between the crystalline and amorphous forms of NPX. PB film spectra exhibited peaks at 1002 for C–H wagging and 1596 cm^{-1} for aromatic C═C stretching also seen in the pure drug spectrum (Figure 2.5d). PB films also exhibited a matching peak at 130 cm^{-1} with the crystalline spectrum absent from the amorphous spectrum. Peaks at 1122, 1340, and 1576 cm^{-1}, corresponding to the NH_2 rock + C═O stretch + C–N stretch, C–N stretch + N–C═O bend + NH_2 rock, and N═N stretch in AZD, respectively, can clearly be seen in both AZD film spectra and the crystalline AZD spectrum, but not in the amorphous spectrum (Figure 2.5e) (Lee et al., 2008; Xie et al., 2013).

Alignment of the drug spectral peaks for both drug-loaded films with those of their respective crystalline drug spectra as opposed to those of the amorphous drug spectra demonstrates that the crystallinity of the drug was maintained throughout the film manufacture process for all drugs under investigation.

2.3.3.7 Dissolution. A comparison between the dissolution profiles of films without SDS and with SDS for each of the five drugs in SDS media is shown in

Figure 2.6. NPX and AZD exhibited statistically similar dissolution profiles with and without SDS according to similarity and difference factors (Boateng et al., 2012; Costa and Lobo, 2001), indicating that the presence of surfactant in the film had little influence on the rate of drug release from films containing these two drugs. Interestingly, FNB, GF, and PB films all exhibited a statistically significant decrease in dissolution rate with the incorporation of SDS than without. This finding was surprising as surfactants generally enhance the rate of release of poorly water-soluble drugs (Bhakay et al., 2014a; Bhakay et al., 2014b). The slower dissolution may be attributed to the greater mechanical strength exhibited by the films containing surfactant. It is more evident when the dissolution profiles are grouped by surfactant content in Figure 2.7, shown for the sake of easier comparison. These results are in line with previous work, which has shown that changes in film formulation, such as film-forming polymer MW (Prodduturi et al., 2005), that result in changes in film mechanical properties may also influence the dissolution rate of the film. Specifically, slower dissolution was observed from films with increasingly greater tensile strength. Likewise, Mangwandi et al. (2014) observed a similar correlation between mechanical properties and dissolution rate in tablets.

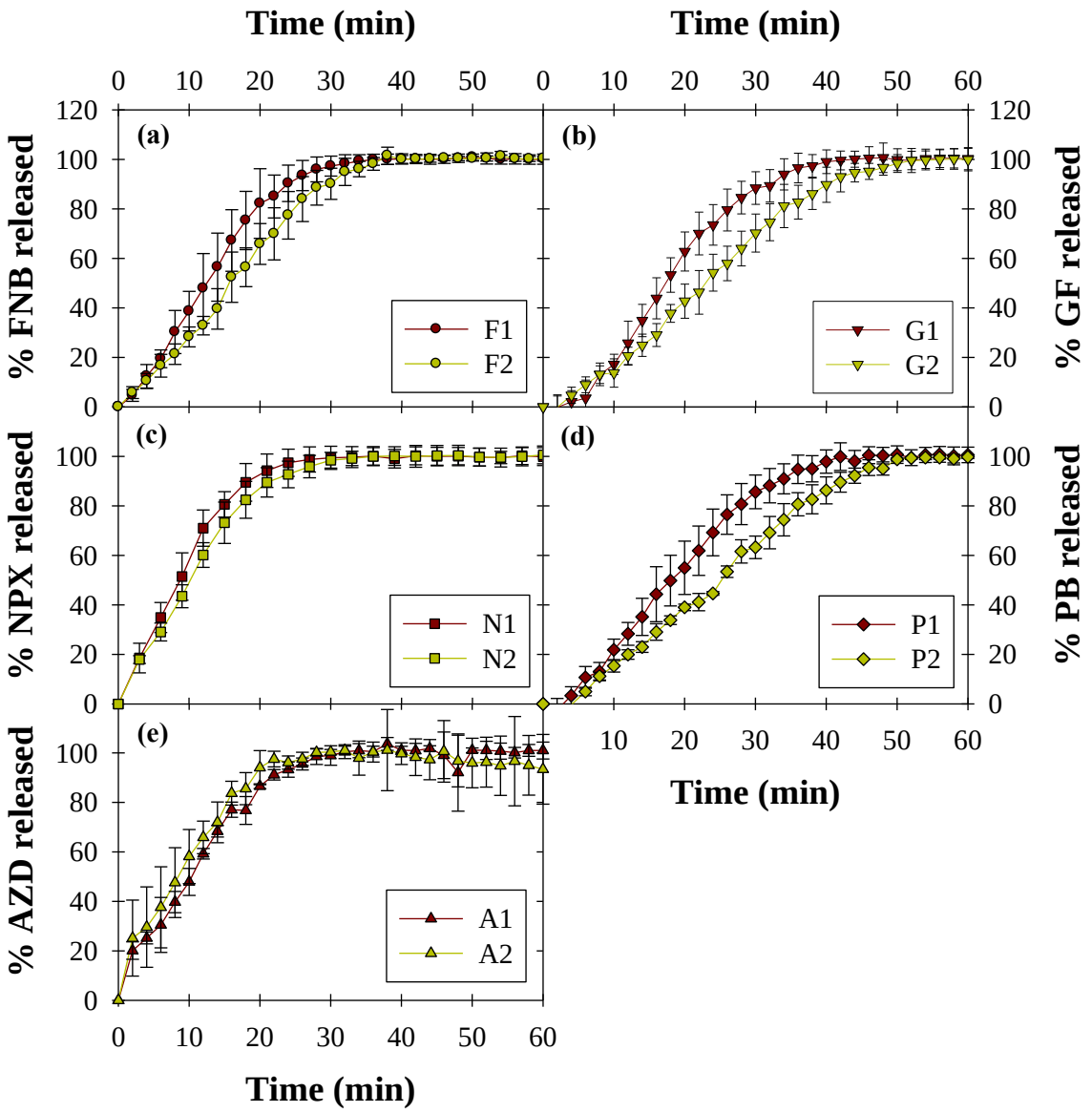

Figure 2.6 Comparison of release profiles from films containing (a) FNB, (b) GF, (c) NPX, (d) PB, and (e) AZD nanoparticles in SDS media.

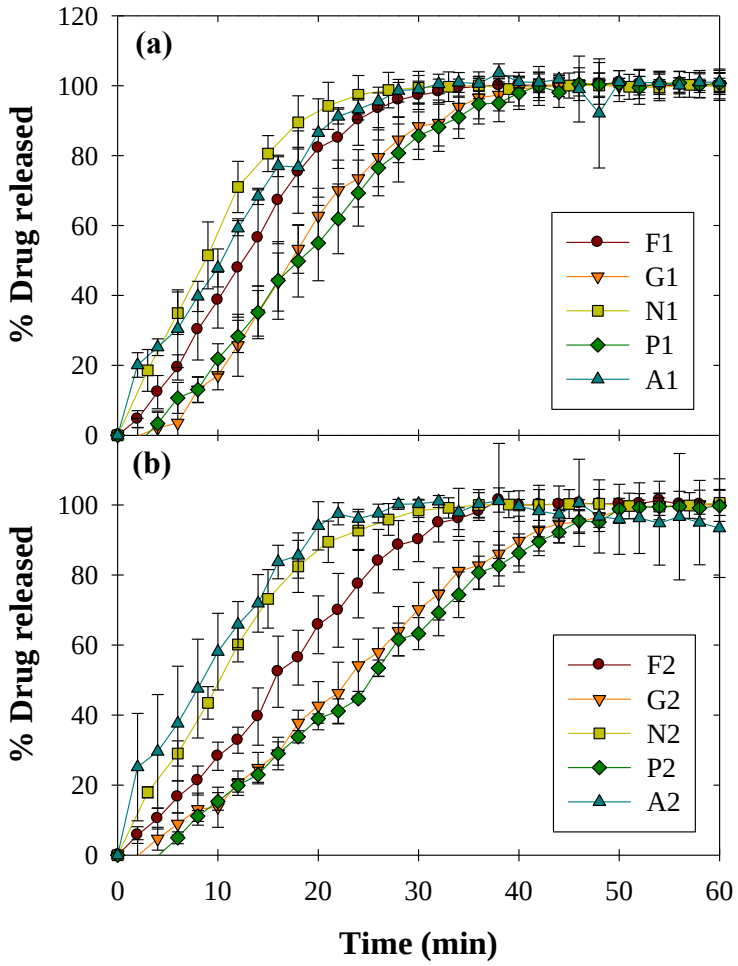

Figure 2.7 Comparison of drug release profiles in SDS media from films containing FNB, GF, NPX, PB, and AZD nanoparticles (a) without SDS and (b) with SDS.

It is hypothesized that, due to the high polymer concentration necessary for film formation, drug release is limited by erosion of the polymer matrix, effectively masking any potential effects of drug properties or surfactant on dissolution rate. As such, it follows that any significant difference in the mechanical properties between films in a polymer matrix erosion-limited system would be manifested in differences between their dissolution profiles. That said, the complex nature of nanoparticle release from polymer films must also be acknowledged. While every effort was made to ensure the following factors were kept as constant as possible, variations in film thickness, gelation, swelling,

etc. may also play a role in determining drug dissolution rate, making it difficult to pinpoint a single source of variation between dissolution profiles. Nonetheless, most films achieved 80% drug dissolution (t_{80}) between 18-28 min in spite of these potential variations as well as the differences in drug solubility and surfactant content between formulations, suggesting that the film format offers reliable and controlled solubilization of the embedded drug nanoparticles.

To further elucidate the potential impact of surfactant on dissolution, similar tests were performed in DI water media for NPX, PB, and AZD films. Such tests were not performed for FNB or GF, as their water solubilities, 0.7 and 8.6 µg/ml, respectively, were too low to make such a test practical for those drugs. As shown in Figure 2.8, despite being released into a surfactant-free medium, PB and AZD films exhibited statistically similar dissolution profiles with and without SDS, further emphasizing that surfactant is unnecessary to achieve enhanced dissolution of drug nanoparticles from films. The slight difference between NPX films may be attributed to the greater mechanical strength of N2 compared to N1, leading to slower dissolution in DI water. This consistency in dissolution demonstrates the robustness of the film format to release a wide variety of poorly water-soluble drug nanoparticles within a similar timeframe, even without the need for surfactant.

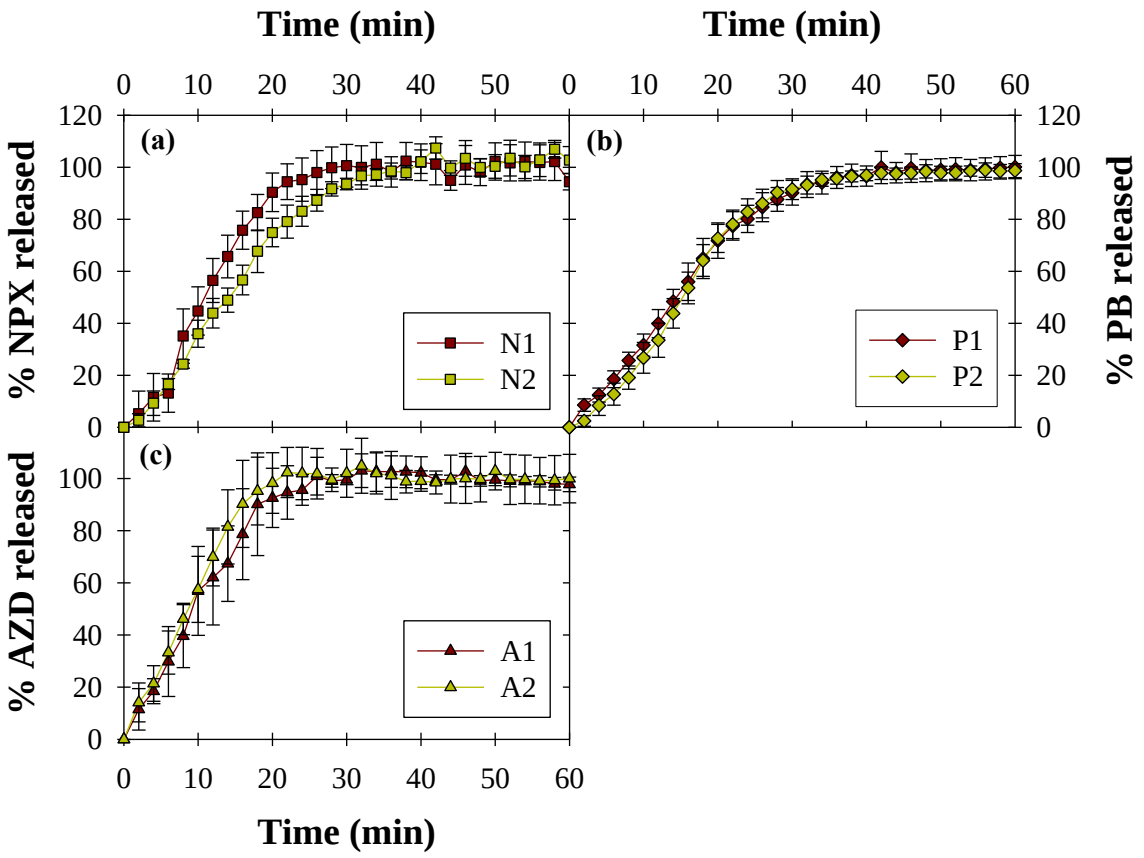

Figure 2.8 Comparison of release profiles from films containing (a) NPX, (b) PB, and (c) AZD nanoparticles in DI water media.

2.4 Conclusions

The ability of the polymer strip film format to effectively stabilize and deliver a variety of BCS class II drug nanoparticles with and without the aid of surfactant was investigated. In general, drug nanoparticles were successfully recovered upon redispersion from FNB, GF, NPX, and AZD films with and without SDS, suggesting surfactant is not required to recover nanoparticles of these drugs from the polymer film. Films exhibited very good content uniformity in terms of drug distribution and thickness variation, even when very small samples were tested (RSD < 4%), demonstrating that

high quality films can be made incorporating a variety of BCS class II drugs. The presence or absence of SDS was found to have little impact on the content uniformity of the films overall, suggesting that surfactant is unnecessary to produce films with good content uniformity.

Overall, all films exhibited fast dissolution from all five drugs. Specifically, most films achieved 80% dissolution between 18 and 28 min with similar dissolution profiles in both SDS and DI water media irrespective of the drug or surfactant content in the film. This consistency in fast dissolution across a wide solubility range of poorly water-soluble drugs further reinforces the robustness of polymer strip film platform for the delivery of poorly water-soluble drugs while the same consistency between formulations with and without surfactant demonstrates the capability of polymer strip films as a surfactant-free format without sacrificing enhanced dissolution rate or drug content uniformity.

The need for relatively high polymer concentrations in film formulations is a unique and important feature of the film format for its use in bioavailability enhancement of BCS class II drug nanoparticles in contrast to other solid dosages incorporating core-shell or spray-died nanocomposite powders. Additional excess polymer is required to achieve a high film precursor suspension viscosity (~8,000 cP), which led to wrinkle-free, flexible films with excellent content uniformity, effective encapsulation of the drug nanoparticles in the film which helps to preserve the drug nanoparticle size upon redispersion of the films in water, and most importantly, fast drug release. All of this was possible without the need for surfactants, which is a unique and novel aspect of the strip film format as demonstrated in this work.

CHAPTER 3

EFFECT OF PLASTICIZER

3.1 Introduction

Generally speaking, plasticizers are additives that increase the plasticity or fluidity of a material. In strip films, this is typically achieved by introducing a plasticizer in the form of a relatively small molecule that is miscible with the film-forming polymer, allowing for molecular-level interaction between the plasticizer and polymer to moderate polymer–polymer interaction, thereby promoting mobility of the polymer chains (Bruce and McGinity, 2008). This is manifested in a depression of the glass transition temperature, as well as decreased tensile strength and increased elongation in the resulting films (Wypych, 2004). This phenomenon has been reported for a multitude of polymer–plasticizer combinations, but such studies have mainly been limited to drug-free films (Aulton et al., 1981; Bodmeier and Paeratakul, 1994; Entwistle and Rowe, 1979; Gutiérrez-Rocca and McGinity, 1994; Honary and Orafai, 2002; Hutchings et al., 1994; Hyppölä et al., 1996; Lim and Hoag, 2013; Lourdin et al., 1997; McHugh and Krochta, 1994; Sakellariou et al., 1986; Thakhiew et al., 2010). Plasticizers are particularly useful in pharmaceutical films, as most film-forming polymers produce hard or brittle films in the absence of plasticizer, resulting in handling/packaging difficulties and poor patient compliance. This has led to investigations of the impact of plasticizer on various properties of polymer films loaded with water-soluble drug (Gottnek et al., 2013; Pongjanyakul and Puttipipatkhachorn, 2007) and amorphous poorly water-soluble drug (Panda et al., 2014). However, this effect has yet to be investigated for films containing

poorly water-soluble drug particles, let alone the effect of plasticizer or plasticizer content on drug release from such films.

While most literature and commercial applications involving polymer films for drug delivery have focused on orodispersible films for water-soluble drugs (Borges et al., 2015a; Dave et al., 2014; Dixit and Puthli, 2009; Garsuch and Breitkreutz, 2010), the potential for successful delivery of poorly water-soluble drugs via strip films had gone untapped until recently. Use of poorly water-soluble drugs introduces two additional challenges to drug delivery: overcoming limited solubility to improve bioavailability (Kesisoglou et al., 2007) and ensuring that the enhanced bioavailability is preserved upon delivery (de Villiers, 1996; Krull et al., 2015a). The two most commonly used methods to overcome these challenges, organic solvent casting (Kumar et al., 2014; Visser et al., 2015) and hot melt extrusion (Prodduturi et al., 2005), both pose inherent limits to drug loading in the film and may lead to instability of the embedded drug (Kipp, 2004). Several particle engineering techniques have demonstrated promise in terms of producing stable poorly water-soluble drug particles for incorporation into and fast dissolution from polymer strip films with less stringent limitations on drug loading, including production of drug nanoparticles via wet stirred media milling (WSMM) (Krull et al., 2016b; Sievens-Figueroa et al., 2012a; Susarla et al., 2015; Susarla et al., 2013), high pressure homogenization (Lai et al., 2015; Shen et al., 2013), liquid antisolvent precipitation (Beck et al., 2013), and melt emulsification (Bhakay et al., 2016). However, none of these studies investigated the impact of plasticizer on film properties as well as dissolution rate.

This chapter demonstrates that the mechanical properties of polymer strip films loaded with poorly water-soluble drug can be manipulated within a desirable range without sacrificing fast dissolution or nanoparticle redispersibility of the embedded poorly water-soluble drug.

3.2 Experimental Procedures

Experimental procedures for the preparation of polymer films containing GF nanoparticles, film mechanical properties, TGA, and SEM are identical to their respective procedures described in Sub-section 2.2.

3.2.1 Materials

Griseofulvin (GF; Letco Medical, Decatur, AL, USA) was selected as a model BCS class II drug. Hydroxypropyl methylcellulose (HPMC; Methocel E15 Premium LV, The Dow Chemical Company, Midland, MI, USA) served as the film-forming polymer. HPMC-E15LV also served as a nanoparticle stabilizer in suspension, along with the surfactant sodium dodecyl sulfate (SDS; Fisher Scientific, Pittsburgh, PA, USA). Glycerin (Sigma–Aldrich, St. Louis, MO, USA), triacetin (Sigma–Aldrich, St. Louis, MO, USA), and polyethylene glycol (PEG-400; Sigma–Aldrich, St. Louis, MO, USA) were selected as film plasticizers for their miscibility with HPMC and limited volatility. Particle size reduction of GF was performed by WSMM according to Sub-section 3.2.2.1. All other materials were used without further processing.

3.2.2 Preparation Methods

3.2.2.1 Preparation of GF Nanosuspension. GF nanosuspension was prepared via WSMM using a Netzsch mill (Microcer, Fine particle technology LLC, Exton, PA,

USA). Methods and stabilizer concentrations were selected according to previous optimization studies (Bilgili and Afolabi, 2012; Monteiro et al., 2013). The suspension consisted of 10% GF (w/w wrt water) dispersed in a stabilizer solution of 2.5% HPMC-E15LV and 0.5% SDS (both w/w wrt water), and was milled for 120 min.

3.2.2.2 Preparation of Film Precursor Suspensions. Formulations for film-forming polymer solutions are listed in Table 3.1. As per Dow® protocol, polymer solutions were prepared by adding the appropriate amounts of HPMC-E15LV and plasticizer (as necessary) to water at 90 ºC, after which the solution was allowed to cool to room temperature under continuous magnetic stirring. Polymer concentrations were selected such that the polymer solutions were sufficiently viscous to ensure a uniform film (Susarla et al., 2013) while not too viscous to hinder mixing or casting. Polymer solutions consisted of 15 wt% HPMC with different plasticizers (glycerin, triacetin, and PEG-400) and plasticizer content (0.0, 2.5, and 5.0 wt%). Plasticizer concentrations were kept at or below 5.0 wt% in order to avoid over-plasticization of the films, which can result in oily films that are difficult to handle. Each of the resulting polymer solutions was mixed with GF nanosuspension in a 2:1 ratio by mass using a Thinky ARE-310 planetary centrifugal mixer (Thinky, Laguna Hills, CA, USA). Polymer solution and nanosuspension were mixed at 2000 rpm for 30 s, followed by 7 min of deaeration at 2200 rpm, to form film precursor suspension. If bubbles were still present in the precursor suspension after mixing, the precursor was left overnight to settle before casting.

Table 3.1 Film-Forming Polymer Solution Formulations Prior to Mixing with GF Nanosuspension

Formulation	Plasticizer	wt% HPMC	wt% plasticizer	wt% water
0.0% Plasticizer	N/A	15.0	0.0	85.0
2.5% Glycerin	Glycerin	15.0	2.5	82.5
5.0% Glycerin	Glycerin	15.0	5.0	80.0
2.5% Triacetin	Triacetin	15.0	2.5	82.5
5.0% Triacetin	Triacetin	15.0	5.0	80.0
2.5% PEG	PEG	15.0	2.5	82.5
5.0% PEG	PEG	15.0	5.0	80.0

3.2.3 Characterization Methods

3.2.3.1 Viscosity of Polymer Solutions and Film Precursor Suspensions. The apparent shear viscosity of polymer solutions and film precursor suspensions was measured with an R/S-CC+ Coaxial Cylinder Rheometer (Brookfield Engineering, Middleboro, MA, USA) equipped with a shear rate controlled coaxial cylinder (CC25) and Lauda Eco water jacket assembly (Lauda-Brinkmann LP, Delran, NJ, USA) for temperature control. Both were subjected to a low shear rate program (0-20 s^{-1}) at 25 ± 0.5 ºC to measure low shear viscosity. Raw data was analyzed using Rheo 3000 software (Brookfield Engineering, Middleboro MA, USA). Experiments were performed a minimum of seven times.

3.2.3.2 GF Particle Size after Milling and Redispersed from Films. GF particle size distributions were measured both in suspension immediately after milling and following redispersion from films utilizing a Coulter LS 13320 Laser Diffraction Particle Size Analyzer (Beckman Coulter, Miami, FL, USA) employing a polarized intensity differential scattering (PIDS) obscuration water optical model. The PIDS was maintained between 40-50% and obscuration was maintained below 8%. Mie scattering theory was

used to calculate particle size distributions. Suspension samples for particle size after milling were prepared by removing a 1.2 ml sample from the holding tank of the mill, dispersing the sample into 4 ml of stabilizer solution (2.5% HPMC-E15LV and 0.5% SDS, both w/w wrt water) via pipette, and vortex mixing for 1 min at 1500 rpm.

In order to evaluate the ability to recover GF nanoparticles from films upon delivery, redispersion samples to determine GF particle size after incorporation into dry films were prepared by dispersing three circular film punches ~0.7 cm^2 in area into 3 ml of deionized water, followed by 3-5 min of vortex mixing at 1500 rpm. These samples were then subjected to the same particle size analysis as the milled suspension samples.

3.2.3.3 Differential Scanning Calorimetry (DSC). A Polymer DSC (Mettler Toledo, Columbus, OH, USA) was used for differential scanning calorimetry. 5-6 mg samples were placed in sealed aluminum pans, initially cooled to -50 ºC at a rate of -10 ºC/min, heated to 250 ºC at 10 ºC/min, cooled to -50 ºC at -10 ºC/min, and again heated to 250 ºC at 10 ºC/min, all under nitrogen flow.

3.2.3.4 Determination of Drug Content and Uniformity in Films. Ten circular samples ~0.7 cm^2 in area were removed from random points throughout each film and dissolved in 250 ml of 5.4 mg/ml SDS solution under continuous stirring for a minimum of 3 h. Despite being roughly $1/10^{th}$ the size of a traditional film dosage, this smaller size was used to help elucidate differences in uniformity between film formulations. The UV absorbance of each sample at the wavelength of maximum absorbance for GF (291 nm) was then measured using a Thermo Scientific Evolution 300 UV-Vis spectrophotometer (Thermo Fisher Scientific Inc., MA, USA). The concentrations of the respective samples were calculated via calibration curve. Content uniformity results are expressed as average

GF weight per unit area of film and average weight percentage of GF in the film over ten samples.

3.2.3.5 Flow-through Cell Dissolution (USP IV). Dissolution experiments were performed using a flow-through cell dissolution apparatus (USP IV; Sotax, Switzerland) with cells of 22.6 mm internal diameter and 0.2 µm Pall HT Tuffryn filters. Dissolution samples were automatically measured in-line every two minutes by the same Thermo Scientific Evolution 300 UV-Vis spectrophotometer (Thermo Fisher Scientific Inc., MA, USA) used for determination of drug content and uniformity in films (Sub-section 3.2.3.4). One circular film sample ~0.7 cm^2 in area was horizontally secured within 5 g of 1 mm glass beads at the bottom of each cell (3 g below the film and 2 g above). 100 ml of 5.4 mg/ml SDS solution (recommended for GF by the United States Pharmacopeia) was circulated through each cell at a flow rate of 16 ml/min and a constant temperature of 37 ± 0.5 ºC. These dissolution protocols were selected for their discriminatory power demonstrated in previous work between films containing nanoparticles, films containing microparticles, and compacted powders (Beck et al., 2013; Bhakay et al., 2016; Sievens-Figueroa et al., 2012b). Dissolution results are reported as GF release as a function of time for an average of six samples from each film. Percentage GF released was calculated based on the expected drug loading in each sample from the drug content assessment performed for each film formulation (Sub-section 3.2.3.4), taking into consideration the weight of each individual film sample.

3.2.3.6 Long-Term Stability of Films. Films designated for long-term stability study were stored in a MicroClimate benchtop climate chamber (Cincinnati Sub-Zero, Cincinnati, OH, USA) at 40 ºC and 75% relative humidity (RH). Following 3 and

6 months of storage under these conditions, films were subjected to redispersion and dissolution tests as outlined in Sub-sections 3.2.3.2 and 3.2.3.5, respectively.

3.2.3.7 Statistical Analysis. All calculations were performed using Microsoft Excel® (Microsoft Office 2010, USA). Results for viscosity, mechanical properties, and dissolution profiles are expressed as mean ± SD (standard deviation) while content uniformity results are expressed as mean with RSD % (relative standard deviation). Dissolution profiles were compared using similarity and difference factors (Boateng et al., 2012; Costa and Lobo, 2001).

3.3 Results and Discussion

3.3.1 Viscosity of Polymer Solutions and Precursor Suspensions

Low shear (2.2 s^{-1}) viscosity measurements for polymer solutions and film precursor suspensions, performed with the objective of mimicking conditions of film casting, are presented in Figure 3.1. The viscosities of the polymer solutions ranged from 9,500-14,000 cP. Upon dilution with aqueous GF nanosuspension that contained about 88.5 wt% water, the viscosities of the film precursor suspensions ranged from 5,000-7,000 cP. Polymer solutions with 5.0% plasticizer exhibited greater viscosities than those with 2.5% plasticizer for all three plasticizers, which may be explained by the fact that the added plasticizers were of greater viscosity (1,400 cP for glycerin, 23 cP for triacetin, and 60 cP for PEG-400) than the water they displaced from the formulation (Table 3.1). These trends were also observed in the film precursor suspensions, although not as prominently due to dilution with GF nanosuspension. However, there was a clear decline in polymer solution viscosity upon inclusion of glycerin and triacetin relative to

the plasticizer-free polymer solution. This may be the result of easier slippage of polymer chains under shearing due to the initial incorporation of plasticizer, which effectively reduced the extent of polymer–polymer interaction and, consequently, polymer solution viscosity.

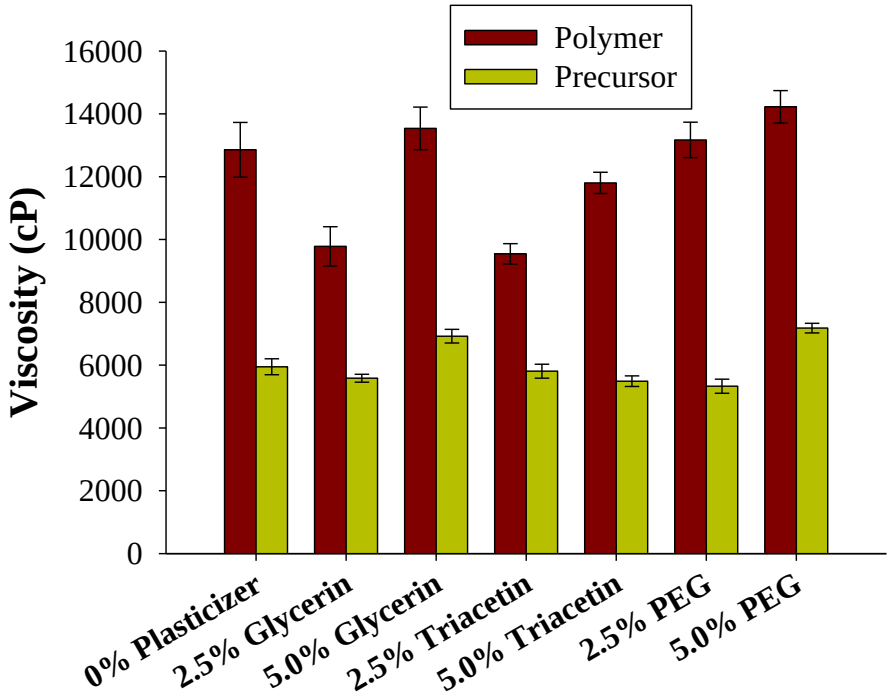

Figure 3.1 Low shear (2.2 s^{-1}) room temperature viscosity of polymer solutions and film precursor suspensions. Values are mean ± SD, n = 7.

3.3.2 GF Particle Size after Milling and Redispersed from Films

Since the purpose of nanomilling poorly water-soluble drug particles is to enhance their dissolution rate and bioavailability, it is crucial that the drug nanoparticles embedded in the polymer matrix do not aggregate prior to or upon delivery. Redispersion testing provides a means by which the size of the poorly water-soluble drug particles released upon delivery can be assessed. As has been shown previously for solid dosage forms containing poorly water-soluble drug nanoparticles (Bhakay et al., 2014b; Bhakay et al.,

2013; Krull et al., 2016b), redispersion offers predictive insight into dissolution, as drug nanoparticle aggregation or growth can lead to slower drug release. In order to investigate the effect of different plasticizers on the ability of the film format to physically stabilize the GF particles, redispersion tests were performed on all films on the day of preparation, as well as after 3 and 6 months of storage under stress conditions (40 ºC, 75% RH) to assess long-term stability (stability results discussed in Sub-section 3.3.3.7). Particle size statistics for the milled GF nanosuspension and GF particles redispersed from films in deionized water after 0, 3, and 6 months of storage are given in Table 3.2 as 10%, 50% (median), and 90% passing size (d_{10}, d_{50}, and d_{90}, respectively).

Table 3.2 Particle Size Distributions of Fresh GF Nanosuspension and Redispersed Film Samples Immediately after Film Preparation, after 3 Months of Storage at 40 ºC, 75% RH, and after 6 Months of Storage at 40 ºC, 75% RH

		d_{10} (µm)	
Formulation	Fresh	3 months	6 months
Suspension	0.099	--	--
0.0% Plasticizer	0.104	0.095	0.115
2.5% Glycerin	0.089	0.098	0.114
5.0% Glycerin	0.092	0.091	0.113
2.5% Triacetin	0.106	0.100	0.114
5.0% Triacetin	0.173	0.064	0.180
2.5% PEG	0.073	0.069	0.113
5.0% PEG	0.093	0.094	0.061
		d_{50} (µm)	
Formulation	Fresh	3 months	6 months
Suspension	0.159	--	--
0.0% Plasticizer	0.231	0.172	0.179
2.5% Glycerin	0.170	0.171	0.185
5.0% Glycerin	0.166	0.166	0.190
2.5% Triacetin	0.241	0.228	0.237
5.0% Triacetin	0.321	0.250	0.301
2.5% PEG	0.169	0.161	0.191
5.0% PEG	0.171	0.212	0.169
		d_{90} (µm)	
Formulation	Fresh	3 months	6 months
Suspension	0.262	--	--
0.0% Plasticizer	0.509	0.309	0.296
2.5% Glycerin	0.317	0.301	0.310
5.0% Glycerin	0.305	0.306	0.328
2.5% Triacetin	0.422	0.404	0.410
5.0% Triacetin	0.556	0.476	0.518
2.5% PEG	0.345	0.343	0.334
5.0% PEG	0.318	0.390	0.364

GF particle redispersion from fresh glycerin and PEG-400 films yielded d_{10} values less than that of the milled suspension and d_{50} values between 160-170 nm, on par with that of the milled suspension, both indicating very good physical stability in the film. While the d_{90} values of the same films were between 300-350 nm compared to

262 nm in the suspension, such differences were expected, as the d_{90} is significantly more sensitive to aggregation. On the other hand, slightly larger nanoparticles were redispersed from fresh triacetin films (d_{50} of 241 nm and 321 nm for 2.5% and 5.0% triacetin, respectively) and the plasticizer-free film (d_{50} of 231 nm) compared to those from glycerin and PEG-400 films (d_{50} between 160-170 nm), which increased in size with increasing triacetin content. That said, even in the 5.0% PEG film, the d_{90} value was only 556 nm, and 100% of all particles were < 1 μm in size (full size distribution not shown). As such, these differences in nanoparticle size are not expected to negatively affect drug dissolution rate from films under sink conditions (Krull et al., 2016b; Murdande et al., 2015).

3.3.3 Film Characterization

3.3.3.1 Differential Scanning Calorimetry (DSC). One of the defining features of a plasticizer is its ability to depress the glass transition temperature (T_g) of a polymer due to their molecular-level interaction (Bruce and McGinity, 2008; Wypych, 2004). To this end, DSC was employed to observe the influence of plasticizer and plasticizer concentration on the T_g of HPMC films loaded with poorly water-soluble drug nanoparticles. However, the DSC signal in HPMC films is very weak (Gómez-Carracedo et al., 2003; Kararli et al., 1990), often making it difficult to observe the glass transition. As such, the first heating cycle was used to determine the T_g for each film.

The impact of plasticizer and plasticizer concentration on the T_g of GF nanoparticle-laden films can be seen in Figure 3.2. These T_g values are in line with those observed in literature, which range between 150-200 ºC depending on the grade of HPMC and method of characterization (Gómez-Carracedo et al., 2003; McPhillips et al.,

1999; Nyamweya and Hoag, 2000). Increasing concentration of all three plasticizers led to a clear reduction in T_g, a trend which has been observed for multiple polymer–plasticizer combinations (Hyppölä et al., 1996; Lin et al., 2000; Ljungberg and Wesslén, 2002, 2003; Pillin et al., 2006; Qussi and Suess, 2006). In spite of the presence of GF nanoparticles (15-20 wt%, Sub-section 3.2.3.4), addition of plasticizer shows a clear impact on the T_g of the films. This suggests that poorly water-soluble drug nanoparticles can be incorporated into polymer films without interfering with the ability of plasticizers to interact with the film-forming polymer. PEG-400 led to the greatest depression of T_g per wt% plasticizer, followed by glycerin and triacetin.

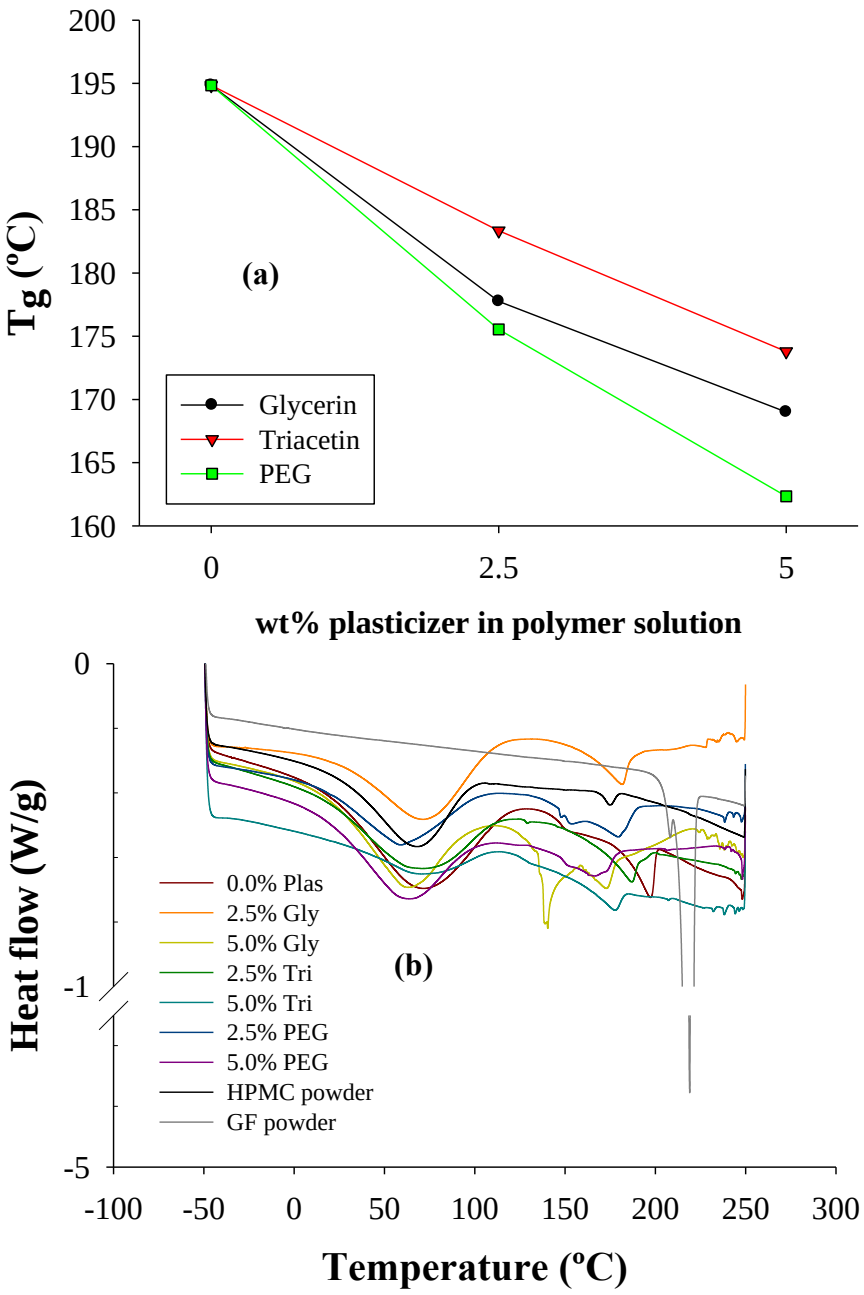

Figure 3.2 (a) T_g and (b) full DSC traces of GF nanoparticle-laden HPMC films containing various amounts of plasticizer.

3.3.3.2 Film Mechanical Properties. The role of plasticizers in influencing the mechanical properties of drug-free polymer films has been thoroughly investigated in literature (Aulton et al., 1981; Bodmeier and Paeratakul, 1994; Entwistle and Rowe,

1979; Gutiérrez-Rocca and McGinity, 1994; Hutchings et al., 1994; Hyppölä et al., 1996; Lim and Hoag, 2013; McHugh and Krochta, 1994). The same has also been investigated for drug-loaded films produced via hot melt extrusion (Repka et al., 1999; Zhu et al., 2006) and solvent casting (Kianfar et al., 2011; Pongjanyakul and Puttipipatkhachorn, 2007). The consensus is that addition of plasticizer to a polymer film formulation leads to a decrease in film strength and an increase in elasticity. However, it is unknown to what extent the influence of plasticizers applies to strip films loaded with poorly water-soluble drug nanoparticles in terms of film mechanical properties.

Figure 3.3 depicts the influence of glycerin, triacetin, and PEG-400 on the mechanical properties of HPMC films loaded with GF nanoparticles. Films with increasing plasticizer content all exhibited decreases in TS, YS, and YM, regardless of which plasticizer was used, suggesting that HPMC films containing poorly water-soluble drug nanoparticles can be effectively plasticized with a variety of plasticizers. Likewise, a general increasing trend in EB was observed with increasing plasticizer content in glycerin and PEG-400 films, although there was no such increase in EB for triacetin films, which has been previously reported in ethylcellulose films (Hyppölä et al., 1996). The order of extent of plasticization according to YS and YM was PEG > glycerin > triacetin, which was in line with the trend in T_g depression observed via DSC (Sub-section 3.3.3.1). This further supports that the presence of poorly water-soluble drug nanoparticles does not interfere with the ability of plasticizers to predictably influence polymer film mechanical properties. The general similarity between trends exhibited in most mechanical properties with increasing plasticizer content for glycerin, triacetin, and

PEG-400 implies that all three plasticizers were similarly effective for HPMC films with embedded drug nanoparticles.

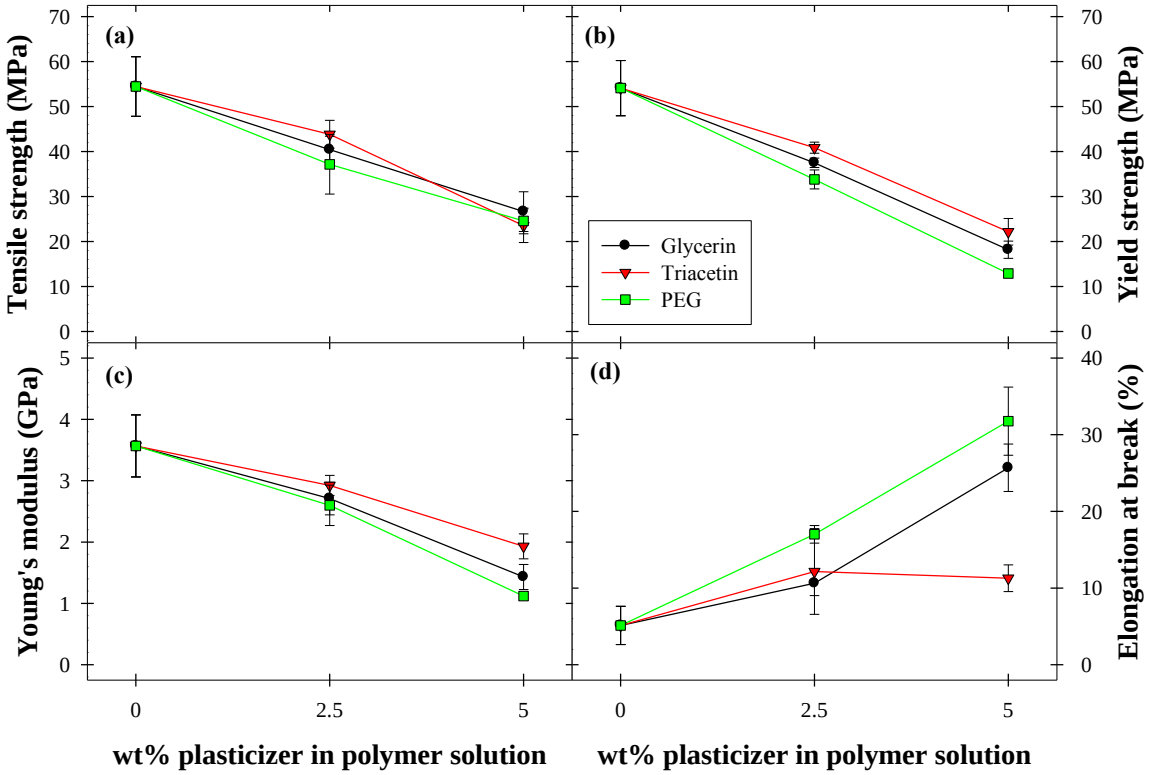

Figure 3.3 (a) Tensile strength, (b) yield strength, (c) Young's modulus, and (d) percent elongation at break of HPMC films with different plasticizers and content containing GF nanoparticles. Values are mean ± SD, n = 4.

3.3.3.3 GF Content and Uniformity in Films. Consistency of drug dosage is critical in any pharmaceutical process. In order to assess the drug content of each film sample and ensure even distribution of drug throughout each film, content uniformity tests were performed for all film formulations. As seen in Table 3.3, all films exhibited 6% RSD or less in terms of film thickness and GF mass variation, despite the fact that the size of each sample was roughly one tenth the size of a typical film dosage (while smaller sample sizes were selected to provide better discrimination between formulations in terms of content uniformity, it is expected that equivalent RSD values for 6 cm^2 samples

would be roughly 1.0-1.5%; results not shown). In addition, triacetin, PEG-400, and plasticizer-free films exhibited 2% RSD or less in terms of wt% GF, while glycerin films had 4% RSD or less. These results suggest that uniform films with embedded drug nanoparticles can be produced with a variety of plasticizers and plasticizer concentrations within the range studied. Film thickness generally increased with increasing plasticizer content due to the fact that addition of plasticizer displaced water from the film precursor formulation (Table 3.1), resulting in less moisture loss, and consequently less thickness reduction during the drying process. The same reasoning applies to the decreasing trend in wt% GF in films with greater plasticizer content, since the residual mass after drying increased with increasing plasticizer content due to less moisture loss.

Table 3.3 Content Uniformity of HPMC Films with Different Plasticizers and Content. Values are an Average of 10 samples ~0.7 cm^2 in Area

Formulation	Thickness (μm)	RSD (%)	GF mass per unit area (mg/cm^2)	RSD (%)	wt% GF	RSD (%)
0.0% Plasticizer	86.9	3.9%	2.48	4.2%	20.9	2.3%
2.5% Glycerin	97.1	4.8%	2.57	5.8%	18.2	3.5%
5.0% Glycerin	108.0	2.9%	2.16	5.5%	15.3	4.2%
2.5% Triacetin	84.4	4.4%	2.05	5.4%	18.7	1.0%
5.0% Triacetin	86.6	6.5%	1.99	5.9%	16.4	2.3%
2.5% PEG	72.2	2.5%	1.68	1.9%	16.6	2.2%
5.0% PEG	91.1	3.4%	1.99	3.2%	15.4	2.2%

3.3.3.4 Dissolution. Dissolution curves for all seven fresh films are presented in Figure 3.4. By visual inspection of the dissolution curves, it is clear that, with the exception of variation in maximum percentage of GF released, there is little difference in dissolution rate between the seven film formulations despite their differences in plasticizer content and, consequently, mechanical properties. This is further supported by

pairwise comparison of the dissolution curves using similarity and difference factors (Boateng et al., 2012; Costa and Lobo, 2001), according to which the only two films that exhibited statistically significant differences in dissolution rate relative to the other five formulations were 2.5% triacetin and 2.5% PEG (Appendix A.1). This result demonstrates that the mechanical properties of polymer films loaded with poorly water-soluble drug nanoparticles can be successfully manipulated by multiple plasticizers with no significant impact on the rate of drug release from the film.

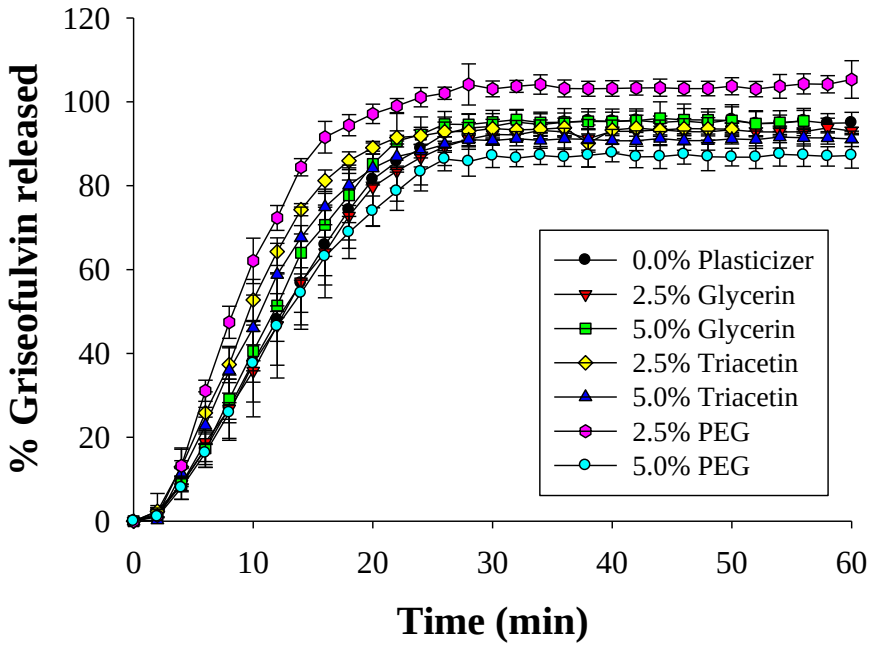

Figure 3.4 Comparison of dissolution profiles between HPMC films loaded with GF nanoparticles containing different plasticizers and plasticizer content. Values are mean ± SD, n = 6.

While investigation of the impact of various CMAs on dissolution of poorly water-soluble drugs from polymer films is ongoing, previous work suggests that, with adequate dispersion and stabilization of drug nanoparticles within the film, the major controlling factor in determining drug release rate is the polymer matrix. Regarding particle size, Sievens-Figueroa et al. (2012b) observed faster dissolution rates for GF

nanoparticles as opposed to microparticles from HPMC films under the same dissolution conditions used in this study, while Krull et al. (2016b) observed the same from pullulan films in deionized water. Both of these studies reiterate the criticality of preserving poorly water-soluble drug particle size in order to maintain enhanced bioavailability upon delivery. Since GF particle size was maintained for all seven formulations in this study (Section 3.3.2), this was not expected to be a source of difference in film dissolution rate. Given proper control of drug particle size, others have demonstrated the impact of other CMAs on poorly water-soluble drug dissolution from films, such as added disintegrants (Susarla et al., 2015) and the drug itself in Chapter 2, due to their influence on polymer erosion (additional CMAs, including film-forming polymer molecular weight (MW) and drug loading, will be the subjects of future work). However, given the hydrophilic and swellable nature of HPMC, the type and amount of plasticizer added did not appear to have a significant influence on the erosion rate of HPMC, resulting in similar dissolution profiles for all films.

While one might have anticipated a direct connection between film mechanical strength and dissolution, this relationship is not a simple one. On the one hand, previous work has shown that films with greater mechanical strength may exhibit slower drug release. Prodduturi et al. (2005) observed slower dissolution for films with greater mechanical strength when varying film-forming polymer MW for hot-melt extruded poly(ethylene oxide) films containing clotrimazole. A similar correlation was found in Chapter 2 where incorporation of different drug nanoparticles into HPMC films led to films of varying mechanical strength, which coincided with their respective differences in dissolution rate. On the other hand, other work, including this study, has suggested that

film mechanical strength does not necessarily affect drug release. Pongjanyakul and Puttipipatkhachorn (2007) observed similar drug permeation rates between acetaminophen tablets coated by sodium-alginate-magnesium aluminum silicate films with varying amounts of glycerin and PEG-400, despite significant differences in the mechanical properties of the film coatings. Lin et al. (1995) noted little difference in permeation profiles of piroxicam from Eudragit E films with varying mechanical properties due to incorporation of four different plasticizers. Krull et al. (2016b) observed similar dissolution rates from GF nanoparticle-laden films of various drug loadings despite significant differences in their mechanical properties. Nonetheless, plasticizer has been shown to be a unique tuning parameter for film mechanical properties that does not appear to impact drug release, unlike film-forming polymer properties, such as MW, which have been shown to affect both. These results suggest that the relationship between film mechanical properties and dissolution is more complex than it first appears, and further investigation is required to elucidate a possible connection.

3.3.3.5 Thermogravimetric Analysis (TGA). TGA was performed on all film formulations and normalized to account for slight variations in GF and SDS content between films according to Susarla et al. (2013) (Figure 3.5). All films exhibited a weight loss between 1.5% and 4.5% up to 100 ºC, which can be attributed to the loss of water within the film. 15 min exposure to 150 ºC resulted in varying degrees of wt% drops between films depending on which and how much plasticizer each film contained, suggesting that this drop, or lack thereof, was due to the presence or absence of plasticizer in the film formulation. Consequently, the plasticizer-free film exhibited a negligible drop in wt% during this time. The extent of weight loss up to 250 ºC between

the three plasticizers was glycerin > triacetin > PEG-400, and films with higher plasticizer concentration experienced greater drops in wt% due to the loss of additional plasticizer.

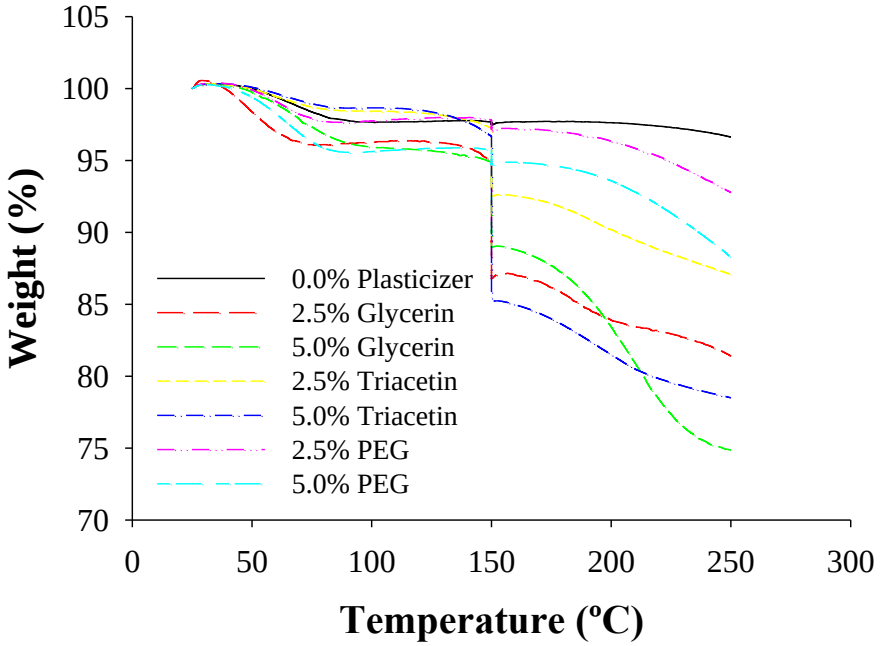

Figure 3.5 Normalized TGA curves for HPMC films with different plasticizers and plasticizer content loaded with griseofulvin nanoparticles.

3.3.3.6 Scanning Electron Microscopy (SEM). Cross-sectional SEM images of all seven film formulations were taken in order to qualitatively assess the size and morphology of the embedded API particles (Figure 3.6). As can be clearly seen in all seven images, the GF nanoparticles were finely dispersed throughout the films with no visible signs of aggregation. This reinforces the assessment of the redispersion results in Sub-section 3.2.3.2 that the polymer matrix is able to physically stabilize the embedded GF nanoparticles regardless of the plasticizer or plasticizer content under investigation.

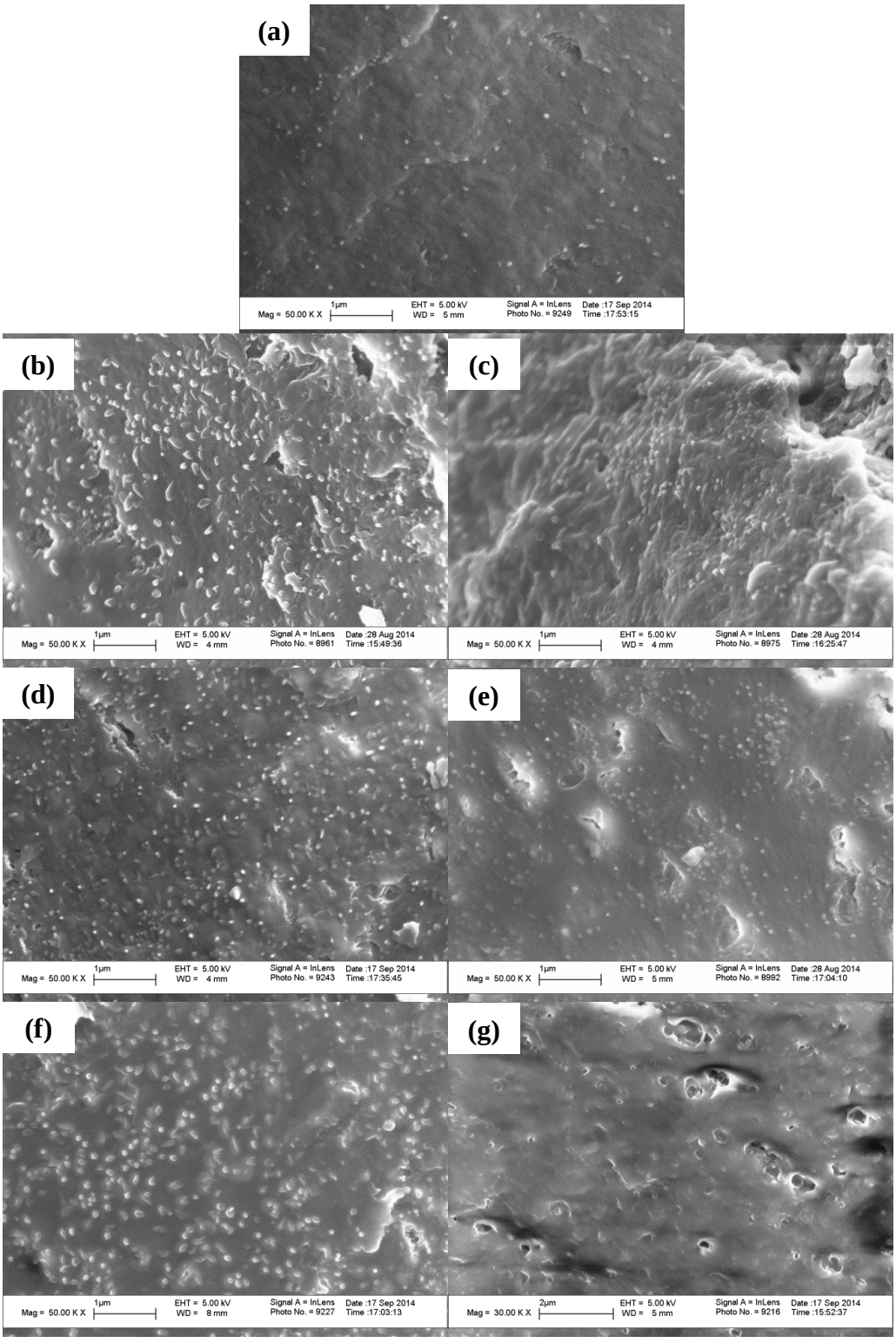

Figure 3.6 Cross sectional SEM images of HPMC films loaded with griseofulvin nanoparticles made from polymer solutions containing (a) no plasticizer, (b) 2.5% glycerin, (c) 5.0% glycerin, (d) 2.5% triacetin, (e) 5.0% triacetin, (f) 2.5% PEG, and (g) 5.0% PEG. Scale bars are 1 µm for (a-f) and 2 µm for (g).

3.3.3.7 Long-term Stability of Films. In order to evaluate the ability of the film format to preserve drug nanoparticle size and enhanced dissolution over an extended period of time, redispersion and dissolution tests were performed for all formulations over the course of 6 months' storage at 40 ºC and 75% RH. First, the long-term physical stability of the GF nanoparticles embedded within the polymer matrix was assessed via redispersion (Table 3.2). While there was some variation in the d_{10}, d_{50}, and d_{90} values of redispersed GF particles between formulations, little variation was observed within any of the seven film formulations during this time. This suggests that long-term stability of poorly water-soluble drug nanoparticles is indeed achievable in polymer strip films containing various plasticizers and plasticizer content.

In order to investigate the impact of long-term storage on the dissolution rate of the films, Figure 3.7 shows dissolution curves for all seven film formulations after 0, 3, and 6 months of storage at 40 ºC and 75% RH. While some films exhibited variation in maximum percentage of GF released before and after storage, little statistical difference in dissolution rate was observed for most of the seven film formulations (Appendix A.1). This suggests that polymer films are capable of successfully stabilizing and releasing poorly water-soluble drug nanoparticles at a consistent rate, even after long-term storage.

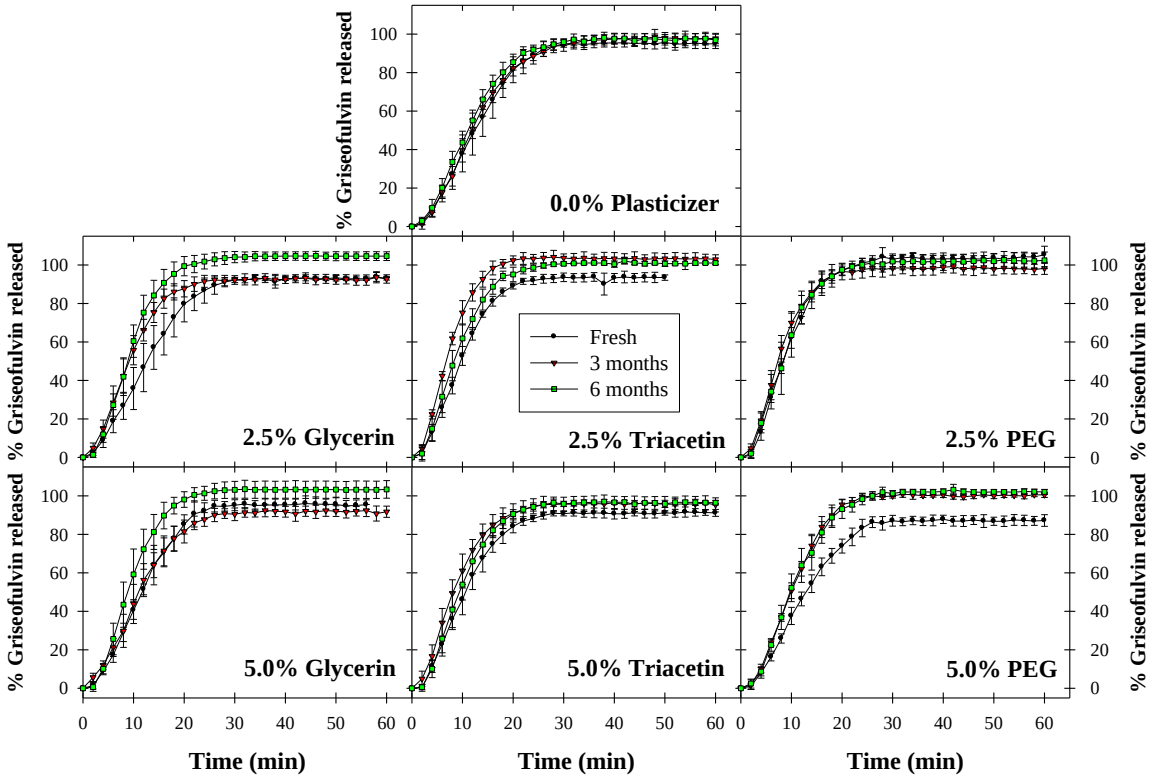

Figure 3.7 Comparison of dissolution profiles for all films immediately after film preparation, after 3 months of storage at 40 ºC, 75% RH, and after 6 months of storage at 40 ºC, 75% RH. Values are mean ± SD, n = 6.

3.4 Conclusions

The objective of this work was to investigate the impact of plasticizer and plasticizer concentration on various properties of strip films loaded with poorly water-soluble drug (GF) nanoparticles. Addition of any of the three plasticizers under investigation (glycerin, triacetin, and PEG-400) led to a depression of film glass transition temperature, a decrease in film tensile strength, and an increase in film elongation at break. However, in spite of these clear differences, there was little difference between the dissolution rates of the films, perhaps due to the robustness with which the drug nanoparticles were stabilized and dispersed. This suggests that film mechanical properties may be successfully manipulated by adjusting the amount of plasticizer used without impacting the rate of

drug release from the films. The similarity between dissolution rates of different films was observed even after the films were stored under stress conditions for six months, demonstrating that the consistency of drug release between formulations is preserved after long-term storage. In addition, the redispersibility of the embedded GF nanoparticles was also preserved after six months' storage, demonstrating the long-term stability of the films. This consistency between films with different plasticizers and plasticizer concentrations will allow formulators the freedom to adjust the strength and elasticity of films containing poorly water-soluble drug without negatively impacting drug release or other film properties.

CHAPTER 4

EFFECT OF FILM-FORMING POLYMER MOLECULAR WEIGHT

4.1 Introduction

One of the greatest strengths of the strip film format is its inherent versatility as a drug delivery platform. With excipients including the film-forming polymer, plasticizing agent, and various other additives, there is a wide array of formulation options available in strip film development, even for poorly water-soluble drugs. Exploration of this flexibility is made even more enticing by the relative simplicity of the film manufacture process as compared to the manufacture of more traditional solid dosage forms (Hoffmann et al., 2011), which has been the subject of recent literature. For instance, some have manipulated the mechanical properties of films containing poorly water-soluble drug in both the amorphous (Panda et al., 2014) and crystalline states in Chapter 3 by adjusting plasticizer and plasticizer concentration while attempting to preserve the enhanced dissolution rate of the drug. Others have investigated the use of viscosity-enhancing agents, such as natural gums or superdisintegrants, for modulation of drug nanoparticle release from films (Krull et al., 2016b; Susarla et al., 2015), although both observed differences in film mechanical properties as well. However, to the best of the authors' knowledge, a simple means of manipulating poorly water-soluble drug release from strip films without significantly affecting film mechanical properties has yet to be demonstrated.

One particularly useful property of polymers as film-forming agents is the variety of molecular weights (MWs) available for a given polymer. Varying polymer MW has been used in several dosage forms as a means of controlling drug release. Ramkissoon-

Ganorkar et al. (1999) observed slower insulin release from higher MW N-isopropylacrylamide/butyl methacrylate/acrylic acid polymeric beads, noting a shift in controlling release mechanism from polymer erosion to drug diffusion. Mittal et al. (2007) observed a similar shift in controlling release mechanism from estradiol-loaded poly(lactic-co-glycolic acid) (PLGA) nanoparticles with increasing PLGA MW. Rowe (1986) observed slower release of a propanolamine derivative from coated granules of ethylcellulose–hydroxypropyl methylcellulose (EC–HPMC) with higher MW EC, presumably due to cracks and flaws in the lower MW film coatings. Omelczuk and McGinity (1992) observed slower theophylline release from tablets made using higher MW grades of PLA up to ~138 kDa, above which no differences in drug release rate were observed. Marucci et al. (2013) observed slower release of metoprolol from pellets coated with hydroxypropyl cellulose–ethylcellulose (HPC–EC) using higher MW EC due to slower HPC leaching and, consequently, slower drug diffusion. Prodduturi et al. (2005) observed slower release of amorphous clotrimazole from higher MW poly(ethylene oxide) films produced via hot melt extrusion. Huang et al. (2013) observed slower water absorption and drug release from higher MW PLGA films loaded with amorphous paclitaxel. However, none of these studies investigated films containing poorly water-soluble drug particles. In addition, existing literature suggests that film-forming polymer MW has a significant effect on film mechanical properties when the concentration of film-forming polymer is held constant (Huang et al., 2013; Lazaridou et al., 2003; Park et al., 1993). A simple means of manipulating drug release rate without significantly affecting film mechanical properties has yet to be demonstrated for drug particle-laden films.

This chapter demonstrates that the release rate of poorly water-soluble drug nanoparticles from polymer films can be manipulated with minimal impact on film mechanical properties or nanoparticle redispersibility.

4.2 Experimental Procedures

Experimental procedures for the preparation of polymer films containing GF nanoparticles, film mechanical properties, TGA, and SEM are identical to their respective procedures described in Section 2.2. Experimental procedures for viscosity, GF particle size after milling and redispersed from films, determination of drug content and uniformity in films, and flow-through cell dissolution (USP IV) are identical to their respective procedures described in Section 3.2.

4.2.1 Materials

Griseofulvin (GF; Letco Medical, Decatur, AL) was selected as a model Biopharmaceutics Classification System (BCS) class II drug. Three different viscosity grades of hydroxypropyl methylcellulose (HPMC; Methocel E15 Premium LV, MW ~14 kDa; E50 Premium LV, MW ~21 kDa; E4M Premium, MW ~88 kDa; The Dow Chemical Company, Midland, MI) served as film-formers. E50 and E4M samples were generously donated by The Dow Chemical Company. HPMC-E15LV also served as a nanoparticle stabilizer during WSMM, along with the surfactant sodium dodecyl sulfate (SDS; Fisher Scientific, Pittsburgh, PA). Glycerin (Sigma–Aldrich, St. Louis, MO) was used as a film plasticizer. GF particle size reduction was performed by WSMM according to Sub-section 4.2.2.1. All other materials were used without further processing.

4.2.2 Preparation Methods

4.2.2.1 Preparation of GF Nanosuspension. GF nanosuspension was prepared via WSMM using a Netzsch mill (Microcer, Fine Particle Technology LLC, Exton, PA). Methods and stabilizer concentrations were selected according to previous optimization studies (Bilgili and Afolabi, 2012; Monteiro et al., 2013). The suspension consisted of 10% GF dispersed in a stabilizer solution of 2.5% HPMC-E15LV and 0.5% SDS (all w/w wrt water), and was milled for 120 min. A single GF nanosuspension formulation was used across all film formulations, as opposed to using different polymer MWs for each film formulation, to ensure consistency in the size and morphology of the milled GF particles (for a thorough investigation of the effect of polymer MW in WSMM, readers are referred to Li et al. (2016)). This meant that the HPMC-E15LV stabilizer, which adsorbed onto the surface of the GF nanoparticles during milling, was present in all film precursors, including those that used E50 and E4M as film-formers. The resulting mass ratios of film-forming polymer to HPMC-E15LV stabilizer were ~9.9 for E50 film precursor formulations and ~3.5 for E4M film precursor formulations.

4.2.2.2 Preparation of Film Precursor Suspension. As per Dow® protocol, polymer solutions were prepared by adding the appropriate amounts of HPMC and glycerin to water at 90 ºC, after which the solution was allowed to cool to room temperature under continuous magnetic stirring. Polymer concentrations were selected such that the polymer solutions were sufficiently viscous to ensure a uniform film while not too viscous to hinder mixing or casting. In order to account for this, as well as to minimize the effect of viscosity variation on film properties seen in previous work (Susarla et al., 2015; Susarla et al., 2013), a “viscosity matching” technique was

employed in which three target viscosity ranges were identified for study across all three HPMC grades: 9,000-10,000 cP ("Low"), 11,000-13,000 cP ("Med"), and 19,000-25,000 cP ("High"). This required careful selection of polymer concentrations in the polymer solution formulations by decreasing polymer concentration with increasing polymer MW, as seen in Table 4.1. The ratio of polymer-to-plasticizer was maintained within each trio of viscosity ranges, although this ratio had to be slightly increased with increasing viscosity to prevent over-plasticization in E4M films (3.0, 3.4, and 3.8, respectively). Each of the resulting polymer solutions was mixed with GF nanosuspension in a 2:1 ratio by mass using a Thinky ARE-310 planetary centrifugal mixer (Thinky, Laguna Hills, CA). Polymer solution and nanosuspension were mixed at 2,000 rpm for 30 s, followed by 7 min of deaeration at 2,200 rpm, to form film precursor suspension. If bubbles were still present in the precursor suspension after mixing, the precursor was left overnight to settle before casting.

Table 4.1 Composition of HPMC Polymer Solution Formulations and Low Shear (2.2 s^{-1}) Room Temperature Viscosity of Polymer Solutions and Film Precursor Suspensions. Viscosities are Mean ± SD, n = 7

Formulation	HPMC grade	wt% HPMC	wt% glycerin	wt% water	Polymer solution viscosity (cP)	Film precursor suspension viscosity (cP)
E15-Low	E15	15.0	5.0	80.0	9,030 ± 190	7,120 ± 350
E15-Med	E15	17.0	5.0	78.0	11,190 ± 350	8,060 ± 1,960
E15-High	E15	19.0	5.0	76.0	N/M	10,250 ± 1,860
E50-Low	E50	9.6	3.2	87.2	9,570 ± 430	7,730 ± 200
E50-Med	E50	10.9	3.2	85.9	12,820 ± 370	10,240 ± 320
E50-High	E50	12.1	3.2	84.7	24,250 ± 830	9,070 ± 350
E4M-Low	E4M	3.3	1.1	95.6	9,710 ± 150	9,970 ± 1,290
E4M-Med	E4M	3.7	1.1	95.2	12,580 ± 370	14,700 ± 2,690
E4M-High	E4M	4.2	1.1	94.8	19,050 ± 330	17,010 ± 3,940

N/M = Not measured (viscosity too high)

4.2.3 Characterization Methods

4.2.3.1 Real-time Surface Dissolution Imaging. A Sirius Surface Dissolution Imager (SDI) UV imaging system (Sirius Analytical Instruments Ltd., East Sussex, UK) was used to gain qualitative insight into the potential drug release mechanisms from films. The SDI employed an ActiPix™ D100 UV Area Imaging System (Paraytec Limited, York, UK) with the use of ActiPix™ D100 software (version 1.2, Paraytec Limited, York, UK). Images were recorded at 3.82 fps with sub-sampling every 10 min and 10 × 1 horizontal binning (each pixel represents 7 × 7 µm). Imaging was performed at 214 nm with the use of a single wavelength filter (10 nm bandwidth) with a pulsed xenon lamp as the light source. A 62.0 × 7.0 × 3.0 mm (L × H × W, W being the path length) quartz dissolution cell was used to house the 3D printed sample holder which was custom-fit for the quartz cell. Flow was controlled using a syringe pump.

Prior to data collection, dark images with the lamp turned off and reference images with blank SDS solution (5.4 mg/ml, also used for USP IV dissolution) were recorded for 10 s each for instrument calibration with the empty sample holder in place. After calibration, data collection was halted to allow for film sample insertion, at which point flow was stopped and the sample holder was removed. A circular film sample, 2 mm in diameter, was secured on the surface of an inert support material placed inside a 2.4 mm high, 2 mm diameter hollow stainless steel cylinder. The cylinder was then placed inside the bottom of the sample holder such that one surface of the film would be exposed to media flow (Figure 4.1), and the sample holder was re-inserted into the quartz cell. Once the sample holder was in place, the cell was filled with dissolution media before data collection and media flow at 0.2 µm/min were initiated. Media temperature was maintained at 37.0 ± 0.5 ºC.

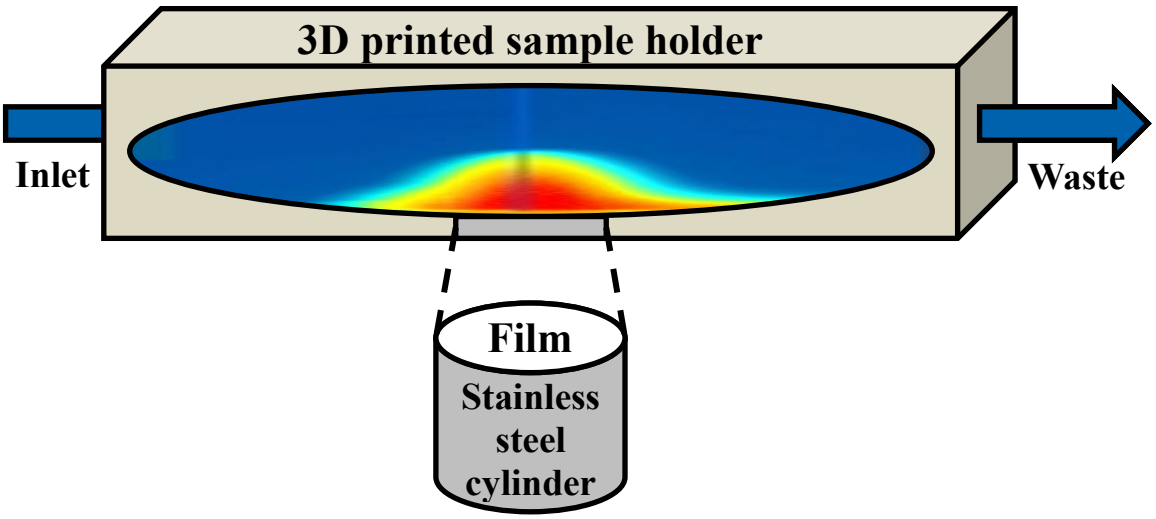

Figure 4.1 SDI film sample holder schematic.

4.2.3.2 Curve Fitting of Dissolution Profiles. In order to gain insight into the potential mechanisms of drug release from films, all dissolution profiles were fitted to the following five models: Equation (4.1), the zero order model, which predicts linear drug release with time, as one would expect from erosion-limited planar systems, where F is the percentage of drug dissolved at time t and k_0 is a constant:

$$F = k_0 t \tag{4.1}$$

Equation (4.2), the first order model, which is commonly employed to describe drug release from reservoir sources (Gibaldi and Feldman, 1967) including drug particle dissolution (Noyes and Whitney, 1897), where k_1 is a constant:

$$F = 100\left(1 - e^{-k_1 t}\right) \tag{4.2}$$

Equation (4.3), the Higuchi equation, or square-root law, developed to describe drug release via diffusion from planar matrices (Higuchi, 1963), where k_H is a constant:

$$F = k_H \sqrt{t} \tag{4.3}$$

Equation (4.4), the Korsmeyer–Peppas equation, or power law, designed to identify the controlling drug release mechanism of a given dosage (Korsmeyer et al., 1983; Peppas, 1985), where k_{KP} is a constant that incorporates geometric and structural characteristics of the system and n is the release exponent:

$$F = k_{KP} t^n \tag{4.4}$$

and Equation (4.5), the Hixson–Crowell equation, or cube-root law, based on the relationship between the surface area and volume of a dissolving particle (Hixson and Crowell, 1931), where k_{HC} is a constant that incorporates the surface area-to-volume relation:

$$F = 100\left[1 - \left(1 - k_{HC} t\right)^3\right] \tag{4.5}$$

These models were selected for both their basis in fundamental dissolution phenomena and their relative simplicity to identify the controlling drug release mechanism from films.

4.2.3.3 Statistical Analysis. Basic calculations were performed using Microsoft Excel® (Microsoft Office 2010). Analysis of variance (ANOVA) and Tukey pairwise comparisons (two-tailed t-tests) were performed using Minitab® (Minitab 17.3.1). Dissolution curve fitting was performed using a script written in Matlab® (R2015b, Mathworks). Results for viscosity, mechanical properties, and dissolution profiles are expressed as mean ± SD (standard deviation) while content uniformity results are expressed as mean with RSD% (relative standard deviation). Dissolution profiles were compared to each other using similarity and difference factors (Boateng et al., 2012; Costa and Lobo, 2001).

4.3 Results and Discussion

4.3.1 Viscosity of Polymer Solutions and Precursor Suspensions

Low shear (2.2 s^{-1}) viscosity measurements for polymer solutions and film precursor suspensions were performed to mimic conditions of film casting (Table 4.1). Viscosity ranges fell within 9,000-9,600 cP, 11,200-12,800 cP, and 19,000-24,000 cP for "low", "medium", and "high" viscosity polymer solutions, respectively. As discussed in Sub-section 4.2.2.2, this viscosity matching approach was necessary in lieu of keeping polymer concentrations constant to ensure film precursor suspensions were castable and did not spread or run upon casting. Appropriately selecting polymer concentrations within each viscosity range was also expected to minimize the impact of polymer solution viscosity on precursor suspension and film properties (Susarla et al., 2015; Susarla et al., 2013) when investigating the impact of film-forming polymer MW. Upon mixture of polymer solution with GF nanosuspension, the resulting film precursor

suspensions generally exhibited lower viscosities than their respective polymer solutions (7,100-10,000 cP, 8,000-14,000 cP, and 9,000-17,000 cP for "low", "medium", and "high", respectively). However, unlike the polymer solutions where viscosities within each class were roughly similar, film precursor suspension viscosity tended to increase slightly with increasing polymer MW, despite being mixed with the same ratio of GF nanosuspension. This may be the result of stronger GF nanoparticle interaction with higher MW HPMC (E4M) compared to lower MW HPMC (E15 and E50).

4.3.2 GF Particle Size after Milling and Redispersed from Films

Retaining poorly water-soluble drug nanoparticle size upon incorporation into and delivery from any solid dosage form is crucial to retaining the enhanced dissolution and bioavailability of the drug. In order to investigate the ability to recover GF nanoparticles from films, all formulations were subjected to redispersion tests in deionized water and the resulting PSDs were compared to that of the original GF nanosuspension. As seen in Figure 4.2 where PSD statistics are reported in the form of 10%, 50% (median), and 90% passing size (d_{10}, d_{50}, and d_{90}, respectively), not only were GF nanoparticles recovered from all film formulations regardless of polymer MW or concentration, but most PSDs were practically identical to that of the original nanosuspension from which the GF nanoparticles were taken. Even in E4M films which exhibited slight increases in measured particle size, only E4M-Low showed any particles larger than 1 μm (< 5%) and none larger than 2 μm. These results demonstrate that poorly water-soluble drug nanoparticles can be successfully recovered from polymer films made using various polymer MWs and concentrations.

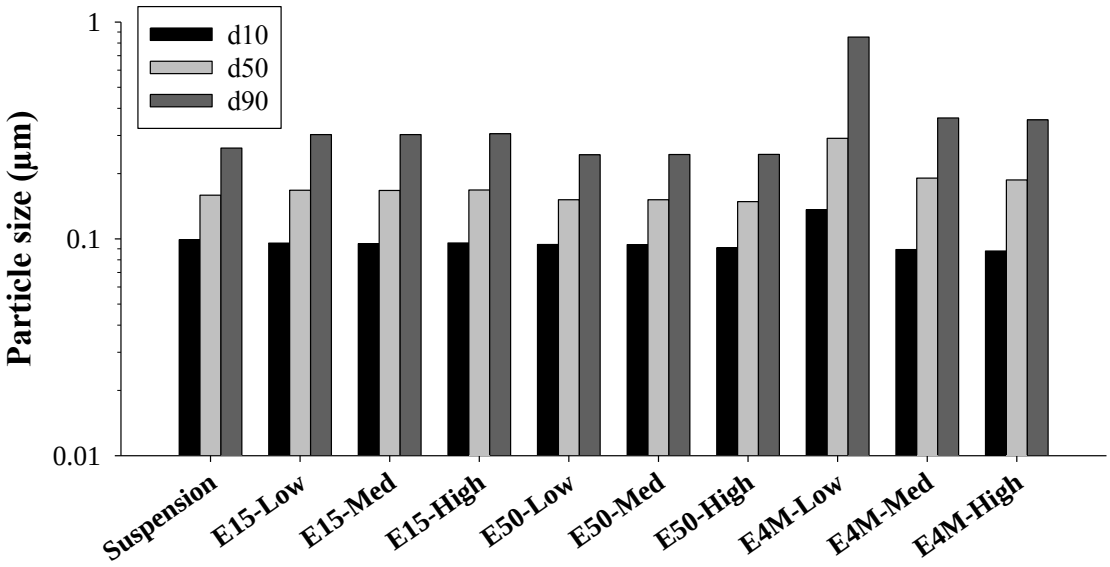

Figure 4.2 Particle size statistics of GF nanosuspension and redispersed film samples.

4.3.3 Film Characterization

4.3.3.1 GF Content and Uniformity in Films. As in any pharmaceutical dosage form, consistency in dosing is critical. In order to assess drug content and uniformity of films, content uniformity tests were performed on all nine film formulations to evaluate thickness, mass of drug per unit area, and drug loading by wt% (Table 4.2). In order to better elucidate possible differences in uniformity between films, smaller sample sizes (~0.7 cm^2) than the conventional film dosage (4-6 cm^2) were used, resulting in larger than expected RSD%. That said, the majority of films still exhibited < 6% RSD in terms of film thickness and GF mass per unit area; in fact, all but one were < 3% RSD in terms of wt% GF. These results demonstrate the robustness of the film manufacture process to produce uniform films with varying polymer MW and concentration.

Table 4.2 Content Uniformity of HPMC Films with Different Polymer MWs and Concentrations. Values are an Average of 10 Samples ~0.7 cm^2 in Area

Formulation	Thickness (μm)	RSD (%)	GF mass per unit area (mg/cm^2)	RSD (%)	wt% GF	RSD (%)
E15-Low	91.6	5.2%	1.81	6.9%	13.7	2.5%
E15-Med	114.2	4.1%	2.14	5.1%	13.7	1.1%
E15-High	110.6	1.6%	1.93	3.2%	12.7	2.5%
E50-Low	64.7	4.4%	1.64	5.2%	18.5	2.4%
E50-Med	70.4	5.7%	1.78	4.9%	18.9	1.1%
E50-High	71.9	3.8%	1.80	4.6%	19.1	2.9%
E4M-Low	34.7	2.7%	1.97	3.3%	43.8	7.4%
E4M-Med	41.4	6.7%	2.02	2.4%	38.3	2.8%
E4M-High	38.5	5.1%	1.93	4.5%	42.0	2.1%

The most obvious trends involve decreasing film thickness and increasing wt% GF with increasing polymer MW. Both of these are a direct result of a greater loss in moisture content during drying as a result of varying polymer concentration due to the necessity of a viscosity matching approach. Since all films were cast at the same 1000 μm thickness but less polymer mass was required to achieve the same viscosity for high MW polymers (Table 4.1), higher MW polymer solutions and precursor suspensions contained greater water content. Consequently, more water, and therefore more mass, was available for evaporation during drying, resulting in thinner dry films with apparently greater GF loading by wt%. This is supported by the fact that the same trend was not observed for GF mass per unit area. Since every polymer solution was mixed with the same amount of GF nanosuspension, the mass of GF per unit area of film should fluctuate around a given value rather than increase or decrease with increasing polymer MW. It is also worth noting that drug loadings of up to 44 wt% were achieved simply by using a higher MW film-forming polymer. If an E4M film is prepared with the current formulation and dried to the same thickness as the E15 films, it would be possible to

achieve a dosage as high as 35 mg. The potential for higher dosage films containing poorly water-soluble drug nanoparticles will be the topic of a future study.

4.3.3.2 Film Mechanical Properties. Mechanical properties of all nine film formulations are shown in Table 4.3. Here, two overarching effects were investigated: the effect of increasing polymer solution viscosity by increasing polymer concentration within each polymer MW class, and the effect of increasing polymer MW within each viscosity range. First, regarding increasing polymer solution viscosity, although there were slight increasing trends in TS, YS, YM, and EB overall within each MW class due to an increase in polymer concentration, most of these trends were not statistically significant ($p < 0.05$). While one might expect more significant increases in film strength and elongation with increasing polymer concentration across a wider range of polymer concentrations, the practical viscosity restrictions necessary for film casting in this work (~7,000-20,000 cP) inherently limited these potential differences. Next, regarding increasing polymer MW within each viscosity range, there was no statistical difference between the TS, YS, or EB of different MW grades (with the exceptions of the YS of E15-Low and the EBs of E15-Med and E4M-Med). However, there was a significant increase in YM and a noticeable decrease in EB with increasing polymer MW overall. That said, the variation in some of the film mechanical property measurements, particularly EB, was not insignificant and should be assessed with caution.

Table 4.3 Mechanical Properties of Films with Different HPMC MWs and Concentrations Containing GF Nanoparticles. Values are Mean ± SD, n = 4

Formulation	Tensile strength (MPa)	Yield strength (MPa)	Young's modulus (GPa)	Elongation at break (%)
E15-Low	16.1 ± 1.6^{c}	14.3 ± 0.4^{d}	1.46 ± 0.13^{d}	11.4 ± 2.8^{abc}
E15-Med	23.5 ± 1.5^{abc}	18.3 ± 0.6^{c}	1.49 ± 0.09^{d}	19.4 ± 2.0^{a}
E15-High	25.4 ± 4.0^{abc}	21.4 ± 0.9^{ab}	1.90 ± 0.03^{cd}	17.3 ± 4.4^{ab}
E50-Low	22.4 ± 4.4^{bc}	18.6 ± 1.2^{bc}	2.86 ± 0.45^{bc}	11.6 ± 1.2^{abc}
E50-Med	27.6 ± 4.1^{ab}	19.6 ± 1.0^{abc}	3.01 ± 0.40^{ab}	12.5 ± 4.1^{abc}
E50-High	32.2 ± 5.2^{a}	21.8 ± 1.7^{a}	3.44 ± 0.05^{ab}	14.3 ± 2.6^{abc}
E4M-Low	24.9 ± 1.4^{abc}	20.9 ± 0.3^{abc}	4.14 ± 0.55^{a}	6.2 ± 0.8^{c}
E4M-Med	25.2 ± 0.4^{abc}	19.8 ± 1.2^{abc}	3.23 ± 0.93^{ab}	7.1 ± 0.2^{bc}
E4M-High	31.8 ± 5.4^{ab}	20.2 ± 2.7^{abc}	3.57 ± 1.11^{ab}	10.5 ± 4.9^{bc}

[a-d]Values in each column that do not share a superscript are statistically different ($p < 0.05$).

Without being limited to a fixed range of polymer solution viscosities, existing literature suggests that changes in film-forming polymer MW may lead to changes in the mechanical properties of the resulting films when the polymer concentration is held constant. Park et al. (1993) observed increases in film TS and YM with increasing polymer MW for methylcellulose (MC) and HPC. EB for MC films also increased with increasing MW, although EB for HPC films appeared to reach a maximum for an intermediate MW rather than increase monotonically. Lazaridou et al. (2003) also observed increasing film TS and EB with increasing pullulan MW. Huang et al. (2013) observed increases in film TS, YS, and YM with increasing PLGA MW, along with decreasing EB. However, while these trends appear to differ from the minimal changes in film mechanical properties with increasing polymer MW observed in this work, it is again worth mentioning that all of their films were prepared using equal concentrations of polymer regardless of their MW. In contrast, films in this work had to be prepared by matching polymer solution viscosity between film-forming polymer MWs, since equal polymer concentrations would have led to precursor suspensions that were either not

viscous enough to form a uniform film or too viscous to cast. As such, there were two competing influences affecting film mechanical properties: increasing polymer MW and decreasing polymer concentration. Kennedy et al. (1994) attributed increases in the apparent modulus of films with increasing polymer MW to an increase in the number of entanglements per polymer chain, leading to additional impediments to strain. The frequency of such entanglements would decrease with a corresponding decrease in polymer concentration, offering a potential explanation for the lack of significant differences in most mechanical properties between films with differing HPMC MWs in this work. The frequency of polymer entanglements is further reduced by a corresponding increase in GF nanoparticle concentration in the dry film for higher polymer MW formulations (despite having the same GF loading by mass), which has also been shown to lead to a reduction in film mechanical properties (Krull et al., 2016b). As such, the inherent viscosity limits posed by the film manufacture process offer a convenient design space in which film-forming polymer MW can be safely adjusted with minimal impact on film mechanical properties.

4.3.3.3 Dissolution. Dissolution profiles for all nine film formulations are shown in Figure 4.3, separated by viscosity range. E4M films for all three viscosity ranges exhibited significantly slower GF release than E15 and E50 films according to similarity and difference factors (Boateng et al., 2012; Costa and Lobo, 2001) (Appendix A.2). This slowing of GF release is even more significant given the fact that E4M films were only 35-40 μm thick. In light of previous work which showed that film thickness is linearly proportional to time of 100% drug release in polymer films loaded with GF nanoparticles (Krull et al., 2016b), one might expect a film cast from the same formulation dried to half

another film's thickness to release twice as fast. In addition, E4M films within each viscosity range were prepared using approximately one-third and one-fifth the mass of polymer required for E50 and E15 films, respectively, to maintain similar viscosities. The fact that E4M films at all three viscosity ranges exhibited significantly slower release than E15 and E50 films despite their reduced thickness and polymer mass demonstrates the ability of the film-forming polymer MW to influence drug release from polymer films without significantly affecting film mechanical properties. That said, no such difference in GF release rate was observed between E15 and E50 films. Since their respective MWs are relatively similar (~14 kDa and ~21 kDa respectively) compared to that of E4M (~88 kDa), the similarity of the E15 and E50 dissolution profiles was likely due to the effect of higher polymer MW being unable to overcome the competing effects of less polymer mass and reduced film thickness.

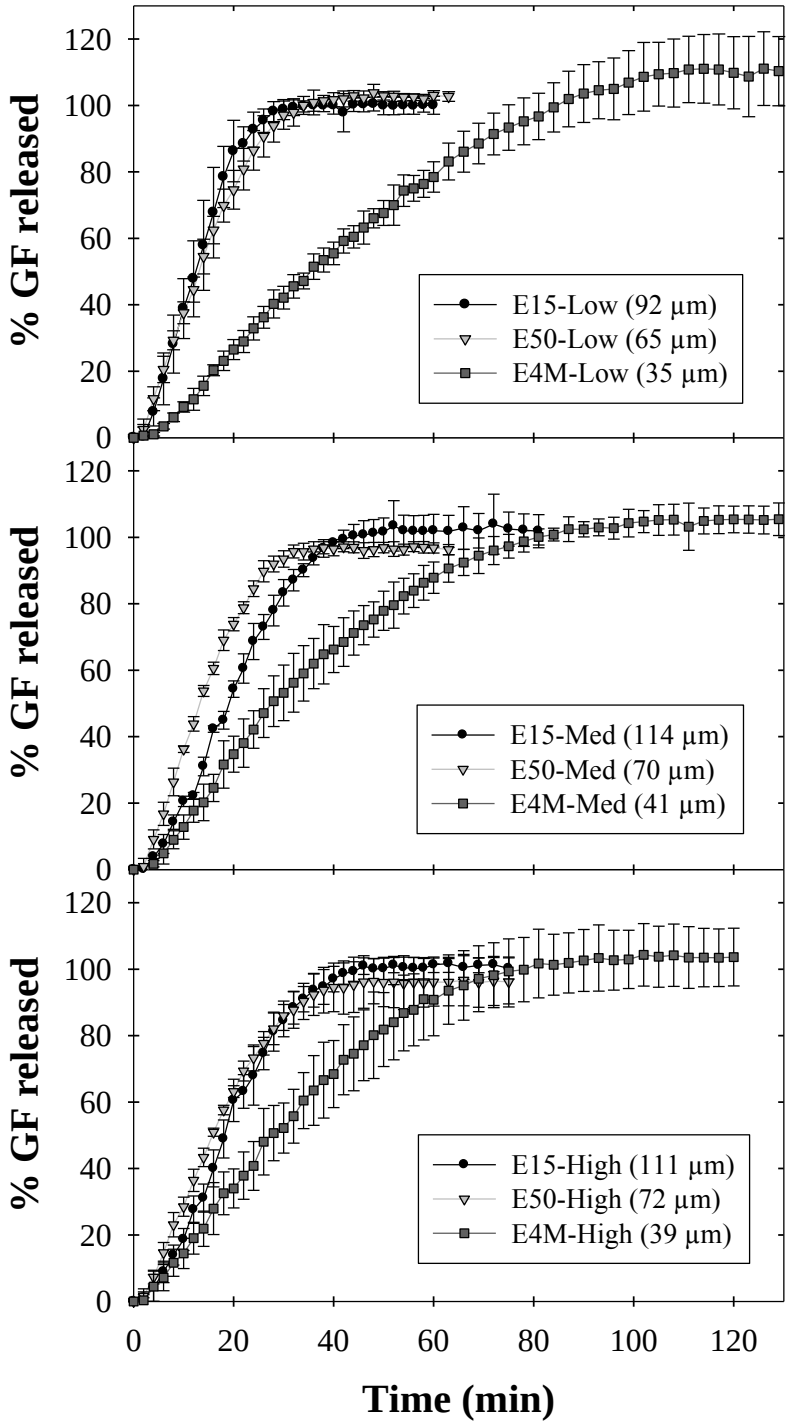

Figure 4.3 Comparison of dissolution profiles between films loaded with GF nanoparticles containing different HPMC MWs and concentrations. Values are mean ± SD, n = 6.

To gain insight into potential drug release mechanisms, the dissolution profiles for all nine film formulations were fitted to zero order, first order, square-root (Higuchi), power law (Korsmeyer–Peppas), and cube-root (Hixson–Crowell) models. The fitting parameters and resulting adjusted R^2 values for these fits are shown in Table 4.4 and Table 4.5, respectively. The Korsmeyer–Peppas equation was the best fit for all nine formulations with adjusted R^2 values of 0.988 and above and a release exponent (*n*) above 1.0 in all cases, suggesting Super Case II transport. This, coupled with the lack of fit by models based on single drug release mechanisms, implies that drug nanoparticle release from these films cannot be explained by a single release mechanism. That said, the adjusted R^2 values of zero order model fits approached those of the Korsmeyer–Peppas model fits with increasing polymer concentration for all three polymer MWs, suggesting that polymer erosion may become the dominating release mechanism when high polymer concentrations are used in film formation, regardless of polymer MW. This is further supported by the fact that the release exponent of the fitted Korsmeyer–Peppas model approaches 1.0 with increasing polymer concentration. Others have also observed a shift in controlling drug release mechanism to drug diffusion with increasing polymer MW in other dosage forms, including polymeric beads (Ramkissoon-Ganorkar et al., 1999) and nanoparticles (Mittal et al., 2007).

Table 4.4 Fitting Parameters Generated by Fitting Dissolution Curves from GF Nanoparticle-loaded HPMC Films of Varying Polymer MW and Concentration to Various Dissolution Models

	Zero order	First order	Higuchi	Korsmeyer–Peppas		Hixson–Crowell
Formulation	k_0 (%/min)	k_1 (min^{-1})	k_H ($\%/min^{1/2}$)	k_{KP} ($\%/min^n$)	n (-)	k_{HC} (min^{-1})
E15-Low	3.95	0.052	12.7	1.56	1.37	0.0158
E15-Med	3.68	0.048	12.0	2.39	1.17	0.0147
E15-High	1.24	0.016	7.0	0.85	1.10	0.0050
E50-Low	2.50	0.032	9.7	0.63	1.47	0.0098
E50-Med	3.75	0.049	12.1	1.79	1.29	0.0149
E50-High	1.63	0.021	8.1	1.00	1.15	0.0066
E4M-Low	2.49	0.030	8.8	0.43	1.64	0.0095
E4M-Med	3.21	0.043	11.6	1.89	1.19	0.0130
E4M-High	1.68	0.022	8.1	1.19	1.11	0.0067

Table 4.5 Adjusted R^2 Values Generated by Fitting Dissolution Curves from GF Nanoparticle-loaded HPMC Films of Varying Polymer MW and Concentration to Various Dissolution Models

Formulation	Zero order	First order	Higuchi	Korsmeyer–Peppas	Hixson–Crowell
E15-Low	0.951	0.876	0.685	0.991	0.903
E15-Med	0.984	0.934	0.749	0.995	0.954
E15-High	0.987	0.952	0.784	0.991	0.967
E50-Low	0.937	0.864	0.670	0.993	0.889
E50-Med	0.963	0.900	0.707	0.991	0.924
E50-High	0.980	0.939	0.764	0.988	0.956
E4M-Low	0.912	0.846	0.634	0.996	0.868
E4M-Med	0.981	0.923	0.745	0.994	0.946
E4M-High	0.990	0.953	0.784	0.994	0.969

As a visual complement to conventional film dissolution studies and analysis, surface dissolution images for low viscosity films are shown in Figure 4.4. E15 films appeared to dissolve readily with little swelling, whereas E50 and E4M films exhibited significant amounts of swelling due to their higher polymer MW, as indicated by the large bump that developed directly above the film samples inside the SDI. This swelling is exemplified by the fact that films made with polymers of increasing MW produced thinner films (~110 μm for E15, ~70 μm for E50, ~40 μm for E4M). Pajander et al.

(2012) also observed a similar increase in extent of swelling between compacts of HPMC viscosity grades equivalent to E15 and E50 using the SDI. It should be noted that these images merely provide visual insight into the film dissolution process and do not necessarily indicate rate of drug release. For instance, although the swelling in E50 films was clearly visible in the SDI while little swelling was observed in E15 films, both films exhibited similar rates of drug release in the USP IV due to the confounding effects of differing polymer mass and film thickness. That said, the SDI images confirm the presence of more significant swelling in higher MW polymer films, even with a corresponding reduction in film thickness.

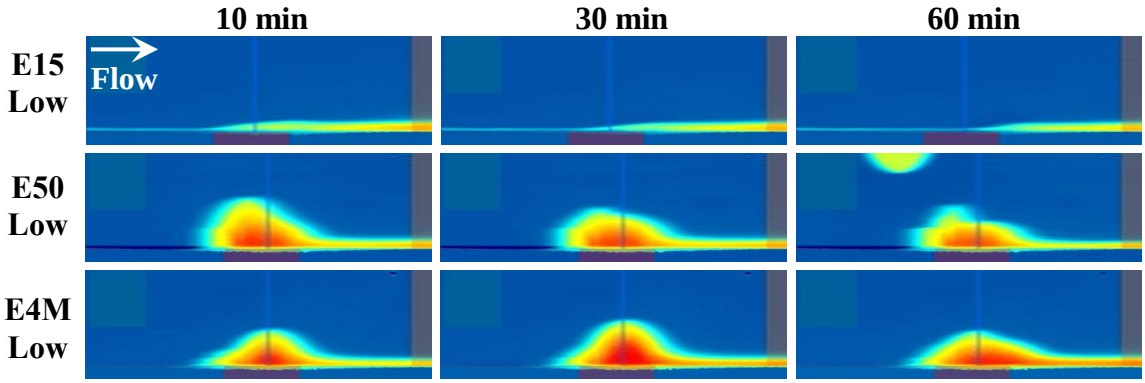

Figure 4.4 Surface dissolution snapshots of low viscosity film formulations. Blue indicates absence of drug while warmer colors indicate higher concentrations of drug (note: the semicircle at the top of the 60 min snapshot of E50-Low is an air bubble, not a part of the film sample).

4.3.3.4 Thermogravimetric Analysis. All nine film formulations were subjected to TGA and the resulting thermograms are shown in Figure 4.5. All films exhibited a weight loss between 2% and 6% up to 100 ºC, most likely due to the loss of water. Increasing the MW of the film-forming polymer led to a significant decrease in film water content (5.3% for E15, 3.8% for E50, 2.5% for E4M; $p < 0.05$) while increasing polymer solution

viscosity within the range of investigation had no significant effect on film water content (3.7% for Low, 4.0% for Med, 4.0% for High; $p < 0.05$). This trend of decreasing water content with increasing polymer MW is even more significant given that film precursor suspensions containing higher MW HPMC had more water content before drying than those made with lower MW HPMC (Table 4.1). The significant weight loss following 15 min of exposure to 150 ºC was likely due to the loss of the plasticizer, glycerin. The average weight loss during this time was ~4% across all films with no significant trend based on film-forming polymer MW or polymer solution viscosity ($p < 0.05$).

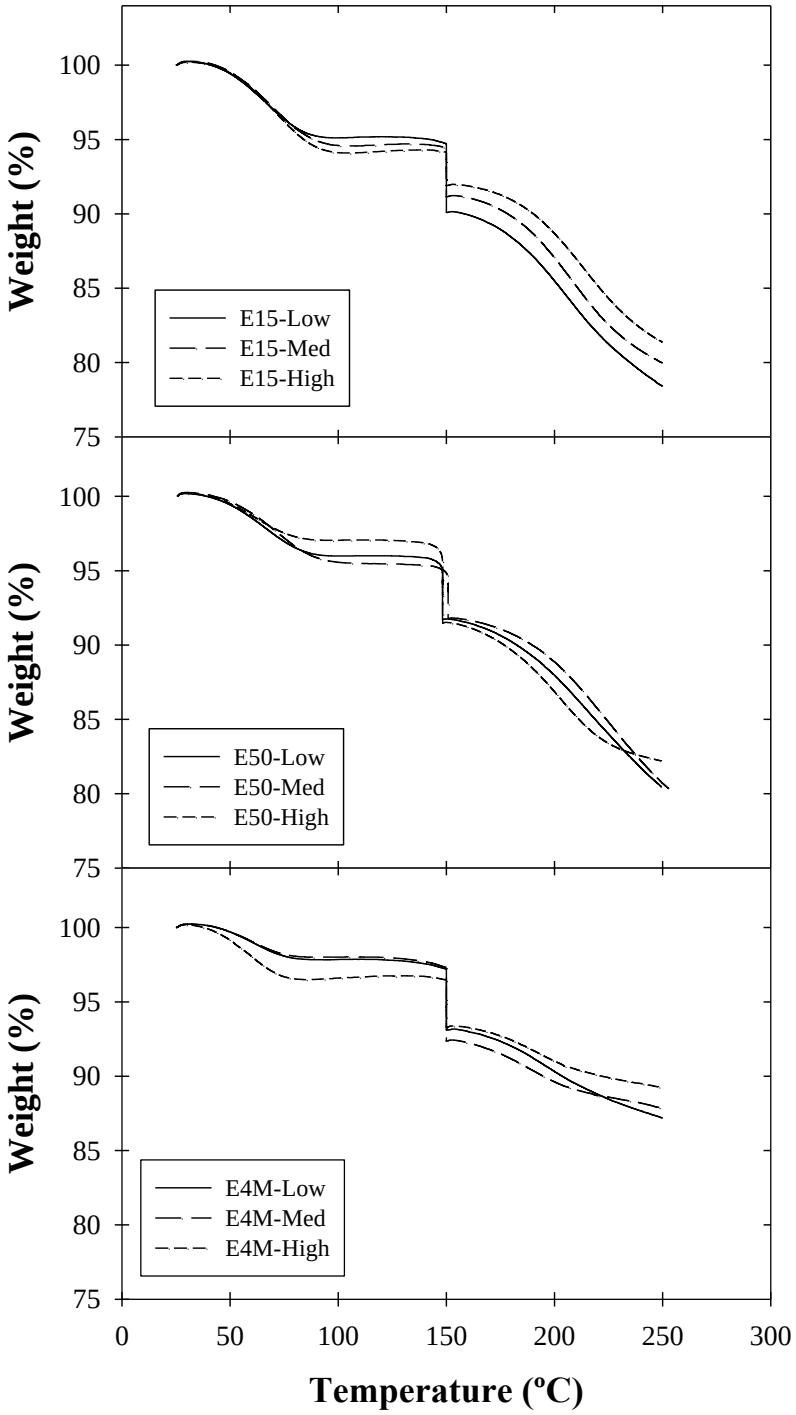

Figure 4.5 TGA curves for films with different HPMC MWs and concentrations loaded with GF nanoparticles.

4.3.3.5 Scanning Electron Microscopy. In order to qualitatively assess the size and morphology of the GF nanoparticles embedded within the films, cross-sectional SEM images were taken of all nine film formulations (Figure 4.6). Finely dispersed primary GF nanoparticles can be observed throughout all nine film formulations with no visual indications of agglomeration, which substantiates the redispersion results discussed in Section 4.3.2. This further supports that poorly water-soluble drug nanoparticles can be physically stabilized without aggregation within the polymer matrix of the films despite variations in film-forming polymer concentration and MW.

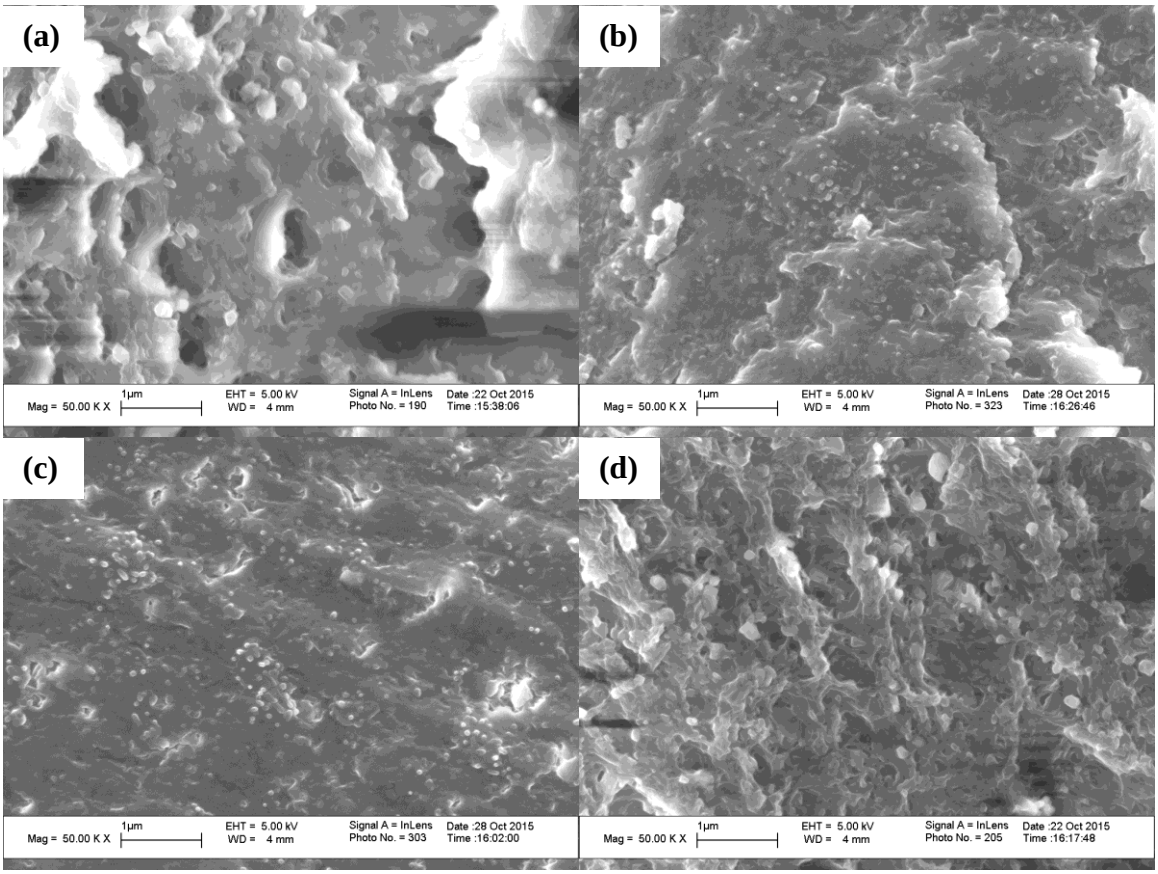

Figure 4.6 Cross-sectional SEM images of (a) E15-Low, (b) E15-Med, (c) E15-High, (d) E50-Low, (e) E50-Med, (f) E50-High, (g) E4M-Low, (h) E4M-Med, and (i) E4M-High films containing GF nanoparticles. Magnification of 50,000× was used for all images. Scale bars indicate 1 µm. (Continued)

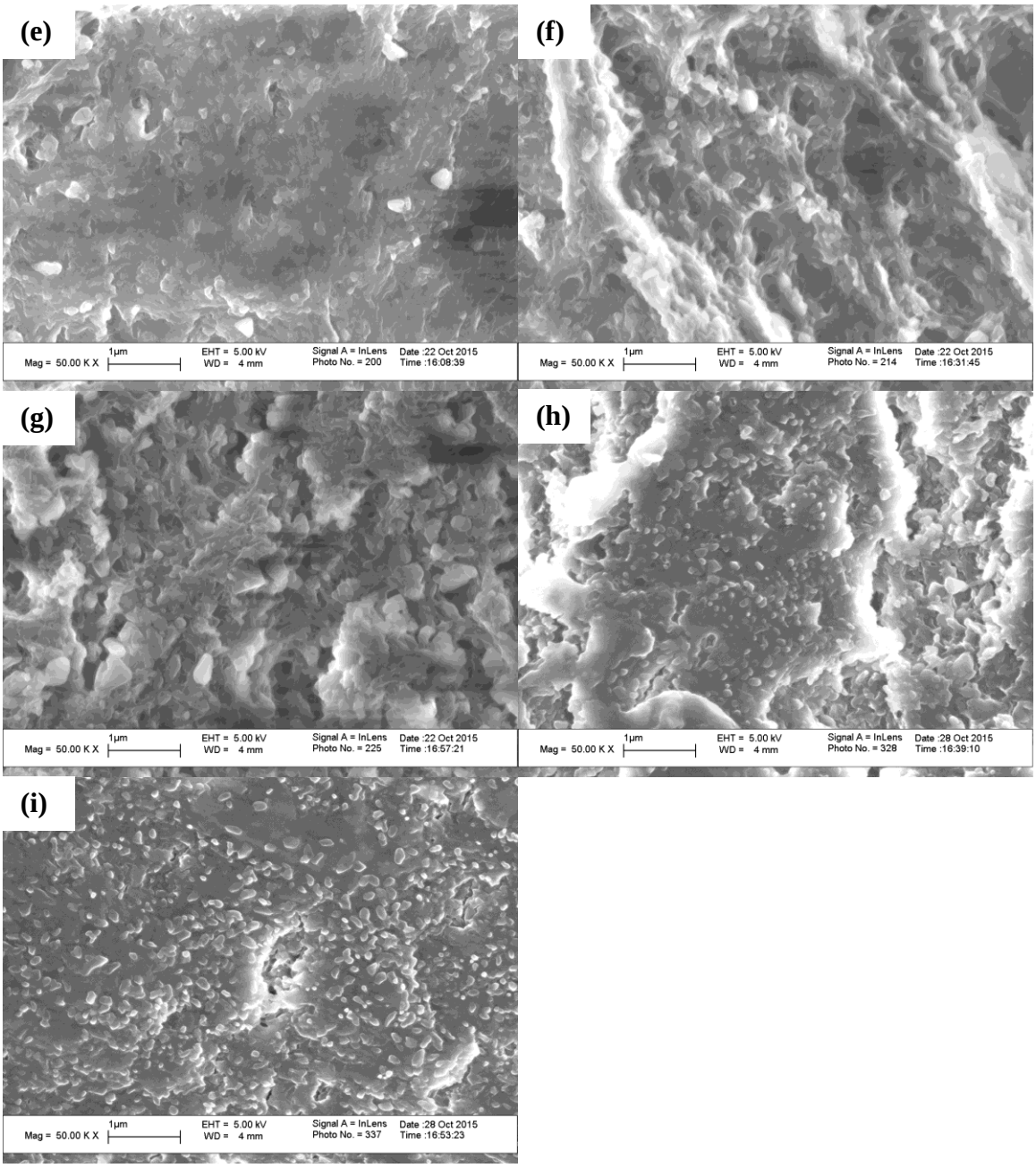

Figure 4.6 (Continued) Cross-sectional SEM images of (a) E15-Low, (b) E15-Med, (c) E15-High, (d) E50-Low, (e) E50-Med, (f) E50-High, (g) E4M-Low, (h) E4M-Med, and (i) E4M-High films containing GF nanoparticles. Magnification of 50,000× was used for all images. Scale bars indicate 1 µm.

4.4 Conclusions

The objective of this work was to investigate the impact of polymer MW and concentration on the properties and dissolution of polymer films loaded with poorly water-soluble drug nanoparticles. A polymer solution viscosity matching approach was necessary in order to ensure film precursor suspensions were castable and to minimize the influence of viscosity on the resulting films. Higher MW E4M films exhibited significantly slower drug release than lower MW E15 and E50 films across three viscosity ranges despite being formed with less polymer mass, which resulted in thinner films. However, despite the noticeable differences in dissolution rate between films made with different polymer MWs within each viscosity range, the respective differences in TS and EB between the same films were relatively minor. This suggests that the release rate of poorly water-soluble drug can be successfully controlled by adjusting film-forming polymer MW with little impact on the mechanical properties of the films if polymer solution viscosity is maintained between formulations. In addition, good content uniformity and nanoparticle redispersibility can be achieved using various film-forming polymer MWs and concentrations, demonstrating the robustness of the film format.

CHAPTER 5

EFFECT OF DRUG LOADING

5.1 Introduction

One perceived limitation shared by all means of incorporating poorly water-soluble drug into films is the existence of an inherent limitation on drug loading (Borges et al., 2015b; Dixit and Puthli, 2009; Hoffmann et al., 2011). While high drug loading in films is already difficult to achieve due to their small size, the means of incorporating drug into films can impose even greater limitations. Since a traditional strip film dosage only contains a fraction of the total mass of a typical tablet or pill, the amount of drug that can be conceivably loaded into a traditional strip film dosage cannot practically match the dosages available in tablets and capsules. In addition, the standard techniques by which poorly water-soluble drugs are incorporated into strip films further restrict the amount of drug that can be loaded into a film dosage, typically up to 30 wt%. In hot melt extruded films, the dissolution rate enhancement of the drug hinges on the stability of the amorphous solid dispersion during cooling and storage. This becomes increasingly difficult with increasing drug loading, resulting in uncontrolled crystallization if the drug loading is too high (Serajuddin, 1999). Similarly, organic solvent casting relies on the stability of drug in the amorphous form, specifically after the solvent in which the drug is dissolved is driven out of the film during drying. If the drug loading in solvent cast films is too high, they too will experience uncontrolled drug crystallization, resulting in a loss of drug dissolution rate enhancement (Hoffmann et al., 2011). Coupled with a drug delivery platform that is already limited in total mass per unit dosage, these additional

restrictions on drug loading have made achieving even moderate dosages in strip films a significant challenge.

Inclusion of engineered drug particles into strip films over the last few years has revealed the potential for higher drug loading in films, although the subject has yet to be fully explored. The majority of work in this area has either focused on establishing a means of particle engineering that is suitable for incorporation into the film platform (Beck et al., 2013; Bhakay et al., 2016; Prodduturi et al., 2005; Sievens-Figueroa et al., 2012a; Visser et al., 2015) or the impact of critical material attributes (CMAs) on their performance (Krull et al., 2016b; Susarla et al., 2015). In most cases, drug loading in films was kept below 20 wt% with none above 30 wt%, presumably to avoid potential confounding influences of high drug loading on other experimental factors under investigation. Woertz and Kleinebudde (2015) claimed to have prepared "acceptable films" with as high as 50 mg of homogenized ibuprofen in a 6 cm^2 dosage, but neglected to demonstrate acceptable mechanical properties or dissolution rates for their films. Steiner et al. (2016) demonstrated HPMC films with up to 45 wt% WSMM naproxen nanoparticles that exhibited "good" mechanical properties, above which films became too stiff for practical application, although they did not investigate dissolution rate. The potential for higher drug loading (40 wt%) in films containing WSMM griseofulvin nanoparticles prepared with high molecular weight (MW) polymer in passing in Chapter 4 when investigating the impact of polymer MW. However, to this point, no study has been able to demonstrate good mechanical properties and enhanced poorly water-soluble drug dissolution rate of strip films with high (> 40 wt%) drug loading.

This chapter investigates the effect of high loadings of poorly water-soluble drugs on polymer strip films, including mechanical properties and drug dissolution rates.

5.2 Experimental Procedures

Experimental procedures for the preparation of polymer films containing GF nanoparticles, film mechanical properties, TGA, and SEM are identical to their respective procedures described in Section 2.2. Experimental procedures for viscosity, GF particle size after milling and redispersed from films, determination of drug content and uniformity in films, and flow-through cell dissolution (USP IV) are identical to their respective procedures described in Section 3.2. Experimental procedures for long-term stability of films and statistical analysis are identical to their respective procedures described in Section 4.2.

5.2.1 Materials

Griseofulvin (GF; Letco Medical, Decatur, AL) was used as a model BCS class II drug. Hydroxypropyl methylcellulose (HPMC; Methocel E15 Premium LV and Methocel E4M Premium, The Dow Chemical Company, Midland, MI) served as the film-forming polymer. HPMC-E15LV also served as a nanoparticle stabilizer in suspension, along with the surfactant sodium dodecyl sulfate (SDS; Fisher Scientific, Pittsburgh, PA). Glycerin (Sigma–Aldrich, St. Louis, MO) was used as a film plasticizer. GF particle size reduction was performed by wet stirred media milling (WSMM) according to Sub-section 5.2.2.1. All other materials were used without further processing.

5.2.2 Preparation Methods

5.2.2.1 Preparation of GF Nanosuspensions. GF nanosuspensions were prepared via wet stirred media milling (WSMM) using a Netzsch mill (Microcer, Fine particle technology LLC, Exton, PA). Methods and stabilizer concentrations were selected according to previous optimization studies (Bilgili and Afolabi, 2012; Monteiro et al., 2013). Suspensions consisted of 10%, 20%, or 30% GF dispersed in a stabilizer solution of 2.5% HPMC-E15LV and 0.5% SDS (all w/w wrt water). All three suspensions were milled for 120 min.

5.2.2.2 Preparation of Polymer Solutions and Film Precursor Suspensions. Formulations for film-forming polymer solutions and film precursor suspensions are listed in Table 5.1. Polymer and plasticizer concentrations for polymer solutions were selected in such a way that all resulting film precursor formulations would be castable but not spread during drying (target viscosity range of 5,000-12,000 cP). This was accomplished using a viscosity matching approach for polymer solution preparation outlined in Sub-section 4.2.2.2 for E15 and E4M polymer solutions, represented by 0's in Table 5.1. Polymer solutions were prepared by adding the appropriate amounts of HPMC and plasticizer to water at 90 ºC, after which the solution was allowed to cool to room temperature under continuous magnetic stirring. Polymer solutions were mixed with GF nanosuspensions using a Thinky ARE-310 planetary centrifugal mixer (Thinky, Laguna Hills, CA) at 2,000 rpm for 30 s, followed by 7 min of deaeration at 2,200 rpm, to form film precursor suspensions. If bubbles were still present in the precursor suspension after mixing, the precursor was left overnight to settle before casting.

Table 5.1 Composition of Polymer Solutions and Film Precursor Suspensions

Formulation	HPMC grade	wt% GF in suspension (wrt water)	Polymer-to-suspension mixing ratio (w/w)	wt% GF	wt% HPMC	wt% Glycerin	wt% SDS	wt% water
DL0-15	E15	N/A	N/A	N/A	15.0%	5.0%	N/A	80.0%
DL1-15	E15	10%	3.6	1.9%	12.2%	3.9%	0.10%	81.8%
DL2-15	E15	10%	1.5	3.5%	9.9%	3.0%	0.18%	83.4%
DL3-15	E15	20%	3.0	4.1%	11.8%	3.8%	0.11%	80.3%
DL4-15	E15	20%	1.6	6.2%	10.1%	3.1%	0.17%	80.5%
DL5-15	E15	30%	2.3	6.8%	11.2%	3.5%	0.13%	78.6%
DL6-15	E15	30%	1.4	9.4%	9.7%	2.9%	0.18%	78.0%
DL0-4M	E4M	N/A	N/A	N/A	3.3%	1.1%	N/A	95.6%
DL1-4M	E4M	10%	3.6	1.9%	3.1%	0.9%	0.10%	94.1%
DL2-4M	E4M	10%	1.5	3.5%	2.9%	0.7%	0.18%	92.8%
DL3-4M	E4M	20%	3.0	4.1%	3.0%	0.8%	0.11%	92.0%
DL4-4M	E4M	20%	1.6	6.2%	2.9%	0.7%	0.17%	90.1%
DL5-4M	E4M	30%	2.3	6.8%	3.0%	0.8%	0.13%	89.5%

Drug loadings in film precursor suspensions were adjusted by varying the drug concentration in WSMM nanosuspensions and polymer-to-nanosuspension mixing ratios (Table 5.1). This combination of factors was necessary in order to ensure the resulting film precursor suspensions were within the castable viscosity range. E15 formulations were designed to achieve the following target GF loadings in their respective dry films: 10 wt% for DL1-15, 20 wt% for DL2-15 and DL3-15, 35 wt% for DL4-15 and DL5-15, and 50 wt% for DL6-15. Similar drug loadings for DL2/3 and DL4/5 were chosen to observe the effects, if any, of adding GF nanoparticles from WSMM suspensions with different drug concentrations. Polymer-to-nanosuspension ratios were kept the same across both E15 and E4M formulations for ease of comparison. DL6-4M produced films that were too brittle for testing and were excluded from analysis.

5.3 Results and Discussion

5.3.1 Viscosity of Polymer Solutions and Precursor Suspensions

Low shear (2.2 s^{-1}) viscosity measurements for polymer solutions and film precursor suspensions, performed with the objective of mimicking conditions of film casting, are presented in Figure 5.1. As explained in Sub-section 5.2.2.2, E15 and E4M polymer solutions (DL0-15 and DL0-4M, respectively) were formulated to have similar viscosities of ~12,000 cP so that, upon mixture with GF nanosuspension, all of the resulting film precursor formulations would be castable. Upon dilution with GF nanosuspension, the viscosity of the resulting film precursor suspensions generally decreased, more so for precursors with lower polymer-to-nanosuspension mixing ratios. It is also worth noting that GF nanosuspensions with greater solids content (30 wt% GF > 20% > 10%) were more viscous, leading to more viscous precursors prepared from higher drug loading nanosuspensions. For the same polymer-to-nanosuspension mixing ratios, E4M precursors generally exhibited greater viscosities than their respective E15 counterparts, possibly suggesting stronger GF nanoparticle interaction with E4M than with E15.

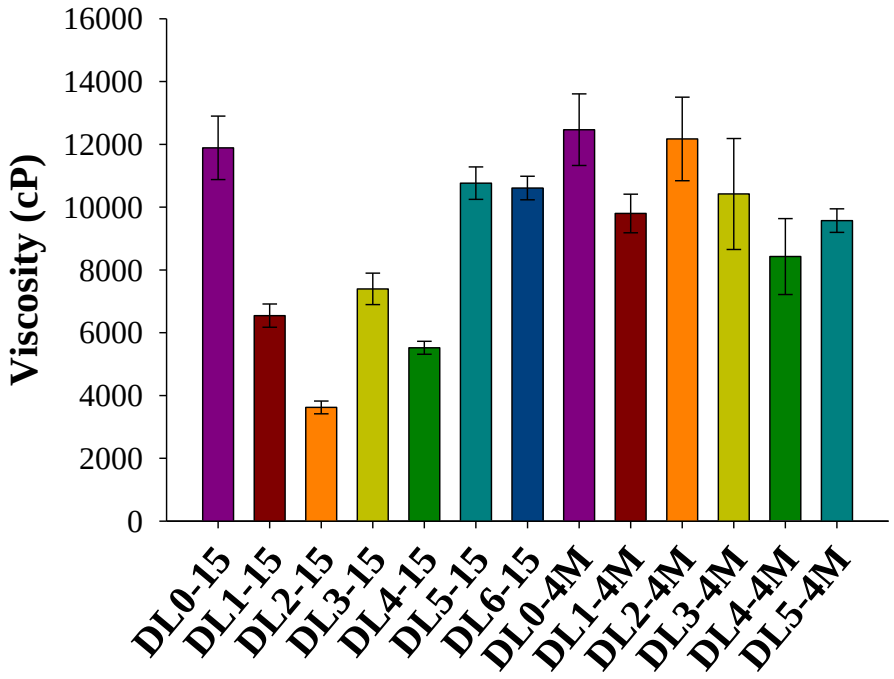

Figure 5.1 Low shear (2.2 s^{-1}) room temperature viscosity of polymer solutions and film precursor suspensions.

5.3.2 Scanning Electron Microscopy (SEM)

Cross sectional SEM images of all films were taken to qualitatively assess the size and morphology of the embedded GF nanoparticles (Figure 5.2). Finely dispersed GF nanoparticles were observed in all images, including both E15 and E4M films. This suggests that negligible drug nanoparticle aggregation within the film and uniform dispersion of embedded GF nanoparticles throughout the HPMC matrix is indeed achievable, even for films with high drug loadings (> 70 wt%).

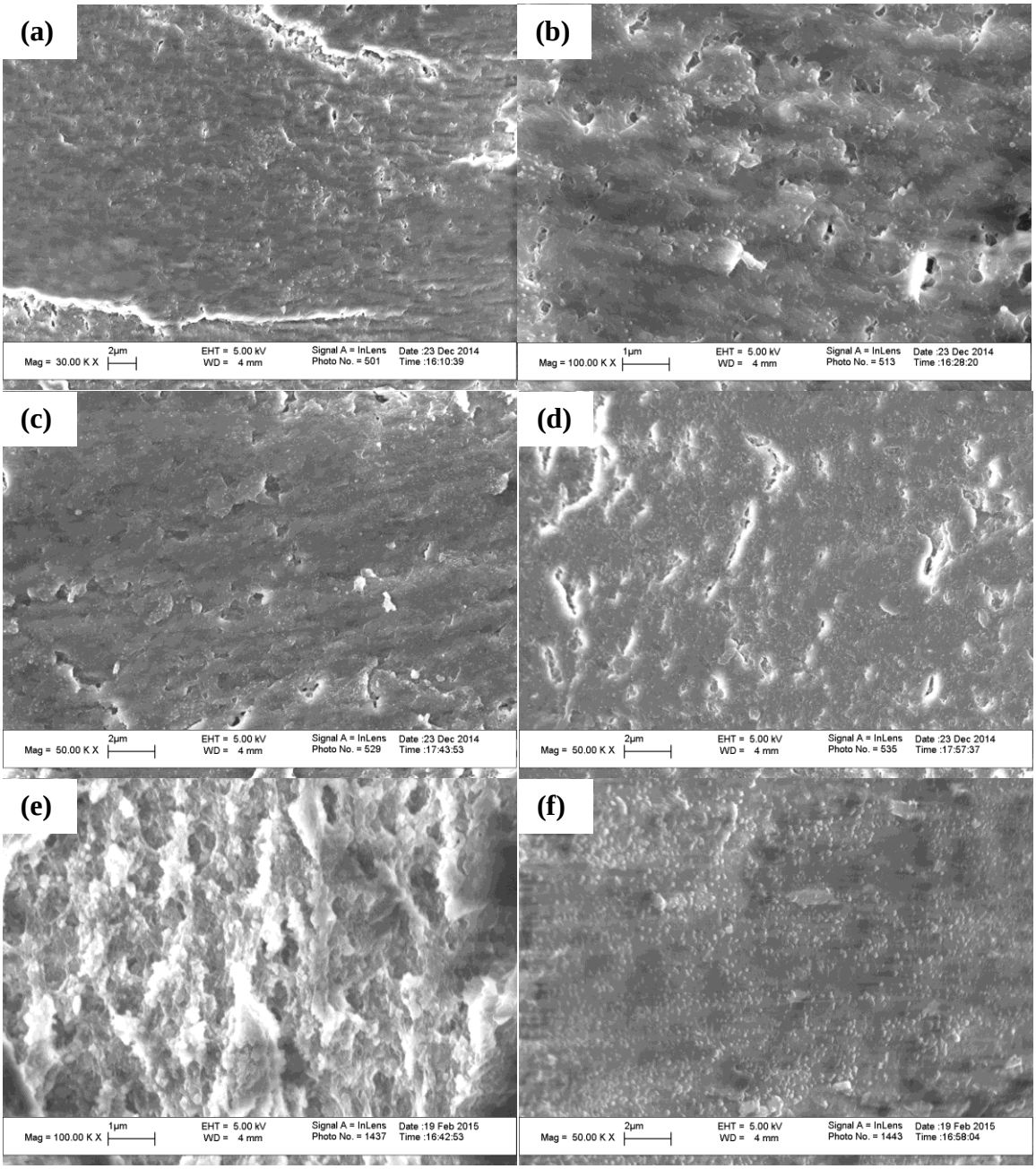

Figure 5.2 Cross sectional SEM images of the following HPMC films with various GF nanoparticle loadings: (a) DL1-15, (b) DL2-15, (c) DL3-15, (d) DL4-15, (e) DL5-15, (f) DL6-15, (g) DL1-4M, (h) DL2-4M, (i) DL3-4M, (j) DL4-4M, and (k) DL5-4M. (Continued)

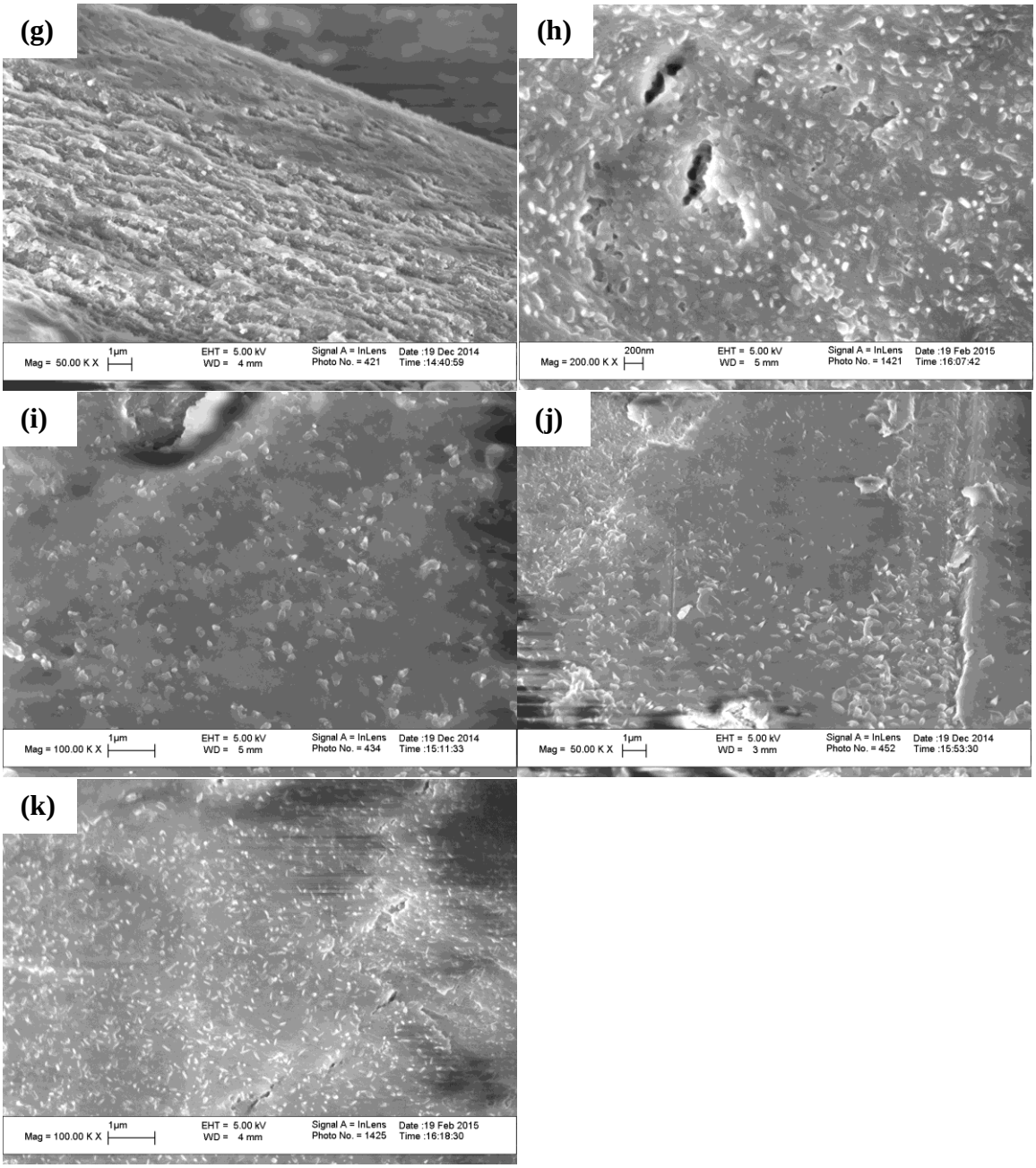

Figure 5.2 (Continued) Cross sectional SEM images of the following HPMC films with various GF nanoparticle loadings: (a) DL1-15, (b) DL2-15, (c) DL3-15, (d) DL4-15, (e) DL5-15, (f) DL6-15, (g) DL1-4M, (h) DL2-4M, (i) DL3-4M, (j) DL4-4M, and (k) DL5-4M.

5.3.3 GF Particle Size After Milling and Redispersed from Films

Since poorly water-soluble drug particles naturally exhibit slow dissolution rates, it is critical that the WSMM nanoparticles do not aggregate upon incorporation into or delivery from films, as their enhanced dissolution rate would be lost. In order to investigate the ability of the film format to stabilize and deliver poorly water soluble drug nanoparticles, even with high drug loading, films were tested for nanoparticle redispersibility in water, and the size distributions of the GF particles redispersed from films were compared to those of the nanosuspensions from which the GF nanoparticles were originally taken. Redispersion tests were performed on all films on the day of preparation, as well as after 3 and 6 months of storage under stress conditions (40 ºC, 75% RH) to assess long-term stability (stability results discussed in Section 5.3.8). Particle size distribution results, reported as 10%, 50% (median), and 90% passing sizes (d_{10}, d_{50}, and d_{90}, respectively), are shown in Figure 5.3, organized by the WSMM suspension from which the films were prepared.

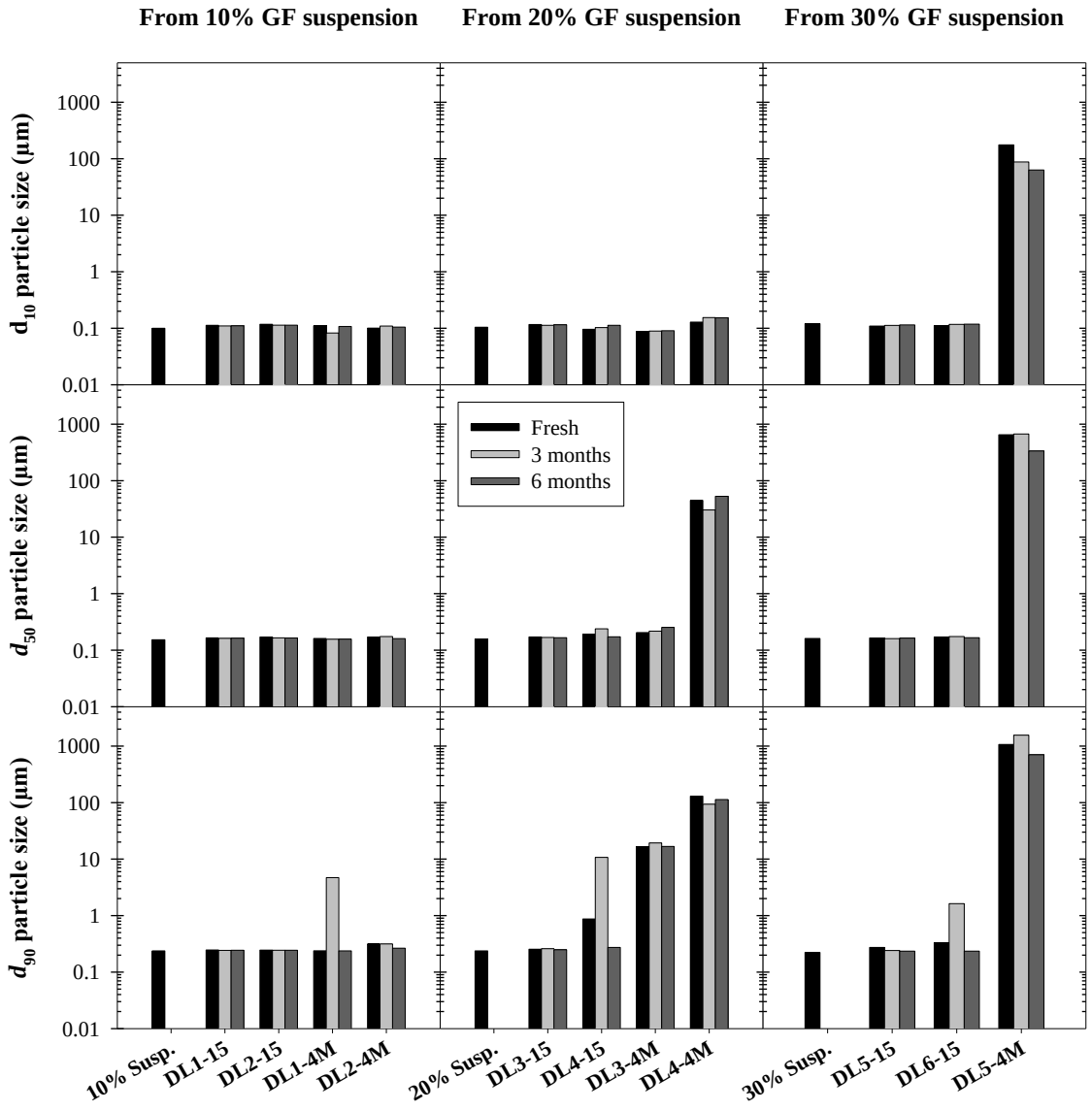

Figure 5.3 d_{10}, d_{50} and d_{90} of GF nanoparticles in suspension and redispersed from HPMC-E15 and E4M films of varying API loading after 0, 3, and 6 months' storage at 40 ºC and 75% RH.

The size of the original GF nanoparticles was recovered from all HPMC-E15 films. The same nanoparticle redispersibility was observed in HPMC-E4M films up to about 50 wt% drug loading (DL2-4M), above which original nanoparticle size could no longer be immediately recovered upon redispersion in water. In fact, coarse drug–polymer agglomerates or clusters were visible by the naked eye during redispersion tests

for DL3-4M, DL4-4M, and DL5-4M films, appearing as undissolved film clusters after the film had physically broken apart during vortex mixing, rather than appearing to grow from suspended particles. However, as shown in the cross sectional SEM images (Section 5.3.2), the GF nanoparticles are well dispersed and stabilized within all films, even those with high drug loading. Therefore, it is likely that the existence and slow dissolution of these drug–polymer agglomerates is due to interactions between the GF nanoparticles and HPMC-E4M during redispersion, rather than GF nanoparticle aggregation during film formation. Although by a different mechanism (flocculation), similar behavior was reported by Wong and Bodmeier (1996) in ethyl cellulose dispersions with HPMC. They observed flocculation at lower HPMC concentrations in dispersions with higher MW HPMC and higher poorly water-soluble solids content (ethyl cellulose), similar to how drug–polymer agglomerates were only observed upon redispersion from high MW HPMC films (E4M) above a certain GF loading (> 50 wt%) in this study.

5.3.4 GF Content and Uniformity in Films

Content uniformity tests were performed on all films in order to assess their drug content and uniformity. These results, shown in Table 5.2, are expressed in terms of film thickness, mass of GF per unit area, and GF loading by wt%. In spite of using a small sample size (roughly $1/10^{th}$ the size of a typical dose) to better elucidate potential differences between films, all HPMC-E15 films exhibited very good uniformity in terms of wt% GF (< 1% RSD) and mg GF/cm^2 (most ~3% RSD). HPMC-E4M films, on the other hand, exhibited greater variability for both, due in part to their decreased thickness. Although all films were cast to be 1000 μm thick before drying, precursor suspensions had varying water concentrations (Table 5.1), the majority of which was lost upon drying.

These differences resulted in thinner films for precursors with higher starting water concentrations, as they had less solids content, in line with the results presented in Sub-section 4.3.3.1. Consequently, although E15 and E4M precursors of the same number (e.g., DL1-15 and DL1-4M) contained roughly the same concentration of GF nanoparticles before drying, greater mass loss during drying drove up the percentage of GF remaining in the E4M films (despite having the same loading by mass per unit area).

Table 5.2 Content Uniformity of Films with Different GF Loadings

Formulation	Thickness (μm)	RSD (%)	wt% GF	RSD (%)	GF mass per unit area (mg/cm^2)	RSD (%)
DL1-15	97.2	2.8%	9.1	0.9%	1.22	4.1%
DL2-15	85.1	3.4%	19.0	0.6%	2.22	3.4%
DL3-15	109.0	2.5%	20.9	0.6%	3.18	2.9%
DL4-15	108.8	4.4%	34.6	0.4%	5.29	3.3%
DL5-15	122.9	2.1%	37.6	0.3%	6.08	2.9%
DL6-15	127.4	4.0%	49.4	0.3%	8.61	4.8%
DL1-4M	27.8	5.6%	30.5	4.6%	1.17	7.2%
DL2-4M	40.1	6.6%	51.4	0.6%	2.87	5.0%
DL3-4M	45.6	6.1%	56.4	3.4%	3.50	6.6%
DL4-4M	57.3	5.7%	69.2	1.4%	5.54	4.8%
DL5-4M	65.6	6.7%	72.8	0.3%	6.04	3.9%

5.3.5 Film Mechanical Properties

TS, YS, YM, and EB were measured for each film, with the exception of DL5-4M which was too brittle for texture analysis. As can be seen in Table 5.3, films generally exhibited TS between 35-45 MPa and YS between 30-40 MPa, demonstrating good mechanical strength regardless of GF nanoparticle loading. There was no observable trend in YM for E15 films with increasing GF nanoparticle loading, while YM appeared to increase significantly in E4M films prepared by suspensions with lower polymer-to-nanosuspension mixing ratios (Table 5.1), indicating increasing stiffness. EB decreased

dramatically with increasing drug nanoparticle loading above ~40 wt% GF. It is no surprise that one of the greatest challenges posed by high drug loading in films is simultaneously maintaining good mechanical properties for manufacture and patient compliance. Typically, film-forming polymer mass must be reduced to account for higher drug loading, reducing the integrity of the resulting film matrix. Although there are currently no fixed guidelines regarding acceptable mechanical properties of pharmaceutical films (Hoffmann et al., 2011), the brittleness of high drug loading films which exhibited EB < 5% was readily apparent as they were being handled. Steiner et al. (2016) also observed brittleness in poorly water-soluble drug nanoparticle-loaded films with similarly high drug loading using a lower MW grade of HPMC as film-forming polymer. Although it may be possible to push the maximum drug particle loading in films above 45-50 wt% while maintaining acceptable film mechanical properties with more thorough formulation development, such as modulation of plasticizer content described in Chapter 3, these results suggest that film brittleness is a major hurdle to overcome to achieve higher drug particle loadings in strip films for practical use.

Table 5.3 Mechanical Properties of Films with Different GF Loadings

Formulation*	Tensile strength (MPa)	Yield strength (MPa)	Young's modulus (GPa)	Elongation at break (%)
DL1-15	38.6 ± 0.8^{bc}	28.9 ± 1.7^{c}	2.38 ± 0.05^{d}	19.6 ± 1.3^{a}
DL2-15	40.7 ± 0.1^{abc}	30.8 ± 1.6^{bc}	2.61 ± 0.16^{d}	18.8 ± 1.6^{ab}
DL3-15	38.0 ± 0.3^{bc}	32.3 ± 3.3^{bc}	2.27 ± 0.21^{d}	18.5 ± 3.6^{ab}
DL4-15	34.5 ± 2.7^{c}	31.0 ± 1.2^{c}	1.99 ± 0.40^{d}	13.9 ± 4.3^{b}
DL5-15	41.7 ± 1.9^{ab}	41.7 ± 1.9^{a}	2.45 ± 0.24^{d}	6.1 ± 0.7^{c}
DL6-15	37.7 ± 7.1^{abc}	37.7 ± 7.1^{abc}	2.67 ± 0.12^{cd}	2.4 ± 0.7^{c}
DL1-4M	46.0 ± 3.0^{a}	35.0 ± 1.2^{abc}	3.63 ± 0.62^{bc}	13.7 ± 1.2^{b}
DL2-4M	38.3 ± 4.5^{bc}	38.3 ± 4.5^{ab}	4.80 ± 0.48^{a}	1.4 ± 0.1^{c}
DL3-4M	38.0 ± 2.1^{bc}	38.0 ± 2.1^{ab}	2.43 ± 0.59^{d}	4.2 ± 1.1^{c}
DL4-4M	42.2 ± 4.6^{abc}	36.1 ± 8.0^{abc}	4.04 ± 0.42^{ab}	2.5 ± 0.3^{c}

*DL5-4M not listed as it was impossible to cut strips due to film brittleness
[a-d]Values in each column that do not share a superscript are statistically different

When comparing directly between HPMC MWs for films with the same drug loading by mass (e.g. DL1-15 and DL1-4M), the observed trends are in line with those presented in Sub-section 4.3.3.2 which also incorporated a polymer solution viscosity matching approach. There was no statistical difference between the TS or YS of E15 and E4M films for most drug loadings (with the exception of TS for DL1). However, YM was generally lower and EB was generally higher for E15 than for E4M, suggesting that E4M films were more brittle than E15 films. As in the previous study, it is worth noting that E4M polymer solution was prepared using a lower concentration of HPMC to match the viscosity of E15 polymer solution to ensure the precursor was castable. As a result, the lower HPMC concentration (and, consequently, higher GF nanoparticle loading by wt%) in E4M films likely confounded the influence of polymer MW on film mechanical properties.

5.3.6 Dissolution

Dissolution curves for fresh films are shown in Figure 5.4, separated by HPMC MW grade. The extent of drug release relative to the estimated drug content established in Sub-section 5.3.4 decreased slightly with increasing GF loading, likely due to increasing deviation from sink conditions. There was a clear increasing trend in total release time for both HPMC-E15 and HPMC-E4M films with increasing drug nanoparticle loading up to ~50 wt% GF. Additional time required to achieve 100% drug release may be partially attributed to other factors, including increasing film thickness (Krull et al., 2016b) and varying polymer concentration as seen in Sub-section 4.3.3.3 with increasing drug loading (Table 1). Above 50 wt% GF, however, the dissolution profiles for E4M films

DL3-4M, DL4-4M, and DL5-4M exhibited statistically similar release rates according to similarity and difference factors (Boateng et al., 2012; Costa and Lobo, 2001) (Appendix A.3). These films also exhibited poor GF nanoparticle redispersibility (Section 5.3.3) and polymer–drug agglomerates were visible upon film disintegration during dissolution testing similar to those observed in redispersion tests. It appears likely that, above 50 wt% drug nanoparticle loading, the dissolution of these polymer–drug agglomerates became the controlling drug release mechanism, particularly for high MW polymers, resulting in similar release rates for all E4M films with high drug loading. When directly comparing drug release rates of E15 and E4M films with similar drug loading by mass (e.g. DL1-15 and DL1-4M), the higher MW E4M films appear to release more slowly than their E15 counterparts for all drug loadings, in line with the results presented in Sub-section 4.3.3.3.

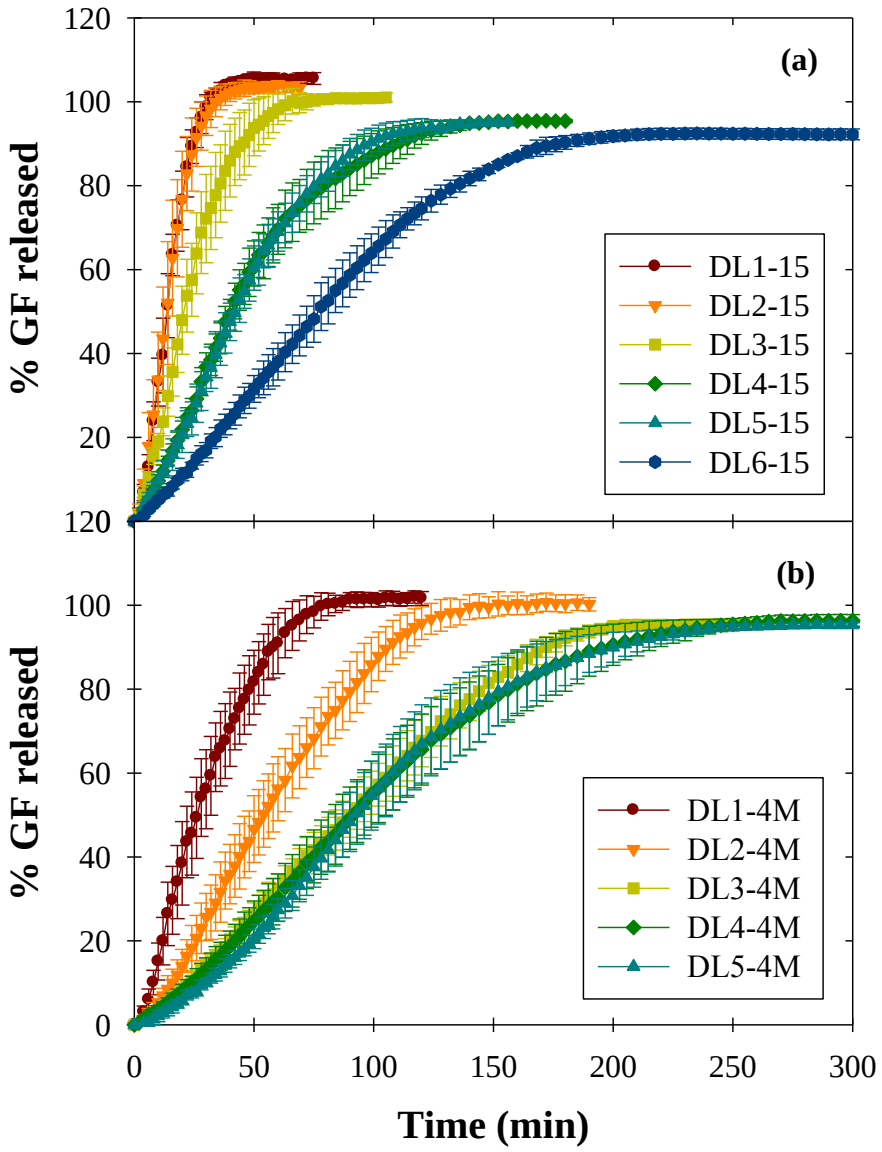

Figure 5.4 Dissolution profiles of HPMC (a) E15 and (b) E4M films with various GF nanoparticle loadings.

5.3.7 Thermogravimetric Analysis (TGA)

TGA curves for E15 and E4M films are shown in Figure 5.5a and Figure 5.5b, respectively. All films exhibited significant mass loss up to 110 ºC, most likely due to the loss of water. E15 films exhibited the greatest such loss on average (~6.5 wt%) compared to E4M films (~4.0 wt%) despite E15 precursor suspensions having less moisture content

than E4M precursor suspensions when cast. In addition, films with higher GF nanoparticle loading generally exhibited less weight loss during this time, suggesting lower moisture content. This may be due to the fact that films with higher GF concentrations exhibit greater overall hydrophobicity, driving out additional moisture during drying, resulting in films with less moisture content. Films with higher GF nanoparticle loading also contained lower concentrations of hydrophilic HPMC, which is expected to retain some moisture even after the film dries, likely resulting in lower moisture content. The significant weight loss after holding at 150 ºC for 15 min was most likely due to the loss of the plasticizer glycerin. Relative weight loss between film formulations during this time was generally in line with the plasticizer concentrations in the precursor suspensions (Table 5.1).

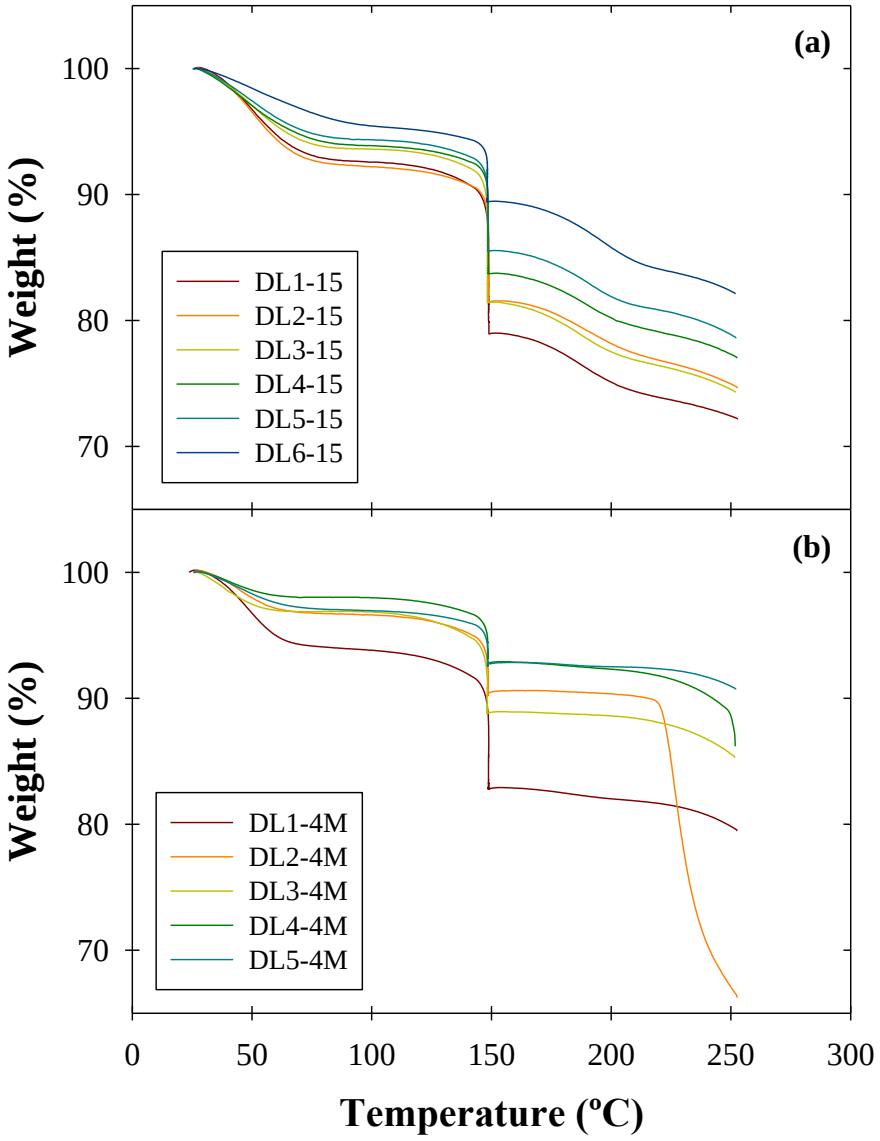

Figure 5.5 TGA curves for HPMC (a) E15 and (b) E4M films with various GF nanoparticle loadings.

5.3.8 Long-term Stability of Films

Redispersion and dissolution tests were performed for all film formulations over the course of six months' storage at 40 ºC and 75% RH to simulate the effects of long-term storage on the ability of the film format to preserve drug nanoparticle size and enhanced drug dissolution rate. First, the effect of long-term storage on the ability to recover GF

nanoparticles from films via redispersion in water was assessed (Figure 5.3). Aside from order of magnitude increases in the d_{90} of a select three films for 3 month samples only (DL1-4M, DL4-15, DL6-15), there was no observable impact of long-term storage on GF nanoparticle redispersibility from films. The ability to recover GF nanoparticles after 6 months of storage under stress conditions was demonstrated for all E15 films and E4M films with 50 wt% drug loading or less. Interestingly, long-term storage did not appear to influence the inability to immediately recover GF nanoparticles from E4M films with higher drug loading, as the particle size statistics for such films did not appear to deviate significantly after storage.

Dissolution tests were also performed on films following 0, 3, and 6 months' storage at 40 ºC and 75% RH in order to investigate the effect of long-term storage on the drug dissolution rate from films. Four of six E15 film formulations exhibited similar rates of drug release after 3 and 6 months' storage according to similarity and difference factors (Appendix A.3) while the remaining two formulations, DL2-15 and DL6-15, were not drastically different (Figure 5.6). This suggests that drug release rates from E15 films are relatively stable, even after long-term storage, for a wide range of drug nanoparticle loadings. On the other hand, while E4M films exhibited similar release profiles after 3 months' storage, they appeared to release drug more quickly after 6 months of storage, particularly from high drug loading films for which polymer–drug agglomerates were observed during initial redispersion and dissolution tests (Figure 5.7). It is possible that prolonged exposure to high humidity weakened the interaction between HPMC-E4M and GF nanoparticles within the film, resulting in faster dissolution of the polymer–drug agglomerates. However, as seen in redispersion tests from the same films, the

agglomerates do not dissolve immediately, requiring a short induction time (~10-20 min) before dissolving.

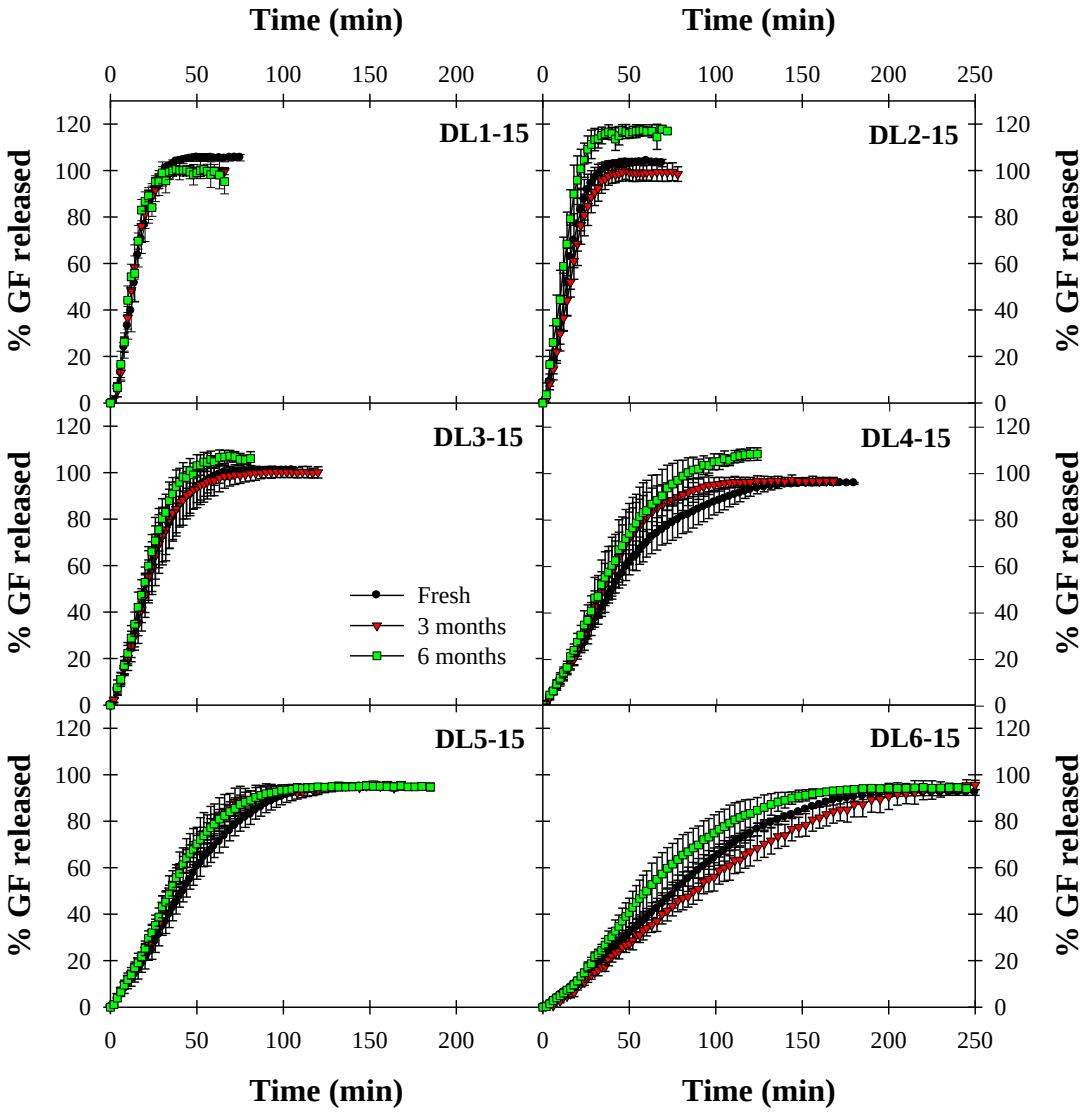

Figure 5.6 Comparison of dissolution profiles for E15 films immediately after film preparation, after 3 months of storage at 40 °C, 75% RH, and after 6 months of storage at 40 °C, 75% RH. Values are mean ± SD, n = 6.

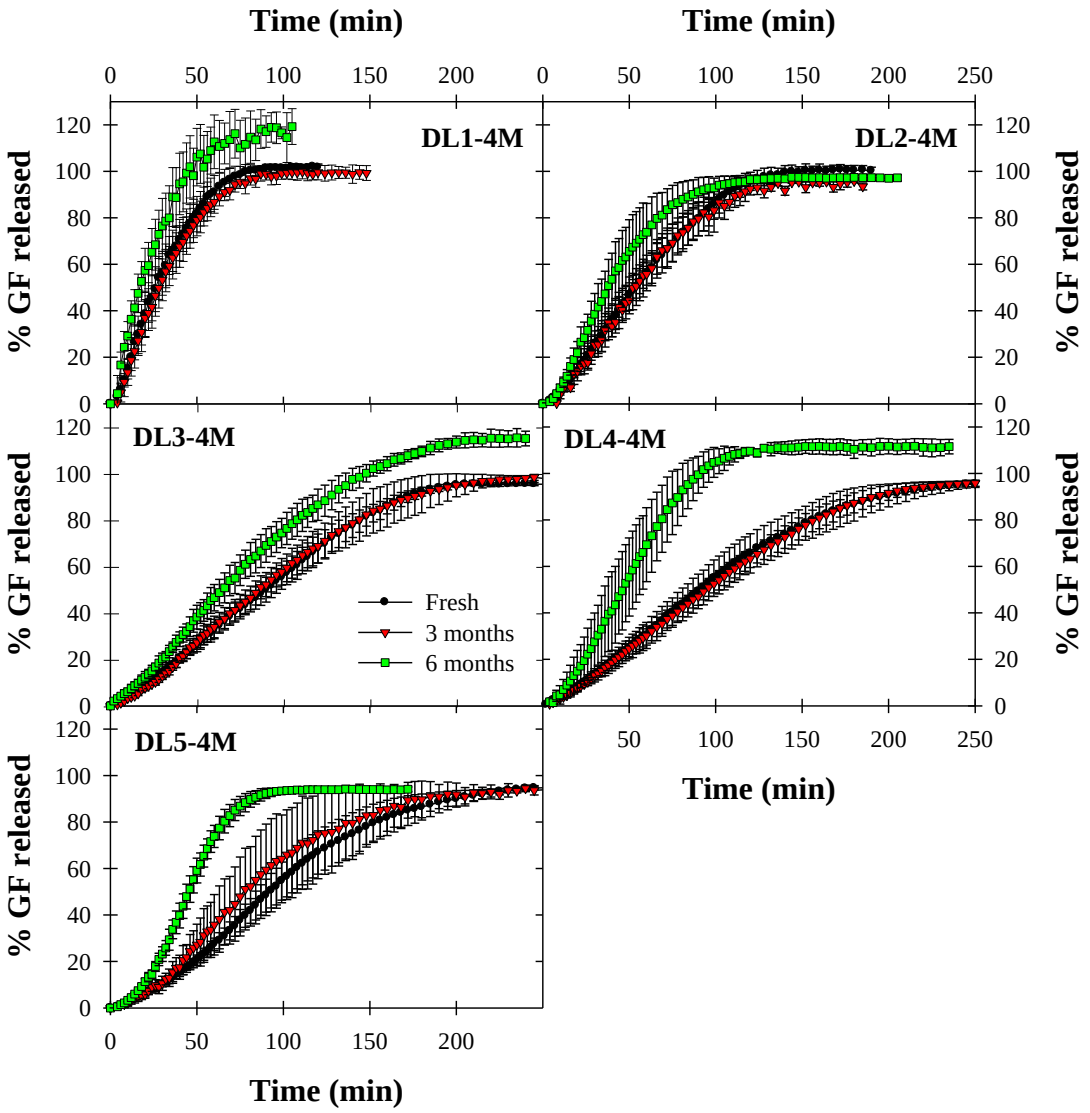

Figure 5.7 Comparison of dissolution profiles for E4M films immediately after film preparation, after 3 months of storage at 40 °C, 75% RH, and after 6 months of storage at 40 °C, 75% RH. Values are mean ± SD, n = 6.

5.4 Conclusions

The objective of this work was to investigate the capability of producing strip film dosages containing high loadings of poorly water-soluble drug nanoparticles with good mechanical properties that retain the enhanced dissolution rate of the drug nanoparticles. While drug loadings of 50 wt% and 73 wt% were achieved in HPMC-E15 and E4M

films, respectively, films with drug loadings above 40-50 wt% were unacceptably brittle, imposing a practical drug loading limitation for films with good mechanical properties. In addition, undissolved polymer–drug agglomerates were observed upon redispersion and dissolution from E4M films with drug loadings above 50 wt%, severely limiting the ability to recover the embedded GF nanoparticles and retain their enhanced dissolution upon delivery. In spite of these challenges, all film formulations exhibited good content uniformity (6% RSD or less) and were able to preserve the size and morphology of the GF nanoparticles. These results suggest that the greatest barriers to producing pharmaceutical films with high loadings of poorly water-soluble drug nanoparticles are overcoming poor film mechanical properties and ensuring recovery of the embedded drug nanoparticles, both of which can be conceivably overcome by further formulation development.

CHAPTER 6

DISSOLUTION MODEL FOR DRUG PARTICLE-LADEN FILMS

6.1 Introduction

One of the most crucial elements when developing a pharmaceutical product is the ability to deliver the appropriate dose at the correct time. This holds true regardless of the dosage form, from tablets to films and everything in-between. Drug release from pharmaceutical systems is commonly controlled by embedding the drug in a polymeric matrix. In doing so, the polymer generally serves as a diffusion barrier for the embedded drug, restricting its release from the dosage form in a controllable manner (Langer and Peppas, 1981). This predictability led to extensive use of simple empirical models such as the Higuchi equation (Higuchi, 1963) for fitting drug release from polymer matrices which did not swell or erode (Peppas, 1985). In addition, these simple models also assume the drug incorporated into the system is water-soluble and that the drug dissolves immediately upon exposure to solvent. However, in systems with swellable/erodible polymer or poorly water-soluble drugs, these simple models break down, necessitating the use of more complex models. Improved understanding of the mechanisms governing controlled release from pharmaceutical products and advancements in computational efficiency have paved the way for the development of mathematical models that predict the rate of drug release from a given system. Such predictive models have typically been used to simulate controlled or extended release, as precision dosing is critical for such applications, but this restriction allows for the implementation of certain assumptions that generally do not apply in immediate release systems.

While predictive modeling for film dissolution has been a growing topic of discussion in recent literature, few proposed models, if any, have been able to encompass all of the nuances present in poorly water-soluble particle-loaded polymer films for immediate release. Siepmann et al. (1999) developed a Fickian diffusion-based mass transport model for swellable polymer tablets containing water-soluble drug and poorly-soluble drug (Siepmann et al., 2013) assuming instantaneous absorption of water. Frenning (2003) modeled drug particle dissolution from a non-swellable, non-erodible planar matrix assuming instant solvent absorption. Wu et al. (2005) simulated release of a water-soluble drug from swellable/erodible polymer tablets while taking water penetration into consideration and only considering polymer dissolution from the tablet surface. Borgquist et al. (2006) simulated release of both soluble and poorly-soluble drug from swellable/erodible poly (ethylene oxide) tablets for extended release (10-30 h), only considering polymer dissolution from the tablet surface. Cabrera et al. (2006) modeled release of arbitrarily placed drug particles from planar polymeric systems assuming a non-swellable, non-erodible matrix, averaging drug particle concentration within layers as continuous drug dissolution sources. Zhang et al. (2006) developed a diffusion–dissolution model for poorly water-soluble drug particle release from polymeric microspheres considering a moving dissolution boundary and particle size distribution. Xiang and McHugh (2011) developed a generalized diffusion–dissolution model for non-swellable, non-erodible polymer matrices containing amorphous drug and dispersed drug particles. However, most of these models focus on diffusion as the limiting drug release mechanism and none of them considered polymer swelling/erosion, poorly water-soluble drug dissolution, and non-instantaneous water absorption simultaneously.

This chapter introduces a predictive mathematical model for poorly water-soluble drug particle release from polymer films developed from first principles and compares simulated dissolution profiles to experimental data from previous chapters.

6.2 Mathematical Model

A schematic of the model for drug nanoparticle release from a film matrix is shown in Figure 6.1. The film has an initial thickness $L = L_0$ at time $t = 0$. While the depicted example shows an impermeable wall boundary at $x = 0$, the same model is also applicable if the wall boundary is replaced by an identical film of equal thickness on the opposite side of the origin due to symmetry, in which case L becomes the half-thickness.

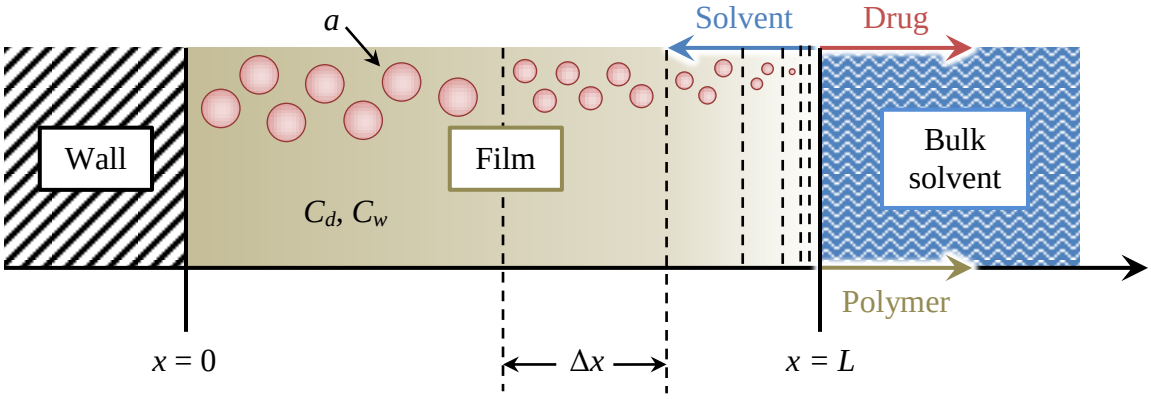

Figure 6.1 Process schematic of drug nanoparticle release from film matrix.

6.2.1 Model Assumptions

The underlying assumptions of the mathematical model are: (i) all mass transport and polymer swelling/erosion is effectively one-dimensional (i.e. occurs strictly in the x direction) since the surface area of the film is orders of magnitude larger than the film thickness, (ii) all drug within the film is initially undissolved, (iii) all diffusion can be described by Fick's second law, (iv) drug particle dissolution can be explained by a rate

equation based on the Noyes–Whitney equation (Noyes and Whitney, 1897), (v) drug particle size is uniform throughout each film cross-sectional layers, but can vary between layers (vi) drug particles are initially spherical in shape and retain their spherical shape throughout dissolution, (vii) drug and solvent diffusion coefficients can be described by a Fujita-type free-volume model, (viii) the total volume of the system is equal to the sum of the volumes of drug, solvent, and polymer in the system, (ix) polymer swelling is homogenous, (x) polymer dissolution occurs strictly at the surface of the film ($x = L$) at a fixed, linear rate until all polymer is dissolved (xi), no dissolved drug exists at the film-solvent boundary (i.e. sink conditions), (xii) external mass transfer resistance is negligible.

6.2.2 Mass Balances

Drug and solvent concentrations throughout the matrix are expressed by $C_d(x, t)$ and $C_w(x, t)$ in Equations (6.1) and (6.2), respectively:

$$\frac{\partial C_d}{\partial t} = \frac{\partial}{\partial x}\left(D_d \frac{\partial C_d}{\partial x} \right) + k_d n a \left(C_s - C_d \right) \tag{6.1}$$

$$\frac{\partial C_w}{\partial t} = \frac{\partial}{\partial x}\left(D_w \frac{\partial C_w}{\partial x} \right) \tag{6.2}$$

where D_d and D_w, are the diffusion coefficients of drug and solvent in equilibrium swollen polymer, respectively, k_d is the drug dissolution rate constant, n is the number of drug particles per unit volume film, a is the surface area of a single drug particle, C_s is the solubility of the drug in the solvent, x is the spatial coordinate, and t is time. The first

term of each is the diffusion rate determined by Fick's second law, and the second term of Equation (6.1) describes dissolution of undissolved drug into the dissolved state. The diffusivities of drug and solvent, D_d and D_w, are assumed to follow a Fujita-type exponential dependence on concentration based on free-volume theory given in Equation (6.3):

$$D_i = D_{ie} e^{-\beta_i (1 - C_i / C_{ie})} \tag{6.3}$$

where i represents either drug or solvent, β_i is a constant, and the subscript e indicates an equilibrium value in fully swollen polymer. The surface area of a single drug particle, a, is given by Equation (6.4):

$$\frac{da}{dt} = -\frac{2k_d}{3m_0} \sqrt{a_0^{\,3} a} \left(C_s - C_d \right) \tag{6.4}$$

where m_0 is the mass of a single drug particle and a_0 is the initial surface area of a single drug particle. The evolution of film thickness, L, can be derived from a total volume balance on the system, given by Equation (6.5), since volumes are assumed to be additive:

$$\begin{aligned} V = LWH = {} & \frac{1}{\rho_d} \int_0^H \int_0^W \int_0^L C_d \left(x, t \right) dxdydz + \frac{1}{\rho_w} \int_0^H \int_0^W \int_0^L C_w \left(x, t \right) dxdydz \\ & + \frac{1}{\rho_p} \left(\rho_p C_{p0} L_0 WH - \int_0^t K_p WH d\hat{t} \right) \end{aligned} \tag{6.5}$$

where V is the total volume of the system, W and H are the width and height of the film, respectively, making up the area perpendicular to all mass transfer, ρ_d, ρ_w, and ρ_p are the densities of drug, solvent, and polymer, respectively, C_{p0} is the initial polymer concentration, K_p is the polymer dissolution rate constant, and $\hat{t}$ is a dummy variable for integration. Since all mass transfer, swelling, and erosion are assumed to occur in the x direction and the cross-sectional area does not change with time, this reduces to Equation (6.6):

$$L = \frac{1}{\rho_d}\int_0^L C_d\left(x,t\right)dx + \frac{1}{\rho_w}\int_0^L C_w\left(x,t\right)dx + \frac{1}{\rho_p}\left(\rho_p C_{p0} L_0 - \int_0^t K_p d\hat{t}\right) \tag{6.6}$$

Differentiating with respect to time yields Equation (6.7):

$$\frac{dL}{dt} = \frac{1}{\rho_d}\frac{d}{dt}\left[\int_0^L C_d dx\right] + \frac{1}{\rho_w}\frac{d}{dt}\left[\int_0^L C_w dx\right] - \frac{1}{\rho_p}\frac{d}{dt}\left[\int_0^t K_p d\hat{t}\right] \tag{6.7}$$

These balance equations are subject to the following initial (Equation (6.8)) and boundary conditions (Equation (6.9)):

$$\begin{array}{llll} t=0 & & L=L_0 & \\ t=0 & 0\le x\le L & C_d=0 & a=a_0 \\ t=0 & 0\le x< L & C_w=0 & \\ t=0 & x=L & C_w=C_{we} & \end{array} \tag{6.8}$$

$$
\begin{aligned}
&x = L \qquad C_d = 0 \qquad C_w = C_{we} \\
&x = 0 \qquad \frac{\partial C_d}{\partial x} = k_d n a \left(C_s - C_d \right) \qquad \frac{\partial C_w}{\partial x} = 0
\end{aligned}
\tag{6.9}
$$

6.2.3 Dimensionless Variables and Parameters

For the sake of generality regarding numerical results and discussion, all proceeding mathematical expressions will be expressed in terms of the dimensionless variables and parameters given by Equation (6.10):

$$
\begin{aligned}
&\overline{C_d} = C_d / C_{de} \qquad \overline{C_w} = C_w / C_{we} \qquad \overline{C_s} = C_s / C_{de} \qquad \overline{D_d} = D_d / D_{we} \\
&\overline{D_w} = D_w / D_{we} \qquad \tau = D_{we} t / L_0^{\,2} \qquad \eta = L / L_0 \qquad y = x / L \\
&\kappa = k_d L_0^{\,2} n a_0 / D_{we} \qquad \overline{K_p} = K_p L_0 / \rho_p D_{we} \qquad \alpha = a / a_0
\end{aligned}
\tag{6.10}
$$

Since the mathematical model under investigation is a moving boundary problem, a front-fixing method was employed. This method was first proposed by Landau (1950) and first applied to a finite-difference scheme by Crank (1957). This coordinate transformation results in an apparent pseudo-convective (second) term in the transformed equations for dimensionless drug ($\overline{C_d}$) and solvent ($\overline{C_w}$) concentrations, given by Equations (6.11) and (6.12), respectively:

$$
\frac{\partial \overline{C_d}}{\partial \tau} = \frac{1}{\eta^2} \frac{\partial}{\partial y} \left(\overline{D_d} \frac{\partial \overline{C_d}}{\partial y} \right) - \frac{y}{\eta} \frac{d\eta}{d\tau} \frac{\partial \overline{C_d}}{\partial y} + \kappa \alpha \left(\overline{C_w}\,\overline{C_s} - \overline{C_d} \right) \tag{6.11}
$$

$$\frac{\partial \overline{C_w}}{\partial \tau} = \frac{1}{\eta^2}\frac{\partial}{\partial y}\left(\overline{D_w}\frac{\partial \overline{C_w}}{\partial y}\right) - \frac{y}{\eta}\frac{d\eta}{d\tau}\frac{\partial \overline{C_w}}{\partial y} \tag{6.12}$$

Following similar transformations, dimensionless particle surface area is given by Equation (6.13):

$$\frac{d\alpha}{d\tau} = -\frac{2}{3}\kappa\sqrt{\alpha}\,\frac{C_{de}}{m_0 n}\left(\overline{C_w}\,\overline{C_s} - \overline{C_d}\right) \tag{6.13}$$

and dimensionless film thickness is given by Equation (6.14):

$$\frac{d\eta}{d\tau} = \frac{\frac{1}{\eta}\left(\frac{C_{de}}{\rho_d}\int_0^1\left[\frac{\partial}{\partial y}\left\{\overline{D_d}\frac{\partial \overline{C_d}}{\partial y}\right\}dy\right] + \frac{C_{we}}{\rho_w}\int_0^1\left[\frac{\partial}{\partial y}\left\{\overline{D_w}\frac{\partial \overline{C_w}}{\partial y}\right\}dy\right]\right) - \overline{K_p}}{1 + \frac{C_{de}}{\rho_d}\left(\int_0^1\left[y\left\{\frac{\partial \overline{C_d}}{\partial y}\right\}dy\right] - \overline{C_d}\Big|_{y=1}\right) + \frac{C_{we}}{\rho_w}\left(\int_0^1\left[y\left\{\frac{\partial \overline{C_w}}{\partial y}\right\}dy\right] - \overline{C_w}\Big|_{y=1}\right)} \tag{6.14}$$

6.2.4 Numerical Procedure

Equations (6.11)-(6.14) were solved simultaneously in Matlab® (R2015b, Mathworks) using ode15s. Since the above is a system of partial differential equations (PDEs), it needed to be reduced to a system of ordinary differential equations (ODEs) in order to be solvable using Matlab. This was accomplished using the finite difference approximations given in Equation (6.15) and Equation (6.16):

$$\frac{\partial \overline{C_j}}{\partial y} \approx \frac{\overline{C_{j+1}} - \overline{C_{j-1}}}{\Delta y_j + \Delta y_{j-1}} \tag{6.15}$$

$$\frac{\partial^2 \overline{C_j}}{\partial y^2} \approx \frac{\left(\frac{\overline{C_{j+1}} - \overline{C_j}}{\Delta y_j} \right) - \left(\frac{\overline{C_j} - \overline{C_{j-1}}}{\Delta y_{j-1}} \right)}{\left(\frac{\Delta y_j + \Delta y_{j-1}}{2} \right)} \tag{6.16}$$

where *j* is an index value indicating a point on the spatial grid *y*. All calculations were performed using double precision values and arithmetic. The total number of grid points necessary, 101 for both τ and *y*, was determined by evaluating the lowest number of points that produced results within 0.1% relative error of the results produced with double the number of points. The same tolerance of 0.1%, relative and absolute, was employed when solving the ODE system. In order to account for the large concentration gradients at the solvent boundary during dissolution, spatial points were distributed according to a geometric progression rate of 1.0125 so that additional points would be present near the solvent boundary.

6.3 Experimental Procedures

Experimental procedures for viscosity, GF particle size after milling and redispersed from films, determination of drug content and uniformity in films, and flow-through cell dissolution (USP IV) are identical to their respective procedures described in Section 3.2.

6.3.1 Materials

Griseofulvin (GF; Letco Medical, Decatur, AL) was selected as a model Biopharmaceutics Classification System (BCS) class II drug. Two different viscosity grades of hydroxypropyl methylcellulose (HPMC; Methocel E15 Premium LV, MW ~14 kDa; and E4M Premium, MW ~88 kDa; The Dow Chemical Company, Midland, MI) served as film-formers. E4M samples were generously donated by The Dow Chemical Company. HPMC-E15LV also served as a nanoparticle stabilizer during WSMM, along with the surfactant sodium dodecyl sulfate (SDS; Fisher Scientific, Pittsburgh, PA). Glycerin (Sigma–Aldrich, St. Louis, MO) was used as a film plasticizer. GF particle size reduction was performed by WSMM according to Sub-section 6.3.2.1. All other materials were used without further processing.

6.3.2 Methods

6.3.2.1 Preparation of GF Nanosuspension. GF nanosuspensions were prepared via WSMM using a Netzsch mill (Microcer, Fine Particle Technology LLC, Exton, PA). Methods and stabilizer concentrations were selected according to previous optimization studies (Bilgili and Afolabi, 2012; Monteiro et al., 2013). The suspensions consisted of 10% GF dispersed in a stabilizer solution of 2.5% HPMC-E15LV and 0.5% SDS (all w/w wrt water). One suspension was milled for 4 min (partially milled) and the other was milled for 120 min (equilibrium particle size). For comparison of particle sizes, a third suspension of identical composition was also prepared but not run through the mill (0 min). A single GF nanosuspension formulation was used across all film formulations, as opposed to using different polymer MWs for each film formulation, to ensure consistency in the size and morphology of the milled GF particles (for a thorough

investigation of the effect of polymer MW in WSMM, readers are referred to Li et al. (2016)). This meant that the HPMC-E15LV stabilizer, which adsorbed onto the surface of the GF nanoparticles during milling, was present in all film precursors, including those that used E4M as film-former.

6.3.2.2 Preparation of Polymer Solutions and Film Precursor Suspensions. Formulations for film-forming polymer solutions and film precursor suspensions are listed in Table 6.1. Three of the most critical material film attributes (CMAs) in determining drug release rate were selected for analysis based on prior experience: dry film thickness (Krull et al., 2016b), film-forming polymer molecular weight (MW) (see Sub-section 4.3.3.3), and drug particle size (Krull et al., 2016b). Polymer and plasticizer concentrations for polymer solutions were selected in such a way that all resulting film precursor formulations would be castable but not spread during drying (target viscosity range of 5,000-12,000 cP). This was accomplished using a viscosity matching approach for polymer solution preparation outlined in Sub-section 4.2.2.2 for the polymer solutions, represented by 0's in Table 6.1. E15 and E4M concentrations in the mixed formulation (B) were selected such that each polymer would contribute roughly equally to the viscosity of the combined polymer solution. Polymer solutions were prepared by adding the appropriate amounts of HPMC and plasticizer to water at 90 ºC, after which the solution was allowed to cool to room temperature under continuous magnetic stirring. Polymer solutions were mixed with GF nanosuspensions in a 2:1 ratio by mass using a Thinky ARE-310 planetary centrifugal mixer (Thinky, Laguna Hills, CA) at 2,000 rpm for 30 s, followed by 7 min of deaeration at 2,200 rpm, to form film precursor

suspensions. If bubbles were still present in the precursor suspension after mixing, the precursor was left overnight to settle before casting.

Table 6.1 Composition and Viscosity of Polymer Solutions and Film Precursor Suspensions

Sample	HPMC	Target d_{50} (nm)	Wet film thickness (μm)	wt% GF	wt% HPMC E15	wt% HPMC E4M	wt% Glycerin	wt% SDS	Viscosity (cP)
A0	E15	N/A	N/A	N/A	18.8%	0.0%	6.3%	N/A	12,910
B0	Mix*	N/A	N/A	N/A	8.2%	1.5%	3.2%	N/A	22,590
C0	E4M	N/A	N/A	N/A	0.0%	3.4%	1.1%	N/A	20,420
A1-50	E15	160	500	2.9%	10.7%	0.0%	3.3%	0.06%	4,610
A1-100	E15	160	1,000	2.9%	10.7%	0.0%	3.3%	0.06%	4,610
A1-150	E15	160	1,500	2.9%	10.7%	0.0%	3.3%	0.06%	4,610
B1-50	Mix*	160	800	2.9%	6.2%	1.0%	2.1%	0.06%	8,190
B1-100	Mix*	160	1,500	2.9%	6.2%	1.0%	2.1%	0.06%	8,190
B1-150	Mix*	160	2,700	2.9%	6.2%	1.0%	2.1%	0.06%	8,190
C1-50	E4M	160	1,550	2.9%	0.0%	2.9%	0.7%	0.06%	11,550
A2-50	E15	630	500	2.9%	10.7%	0.0%	3.3%	0.06%	4,110
A2-100	E15	630	1,000	2.9%	10.7%	0.0%	3.3%	0.06%	4,110
A2-150	E15	630	1,550	2.9%	10.7%	0.0%	3.3%	0.06%	4,110
B2-50	Mix*	630	800	2.9%	6.2%	1.0%	2.1%	0.06%	5,440
C2-50	E4M	630	1,550	2.9%	0.0%	2.9%	0.7%	0.06%	7,270
A3-50	E15	15,000	500	2.9%	10.7%	0.0%	3.3%	0.06%	5,560
A3-100	E15	15,000	1,150	2.9%	10.7%	0.0%	3.3%	0.06%	5,560
A3-150	E15	15,000	1,550	2.9%	10.7%	0.0%	3.3%	0.06%	5,560
B3-50	Mix*	15,000	800	2.9%	6.2%	1.0%	2.1%	0.06%	6,240
C3-50	E4M	15,000	1,550	2.9%	0.0%	2.9%	0.7%	0.06%	7,400

*Mix refers to an equal viscosity mixture of E15 and E4M

6.3.2.3 Preparation of GF Nanoparticle-Laden Films. Film precursor suspension was manually cast onto a stainless steel substrate with a doctor blade (Elcometer, MI) at varying thickness according to Table 6.1 such that 50, 100, and 150 film formulations would be approximately 50, 100, and 150 μm in dry thickness, respectively. Wet films were then dried in the convective zone of a Lab-Cast Model TC-71LC Tape Caster (HED International, NJ) in batch mode at 50 ºC under laminar air flow for a period of 1 h

(Davé et al., 2014). The films were peeled from the substrate after drying and stored in individual sealed plastic bags for characterization.

6.4 Results and Discussion

6.4.1 System Parameters and Film Properties

In order to accurately predict the dissolution performance of a given film, several system parameters and film properties must be identified. System parameters for the various components used in this study are shown in Table 6.2. These values were used in all model calculations (with the exception of k_d which will be explained in Section 6.4.3). In terms of film properties, some are fixed based on formulation (e.g. polymer MW and initial polymer concentration) while others must either be confirmed or measured (e.g. drug mass per unit area, dry film thickness, and drug particle size). These properties for all film formulations under investigation are shown in Table 6.3.

Table 6.2 System Parameters

Component	Type	Property	Symbol	Value	Unit	Reference
Griseofulvin	Drug	Solubility in 5.4 mg/ml SDS	C_S	33.7	mg/cm^3	Mosharraf and Nyström (1995)
Griseofulvin	Drug	Diffusion coefficient in swollen polymer	D_{de}	2.0×10^{-6}	cm^2/s	This work
Griseofulvin	Drug	Density	ρ_d	1.40	g/cm^3	-
Griseofulvin	Drug	Concentration dependence constant for Equation (6.3)	β_d	2.0	-	-
Griseofulvin	Drug	Surface-specific dissolution rate	k_d	2.9×10^{-4}	cm/s	Mosharraf and Nyström (1995)
5.4 mg/ml SDS in water	Solvent	Diffusion coefficient in swollen polymer*	D_{we}	1.7×10^{-5}	cm^2/s	Masaro et al. (1999)
5.4 mg/ml SDS in water	Solvent	Density*	ρ_w	1.00	g/cm^3	-
5.4 mg/ml SDS in water	Solvent	Concentration dependence constant for Equation (6.3)*	β_w	2.0	-	-
HPMC in water	Polymer	Density	ρ_p	1.29	g/cm^3	Dow (2002)

*Values taken for water assuming 5.4 mg/ml SDS solution behaves similarly to water

Table 6.3 Properties of Individual Films Determined by Formulation or Experiment

Sample	Average HPMC MW (g/mol)	d_{50} of redispersed particles (nm)	Dry film thickness (µm)	Drug mass per unit area (mg/cm^2)	Polymer mass per unit area (mg/cm^2)
A1-50	14,167	161	44.5	0.74	2.71
A1-100	14,167	162	82.2	1.74	6.33
A1-150	14,167	154	126.3	2.50	9.10
B1-50	63,410	161	49.9	1.35	3.35
B1-100	63,410	160	96.3	2.73	6.77
B1-150	63,410	160	129.8	3.79	9.39
C1-50	87,800	156	52.0	2.33	2.33
A2-50	14,167	1,804	35.8	0.67	2.45
A2-100	14,167	1,535	89.4	1.58	5.74
A2-150	14,167	2,179	117.9	2.50	9.11
B2-50	63,410	5,492	48.6	1.31	3.25
C2-50	87,800	26,714	68.1	2.94	2.94
A3-50	14,167	13,608	39.9	0.69	2.53
A3-100	14,167	15,115	90.1	1.73	6.30
A3-150	14,167	10,695	132.7	2.73	9.94
B3-50	63,410	9,464	54.1	1.37	3.40
C3-50	87,800	10,077	64.1	2.83	2.83

Other parameters, such as C_{we} and K_{p0}, were expected to be dependent on the MW of the film-forming polymer. This is due to the fact that higher MW HPMC exhibits significantly more swelling and erodes more slowly when exposed to solvent. To account for these phenomena, these parameters were fitted to experimental dissolution data for films incorporating GF particles milled to an equilibrium median size of ~160 nm (denoted by a 1 in Table 6.3). The resulting relationships are expressed in Equation (6.17) and Equation (6.18), respectively:

$$C_{we} = \left(3.40 \times 10^{-6}\right) \times MW + 0.652 \tag{6.17}$$

$$K_{p0} = \left(-3.84 \times 10^{-11}\right) \times MW + 3.52 \times 10^{-6} \tag{6.18}$$

6.4.2 Influence of System Parameters

In order to assess the capability of the mathematical model to capture changes in relevant system parameters, a sensitivity analysis was performed in which nine parameters were adjusted above and below a base value to observe their impact on the release profiles of poorly water-soluble drug particle-laden polymer films (Figure 6.2). The base values selected were those used for formulation A1-100.

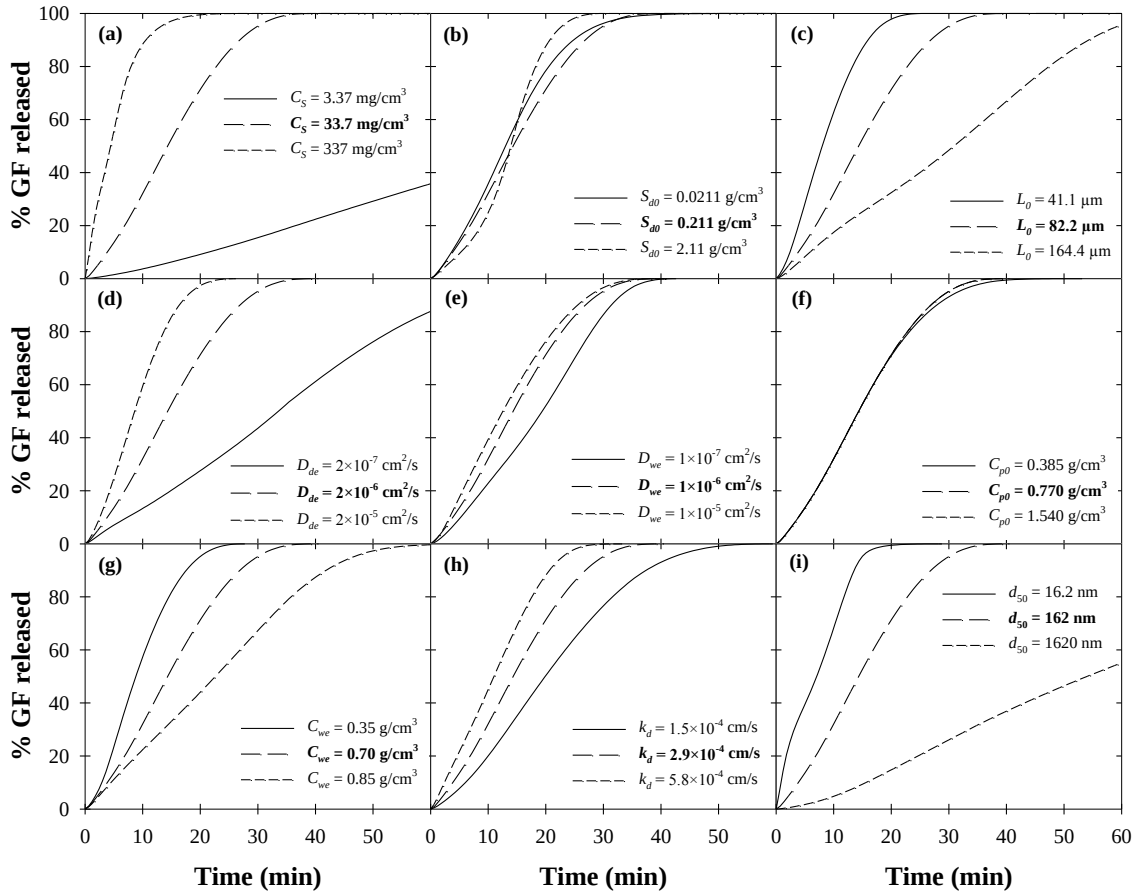

Figure 6.2 Predicted impact of the following system parameters on release profiles of poorly water-soluble drug particle-laden polymer films based on the mathematical model: (a) C_S, (b) S_{d0}, (c) L_0, (d) D_{de}, (e) D_{we}, (f) C_{p0}, (g) C_{we}, (h) k_d, and (i) d_{50}. Bold lettered values in each legend are based on formulation A1-100.

Figure 6.2a reveals an expected trend of slower predicted dissolution for less soluble drug (C_S). Specifically, below a critical solubility, drug particle dissolution becomes the dominant release mechanism, resulting in a dramatic decrease in predicted release rate. Interestingly, initial undissolved drug concentration (S_{d0}) did not appear to have a significant impact on rate of drug release (Figure 6.2b). This was partially due to the fact that, above a critical loading, the polymer film is likely to erode away entirely before the drug particles have dissolved, fully exposing the previously embedded drug particles to the bulk solvent and accelerating their dissolution. It is also worth noting that

the highest drug loading shown in Figure 6.2b exceeds what can be practically achieved in films (more than three times initial polymer concentration) and is simply shown as an extreme example. Figure 6.2c revealed the expected trend that increasing initial film thickness (L_0) leads to a roughly proportional increase in predicted total release time. The slight dip in dissolution rate observed in the dissolution profile predicted for the thickest film is likely the result of additional time required for complete swelling, as the dissolution rate picks up again after the solvent concentration throughout entire film reaches C_{we}. Faster predicted drug release can be observed with increasing D_{de} in Figure 6.2d, as drug diffusion occurs fast enough to no longer limit the rate of drug release. Increasing the rate of solvent diffusion (D_{we}) also led to faster predicted drug release (Figure 6.2e), although this change was not as significant considering the system under investigation (HPMC) is hygroscopic and known to absorb water relatively quickly. The initial delay in drug release for the lowest D_{we} value is indicative of an induction period where sufficient solvent necessary for steady-state drug particle dissolution and diffusion through the polymer matrix has not yet been achieved. Since the sole contribution of polymer is to serve as a fixed mass eroding away at a fixed rate, C_{p0} is only expected to contribute to the thickness change of the film. As such, C_{p0} predictably had little impact on the predicted rate of drug release in Figure 6.2f. Increasing equilibrium solvent concentration (C_{we}) led to slower predicted drug release in Figure 6.2g. This decrease was likely due to the increase in solvent absorption capacity of the film and increased polymer swellability, since the embedded poorly water-soluble drug particles already have sufficient solvent to dissolve, even at low solvent concentrations. For comparison, the model predicts the film with C_{we} = 0.85 to swell to twice the thickness of the film with

C_{we} = 0.35, effectively doubling its total release time. As seen in Figure 6.2h, increasing drug dissolution rate (k_d) led to an expected increase in predicted drug release rate. Finally, increasing median drug particle size led to a significant decrease in predicted drug release rate (Figure 6.2i), as one would expect when drug particle dissolution is governed by the Noyes–Whitney equation. Overall, the results of the sensitivity analysis are in line with their defining principles and demonstrate the capability of accurately capturing the expected behavior of different systems.

6.4.3 Comparison with Experimental Results

6.4.3.1 Model Comparisons with Formulations for Model Development.

Comparison of experimentally determined dissolution profiles for the formulations shown in Table 6.3 and their respective mathematical model predictions are shown in Figure 6.3, Figure 6.4, and Figure 6.5. Despite originally varying between 90-110% expected drug release (most likely due to experimental error regarding assessment of drug content), all dissolution profiles were normalized to 100% drug release for the sake of comparison. It should be noted that k_d had to be varied between formulations based on drug particle size in order to achieve representative fits (2.91×10^{-4}, 4.36×10^{-3}, and 0.116 cm/s for 1, 2, and 3 formulations, respectively). For consistency, these values were fit to the experimental data under the assumption that the drug particles released from the film were the same size as those in the nanosuspension from which they were taken (d_{50} values of 0.164, 0.555, and 17.470 μm, respectively). This is in contrast to the presented model predictions that were calculated taking the size of the drug particles redispersed from the films in DI water (Table 6.3) into account.

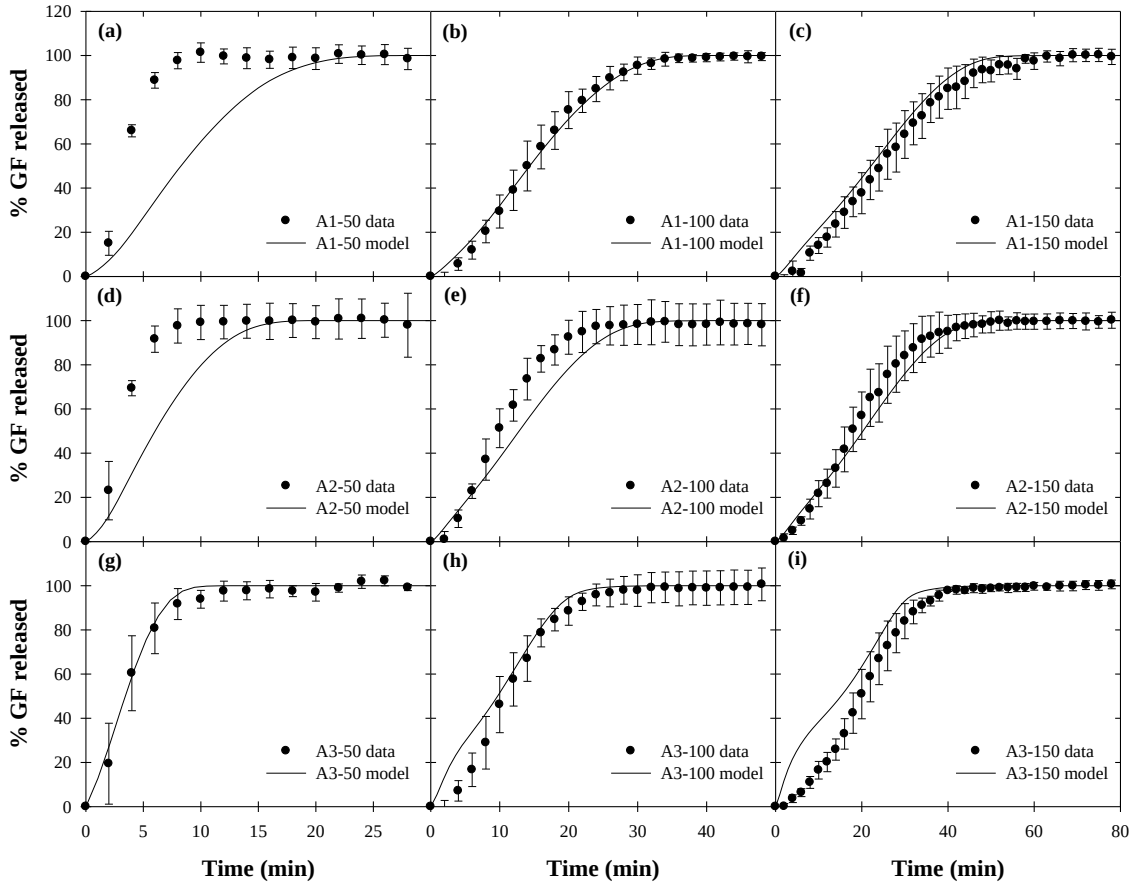

Figure 6.3 Comparison of experimentally determined dissolution rates from HPMC-E15 formulations and numerically predicted dissolution profiles for the same formulations. $k_d = 2.91\times10^{-4}$ cm/s for A1 formulations, $k_d = 4.36\times10^{-3}$ cm/s for A2 formulations, and $k_d = 0.116$ cm/s for A3 formulations.

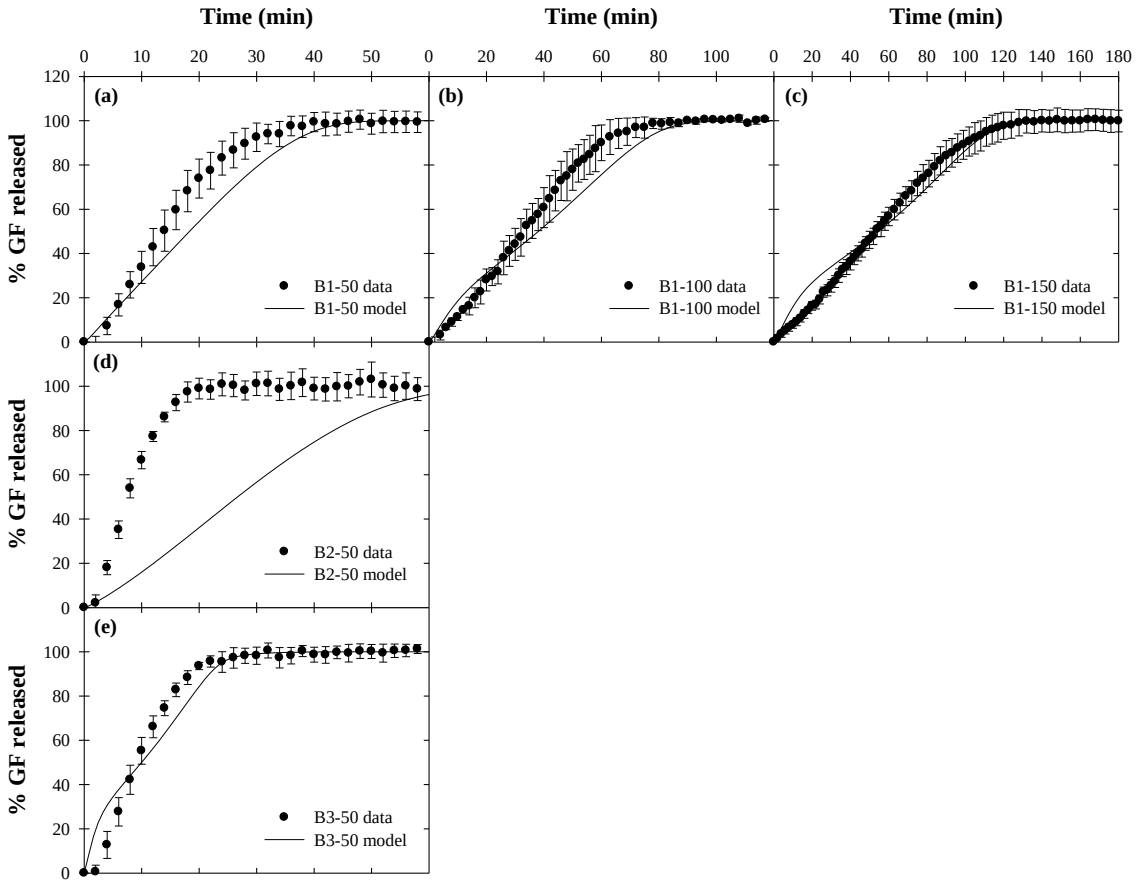

Figure 6.4 Comparison of experimentally determined dissolution rates from HPMC-E15/E4M mixture formulations and numerically predicted dissolution profiles for the same formulations. k_d = 2.91×10^{-4} cm/s for B1 formulations, k_d = 4.36×10^{-3} cm/s for B2-50, and k_d = 0.116 cm/s for B3-50.

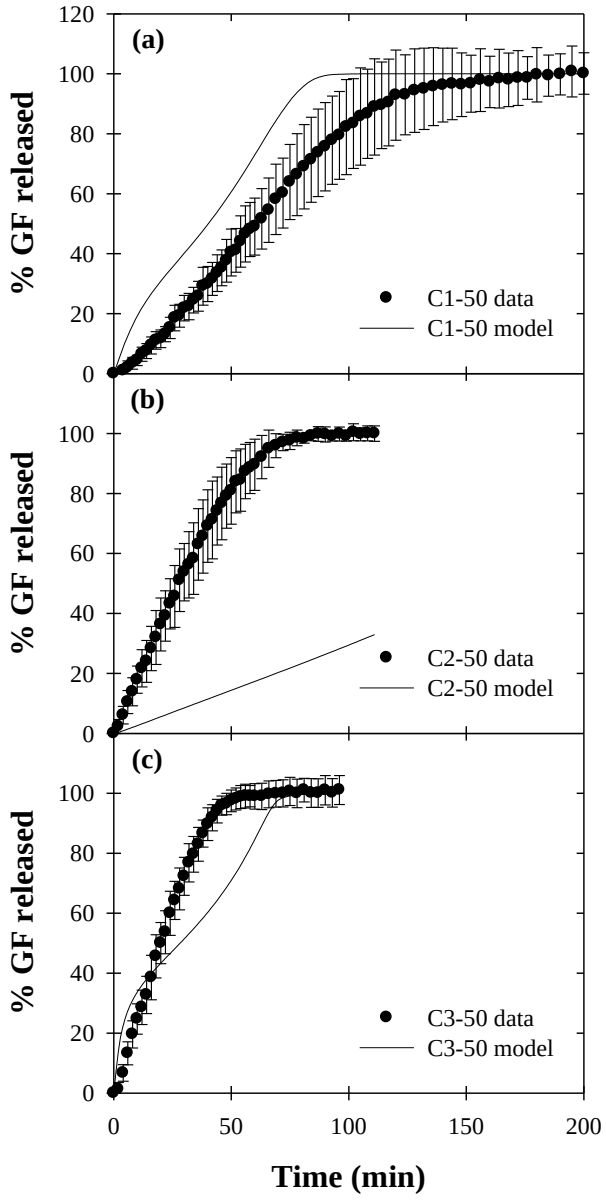

Figure 6.5 Comparison of experimentally determined dissolution rates from HPMC-E4M formulations and numerically predicted dissolution profiles for the same formulations. k_d = 2.91×10^{-4} cm/s for C1-50, k_d = 4.36×10^{-3} cm/s for C2-50, and k_d = 0.116 cm/s for C3-50.

Overall, the mathematical model appeared to fit the experimental dissolution profiles reasonably well, typically within the range of experimental error. The expected sigmoidal shape was apparent in all predicted curves, with the exception of the unmilled microparticle formulations due to the inflation of k_d. Slower release was observed with

increasing film thickness in all applicable cases (all As and B1), in line with previous work (Krull et al., 2016b). The model was able to successfully predict slower release from thicker films, demonstrating the ability to account for changing film thickness. Slower drug release was generally observed with increasing film-forming polymer molecular weight, in line with the dissolution results from Sub-section 4.3.3.3. The mathematical model was able to account for this as well by establishing linear relationships between C_{we}, K_{p0}, and HPMC MW (Equation (6.17) and Equation (6.18), respectively). The most apparent shortcoming of the mathematical model was its underestimation of the dissolution rate of GF particles larger than a few hundred nm. This result was rather unexpected considering extensive work supporting faster solubilization and dissolution of nanoparticles relative to microparticles due to the increase in surface area-to-volume ratio (Hu et al., 2004; Thorat and Dalvi, 2012). Previous work also observed a noticeable decrease in GF release rate from films with increasing particle size (Krull et al., 2016b). It is possible that the solubilization effect of SDS in the dissolution media negated the anticipated impact of drug particle size on dissolution, resulting in the necessity to drastically increase k_d to match the experimentally determined dissolution profiles.

The slower-than-observed release predicted for formulations B2-50 and C2-50 was likely due to the unusually high d_{50} values measured when the GF nanoparticles for those films were redispersed in water. Since the objective of the redispersion technique was employed to assess the ability to recover the embedded drug particles in water, it is not unexpected that this technique will sometimes fail to accurately reflect the conditions of dissolution, especially if the dissolution medium differs from the redispersion medium.

The slower-than-observed release predicted for A1-50, A2-50, B2-50, and C1-50 formulations might be explained by film disintegration, a prevalent phenomenon in thin films not explained by diffusion or dissolution. Below ~50 μm in thickness, the HPMC-based films are prone to physically break apart or disintegrate, leading to accelerated drug release due to the massive increase in film surface area exposed to solvent.

6.4.3.2 Model Comparisons with Formulations from Chapter 4. In order to test the predictive capabilities of the dissolution model, the model was used to predict the dissolution rate of films from the polymer molecular weight study in Chapter 4. Properties of the films used as input parameters for the model can be found in Table 6.4. A comparison of the experimentally determined dissolution profiles for these films and direct comparisons to their respective predicted dissolution profiles can be found in Figure 6.6. The dissolution model proved to be a reasonable fit for all E15 and E50 films, even without modifying k_d. However, it was necessary to change k_d in order to achieve reasonable fits for E4M films, although these changes were very slight (within 50%) in comparison to those necessary in Sub-section 6.4.3.1. The slower-than-expected release from E4M films relative to the model prediction may be attributed to stronger interaction between GF nanoparticles and high MW polymer (E4M) compared to lower MW polymer (E15 and E50), as noted in Section 5.3.6. That said, comparison with experimental data from Chapter 4 demonstrates that the model was able to successfully predict release profiles from films with varying initial polymer mass and film thickness.

Table 6.4 Parameters from Molecular Weight Study Films Used for Predictive Model

Sample	Average HPMC MW (g/mol)	d_{50} of redispersed particles (nm)	Dry film thickness (μm)	Drug mass per unit area (mg/cm^2)	Polymer mass per unit area (mg/cm^2)
E15-Low	14,167	168	91.6	1.82	6.62
E15-Med	14,167	167	114.2	2.14	8.77
E15-High	14,167	168	110.6	1.93	8.77
E50-Low	21,000	151	70.4	1.78	4.82
E50-Med	21,000	152	64.7	1.64	3.96
E50-High	21,000	148	74.5	1.81	5.40
E4M-Low	87,800	291	34.7	1.97	1.97
E4M-Med	87,800	191	41.4	2.02	2.19
E4M-High	87,800	187	38.5	1.93	2.32

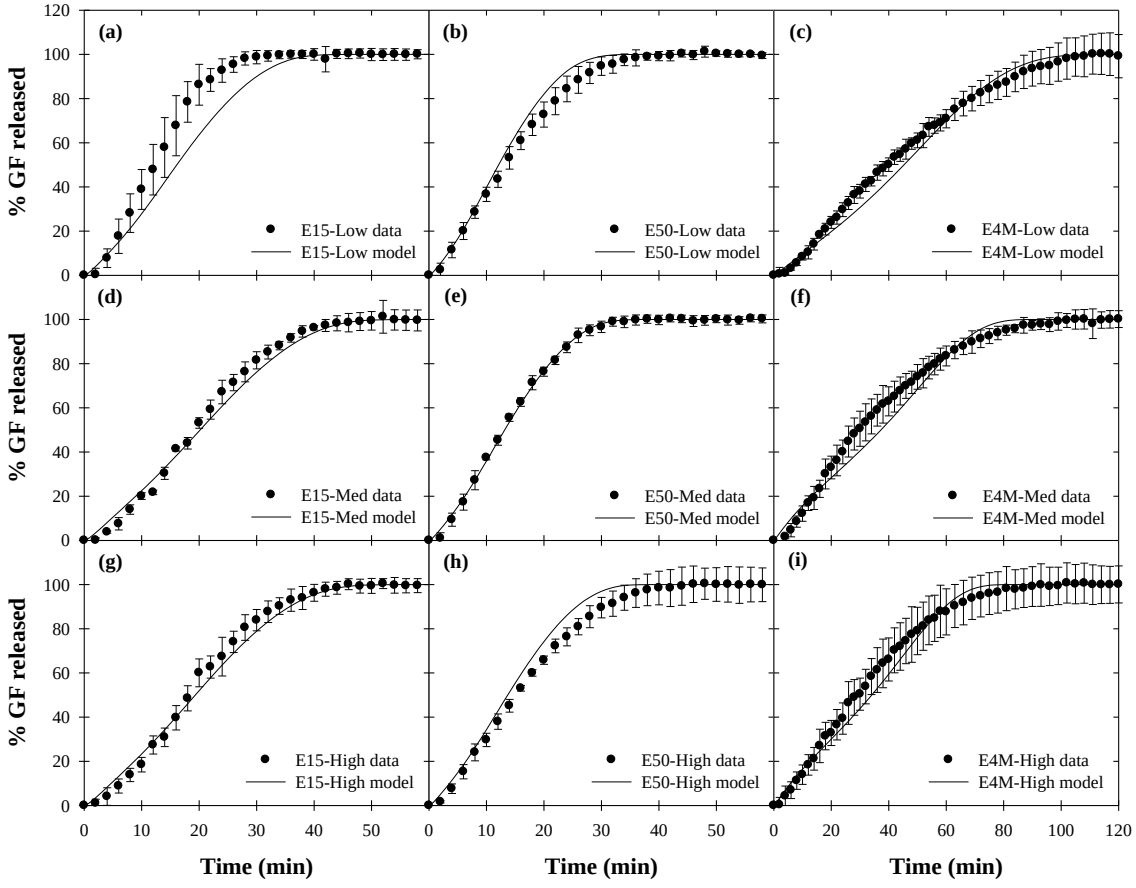

Figure 6.6 Comparison of experimentally determined dissolution rates from films loaded with GF nanoparticles containing different HPMC MWs and concentrations and numerically predicted dissolution profiles for the same formulations. k_d = (a,b,d,e,g,h) 2.9×10^{-4} cm/s, (c) 1.7×10^{-4} cm/s, and (f,i) 2.3×10^{-4} cm/s.

6.4.3.3 Model Comparisons with Formulations from Chapter 5. In order to further test the predictive capabilities of the dissolution model, the model was used to predict the dissolution rate of films from the drug loading study in Chapter 5. Properties of the films used as input parameters for the model can be found in Table 6.5. A comparison of the experimentally determined dissolution profiles for E15 films from this study and direct comparisons to their respective predicted dissolution profiles can be found in Figure 6.7, while the same for E4M films can be found in Figure 6.8. The dissolution model was a suitable fit for low loading E15 films, but required k_d steadily decrease with increasing drug loading (down to 10% its original value for DL6-15, 49 wt% GF). A similar decrease in k_d was also necessary for E4M films up to DL3-4M. Potential sources for these discrepancies are difficult to identify due to the number of parameters changing simultaneously as the WSMM nanosuspension loading and polymer-to-nanosuspension mixing ratio were varied to prepare films with different drug loadings (Table 5.1). These differences may be due in part to the fact that, for high drug loading films, the model predicted complete erosion of the polymer matrix before all of the drug particles had dissolved due to the significant increase in drug-to-polymer ratio. This prediction anticipated complete release of undissolved drug particles into the bulk solvent and unhindered dissolution, leading to predicted drug release that was faster than observed. Since drug release from high loading E4M films was likely the result of disintegration into slowly dissolving polymer–drug agglomerates rather than simple dispersion the embedded GF nanoparticles (Section 5.3.6), the dissolution model severely under-predicted drug release rates from those films based on the size of the agglomerates, and significant increases in k_d were required to compensate (1.2×10^{-2} and 2.0×10^{-1} cm/s

for DL4-4M and DL5-4M, respectively). This did not come as a surprise, as the diffusion–dissolution model was not developed to predict molecular level interaction between film components. That said, dissolution model predictions for the drug loading study films exposed a potential flaw in the current form of the model, which over-predicts drug release rates from films that erode before all of the embedded drug particles have dissolved.

Table 6.5 Parameters from Drug Loading Study Films Used for Predictive Model

Sample	Average HPMC MW (g/mol)	d_{50} of redispersed particles (nm)	Dry film thickness (μm)	Drug mass per unit area (mg/cm^2)	Polymer mass per unit area (mg/cm^2)
DL1-15	14,167	165	97.2	1.22	7.79
DL2-15	14,167	171	85.1	2.22	6.19
DL3-15	14,167	171	109.0	3.18	9.18
DL4-15	14,167	192	108.8	5.29	8.52
DL5-15	14,167	164	122.9	6.08	9.91
DL6-15	14,167	172	127.4	8.61	8.70
DL1-4M	87,800	161	27.8	1.18	1.88
DL2-4M	87,800	170	40.1	2.87	2.33
DL3-4M	87,800	205	45.6	3.50	2.56
DL4-4M	87,800	44,705	57.3	5.54	2.49
DL5-4M	87,800	652,041	65.6	6.04	2.54

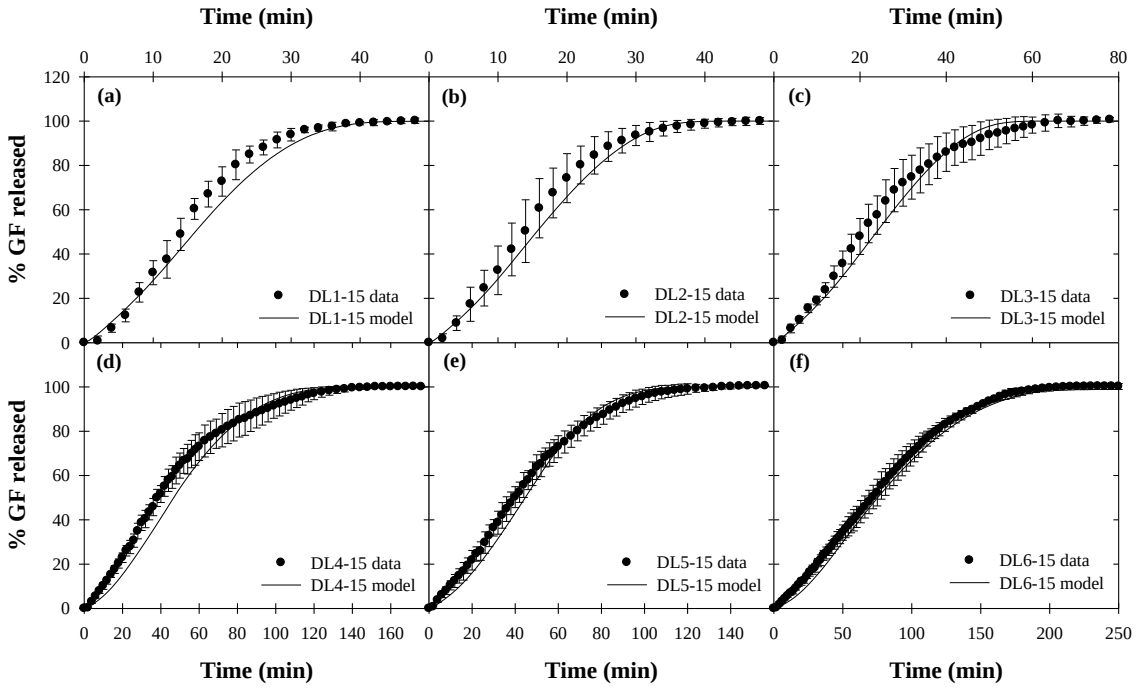

Figure 6.7 Comparison of experimentally determined dissolution rates from HPMC-E15 formulations with varying GF loading and numerically predicted dissolution profiles for the same formulations. k_d = (a,b) 2.9×10^{-4} cm/s, (c) 1.9×10^{-4} cm/s, (d) 5.8×10^{-5} cm/s, (e) 6.5×10^{-5} cm/s, and (f) 2.9×10^{-5} cm/s.

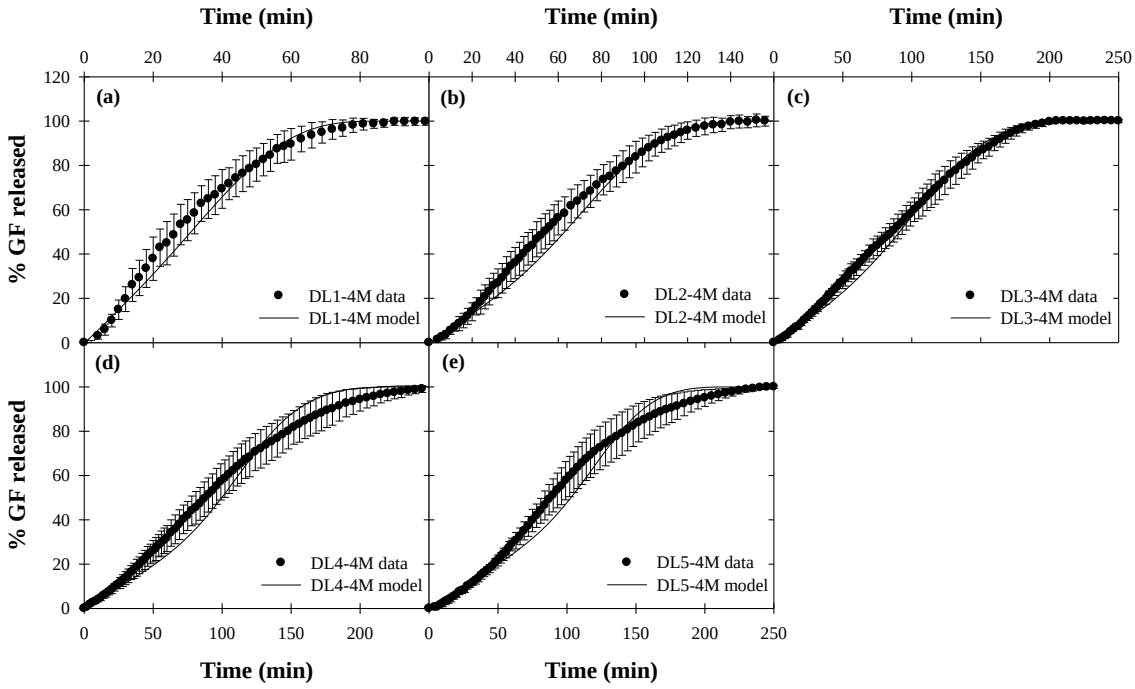

Figure 6.8 Comparison of experimentally determined dissolution rates from HPMC-E4M formulations with varying GF loading and numerically predicted dissolution profiles for the same formulations. k_d = (a) 1.3×10^{-4} cm/s, (b) 6.5×10^{-5} cm/s, (c) 4.8×10^{-5} cm/s, (d) 1.2×10^{-2} cm/s, and (e) 2.0×10^{-1} cm/s.

6.5 Conclusions

The objective of this work was to develop a mathematical model based on first principles that would be able to predict the rate of drug release from polymer films with embedded poorly water-soluble drug nanoparticles. The model simultaneously tracked dissolved drug concentration, solvent concentration, undissolved drug particle size, and film thickness as a function of time throughout the dissolution process. The moving film–solvent boundary was fixed via coordinate transformation and the resulting coupled system of ODEs was solved numerically. Property-dependent relationships were developed for system parameters such as C_{we} and K_{p0} based on experiments used to investigate the impact of film thickness, film-forming polymer MW, and drug particle

size on drug release and subsequently incorporated into the model. When compared to experimentally determined dissolution profiles from previous chapters, dissolution model predictions were reasonably close to the observed release rates. Some aspects of the model, including under-prediction of the dissolution rate of large drug particles and over-prediction of the dissolution rate of high drug-to-polymer films, require further refinement before application to more general systems. That said, the dissolution model demonstrated the ability to react predictably to changes in system parameters, simulate the expected shape of the dissolution profile, and flawlessly reflect changes in film thickness and polymer MW when compared to experimental data.

CHAPTER 7

OVERALL CONCLUSIONS AND FUTURE WORK

7.1 Overall Conclusions

In the preceding chapters, the robustness and versatility of polymer strip films as a delivery platform for poorly water-soluble drug nanoparticles were demonstrated. The relationships elucidated by these studies were then used to develop a mathematical model to predict the rate of drug release from such films based on several film CMAs.

The robustness of the polymer strip film format was demonstrated in Chapter 2 by incorporating nanoparticles of five different BCS class II drugs (FNB, GF, NPX, PB, and AZD) into films for fast dissolution. Good content uniformity, nanoparticle redispersibility, and similar release rates were observed from films regardless of the changes in properties across the five drugs, suggesting the film format is capable of stabilizing and delivering a wide variety of poorly water-soluble drugs. In addition, these advantages were maintained even after surfactant was removed from the formulation, which was previously thought to be necessary in order to achieve good nanoparticle redispersibility and fast dissolution. This suggests that polymer strip films may also serve as a truly surfactant-free delivery platform for poorly water-soluble drugs without sacrificing enhanced dissolution or good drug content uniformity. The ability to predictably adjust film mechanical properties by changing plasticizer concentration in films without impacting drug dissolution rate was demonstrated in Chapter 3. Conversely, the ability to predictably adjust drug dissolution rate from films by changing film-forming polymer MW (while maintaining similar polymer solution viscosity) with

minimal impact on film mechanical properties was demonstrated in Chapter 4. Together, plasticizer concentration and film-forming polymer MW offer a unique combination of easily changed film formulation properties that can be used to tailor final product qualities such as film mechanical properties and drug dissolution rates for specific applications without negatively impacting the advantages of the strip film format. Chapter 5 demonstrated the capability of the strip film format to stabilize and deliver poorly water-soluble drug nanoparticles up to 50 wt% drug in the dry film, challenging the prior misconception that drug loading in films was severely limited. Finally, a mathematical model was developed in Chapter 6 to predict the rate of drug release from drug particle-laden polymer films based on many of the film properties investigated in the preceding chapters.

Chapter 1 discussed the relative infancy of the polymer strip film format regarding delivery of poorly water-soluble drug nanoparticles, the need for further formulation development to investigate the robustness and versatility of the platform, and a lack of fundamental understanding regarding how those formulation aspects impact film properties. In response, this dissertation work explored all aspects of film formulation, including film-forming polymer, plasticizer, drug stabilizer, and the drug itself, in an effort to determine the effect each has on the product quality of the resulting film. In addition, the impact of each formulation aspect on the rate of drug release from films was used to develop a predictive mathematical model. The knowledge gained from this work will be instrumental in developing strip films containing poorly water-soluble drug for targeted applications, as the formulation aspects investigated may be easily

changed to have predictable effects on various critical quality attributes of the resulting films.

7.2 Future Work

7.2.1 Thick Films for Buccal Delivery and Composite Films for Controlled Delivery of Multiple Drugs

All of the films in this work were designed for oral use, generally for oral dispersion and fast release. While the effect of controlled changes in film thickness on dissolution rate was investigated in part in Chapter 6, no films in this work were above 130 μm in thickness. One simple extension would be to develop thicker films for buccal delivery. These films would be designed to adhere to the buccal mucosa in the mouth for the drug to permeate through, directly entering the blood stream. Another natural extension of thin films would be to stack several films together to form a composite film. These composite films could be prepared using different film-forming polymers in each layer for more precise control of drug release or containing different drugs in each layer.

7.2.2 Dissolution Model Expansion to Account for Other Types of Polymers

The dissolution model developed in Chapter 6 was centered on HPMC, a swellable hydrophilic polymer that demonstrated relatively constant dissolution over time. As a result, constant polymer dissolution from the film surface until all polymer had dissolved was assumed with no observed negative impact on the ability to match experimentally determined dissolution profiles. However, not all polymers behave the same way. Some exhibit homogenous dissolution where the entire matrix dissolves simultaneously rather than just the film surface. In specific cases, polymers may be broken into two distinct regions during dissolution: a glassy (dry) layer and a rubbery (wet) layer, which exhibit

different properties. Accounting for these types of polymers in the dissolution model will require tracking of polymer concentration throughout the film, as well as the potential swelling front separating the glassy and rubbery regions.

7.2.3 Mathematical Model for Prediction of Drying Rate from Drug Particle-loaded Polymer Films

While the focus of this dissertation has been on the impact of film formulation on product quality, scale-up of processing techniques will be an important task for future efforts. One process in particular that has a significant impact on the quality of the resulting film is drying. Not only does the film need to dry within a sufficiently brief amount of time to be considered economically feasible, but the residual solvent content and drug particle morphology must be carefully controlled. To this end, a numerical drying model may be developed to predict changes in the amount of solvent, temperature, and solvent weight fraction profiles of the drying film over time based on first principles. This model should account for heating by conduction, convection, and potentially radiation, as well as time-varying film thickness. The resulting predictions can be used to optimize the film drying process to produce adequately dried films that exhibit desirable product qualities in the least amount of time.

APPENDIX

DISSOLUTION PROFILE COMPARISON

Pairwise comparison of dissolution profiles was performed using similarity and difference factors as described by Boateng et al. (2012) and Costa and Lobo (2001). Since difference factors are dependent on which of the two curves is used as a reference, both possible values of f_1 are presented as f_1a and f_1b for each pair of dissolution profiles. Pairs that exhibit $f_1 < 15$ and $f_2 > 50$ are considered statistically similar.

A.1 Effect of Plasticizer

f_1 and f_2 values for comparison of dissolution profiles of fresh films are shown in Table A.1. The same for each of the seven film formulations after 0, 3, and 6 months of storage at 40 ºC, 75% RH are shown in Table A.2-A.8.

Table A.1 Similarity (f_2) and Difference (f_1) Factors for Comparison of Dissolution Profiles of Fresh Films Loaded with GF Nanoparticles

2.5% Glycerin	f_1a	2.7					
	f_1b	2.3					
	f_2	88.3					
5.0% Glycerin	f_1a	5.5	6.5				
	f_1b	6.2	8.5				
	f_2	72.9	68.0				
2.5% Triacetin	f_1a	19.6	17.8	17.0			
	f_1b	22.7	23.7	17.4			
	f_2	46.6	45.3	52.9			
5.0% Triacetin	f_1a	13.3	13.2	9.0	8.9		
	f_1b	11.8	13.5	7.1	6.9		
	f_2	58.4	56.0	67.5	66.4		
2.5% PEG	f_1a	27.9	24.9	27.0	12.5	15.0	
	f_1b	34.9	36.0	29.8	13.5	21.2	
	f_2	36.1	35.4	39.8	56.4	46.8	
5.0% PEG	f_1a	6.1	5.0	11.4	26.4	16.9	37.3
	f_1b	4.8	4.5	7.9	17.9	15.0	23.4
	f_2	71.4	76.1	60.7	43.5	51.9	34.7
Formulation		No Plasticizer	2.5% Glycerin	5.0% Glycerin	2.5% Triacetin	5.0% Triacetin	2.5% PEG

Table A.2 Similarity (f_2) and Difference (f_1) Factors for Comparison of Dissolution Profiles of Films Loaded with GF Nanoparticles Containing No Plasticizer Immediately after Film Preparation, after 3 Months of Storage at 40 ºC, 75% RH, and after 6 Months of Storage at 40 ºC, 75% RH

3 months	f_1a	3.8	
	f_1b	3.7	
	f_2	80.7	
6 months	f_1a	10.2	7.3
	f_1b	11.0	8.1
	f_2	62.4	69.7
No Plasticizer		Fresh	3 months

Table A.3 Similarity (f_2) and Difference (f_1) Factors for Comparison of Dissolution Profiles of 2.5% Glycerin Films Loaded with GF Nanoparticles Immediately after Film Preparation, after 3 Months of Storage at 40 ºC, 75% RH, and after 6 Months of Storage at 40 ºC, 75% RH

3 months	f_1a	21.1	
	f_1b	26.9	
	f_2	42.4	
6 months	f_1a	23.1	8.5
	f_1b	34.2	9.9
	f_2	36.3	62.6
2.5% Glycerin		Fresh	3 months

Table A.4 Similarity (f_2) and Difference (f_1) Factors for Comparison of Dissolution Profiles of 5.0% Glycerin Films Loaded with GF Nanoparticles Immediately after Film Preparation, after 3 Months of Storage at 40 ºC, 75% RH, and after 6 Months of Storage at 40 ºC, 75% RH

3 months	f_1a	5.5	
	f_1b	4.5	
	f_2	75.8	
6 months	f_1a	22.6	16.7
	f_1b	26.3	24.0
	f_2	42.9	45.4
5.0% Glycerin		Fresh	3 months

Table A.5 Similarity (f_2) and Difference (f_1) Factors for Comparison of Dissolution Profiles of 2.5% Triacetin Films Loaded with GF Nanoparticles Immediately after Film Preparation, after 3 Months of Storage at 40 ºC, 75% RH, and after 6 Months of Storage at 40 ºC, 75% RH

3 months	f_1a	22.1	
	f_1b	33.1	
	f_2	39.0	
6 months	f_1a	11.5	21.3
	f_1b	12.6	15.5
	f_2	58.5	49.2
2.5% Triacetin		Fresh	3 months

Table A.6 Similarity (f_2) and Difference (f_1) Factors for Comparison of Dissolution Profiles of 5.0% Triacetin Films Loaded with GF Nanoparticles Immediately after Film Preparation, after 3 Months of Storage at 40 ºC, 75% RH, and after 6 Months of Storage at 40 ºC, 75% RH

3 months	f_1a	16.3	
	f_1b	18.9	
	f_2	49.3	
6 months	f_1a	8.0	10.1
	f_1b	10.3	11.2
	f_2	62.8	62.2
5.0% Triacetin		Fresh	3 months

Table A.7 Similarity (f_2) and Difference (f_1) Factors for Comparison of Dissolution Profiles of 2.5% PEG Films Loaded with GF Nanoparticles Immediately after Film Preparation, after 3 Months of Storage at 40 ºC, 75% RH, and after 6 Months of Storage at 40 ºC, 75% RH

3 months	f_1a	10.0	
	f_1b	11.5	
	f_2	61.3	
6 months	f_1a	4.5	7.3
	f_1b	4.4	6.2
	f_2	76.5	66.6
2.5% PEG		Fresh	3 months

Table A.8 Similarity (f_2) and Difference (f_1) Factors for Comparison of Dissolution Profiles of 5.0% PEG Films Loaded with GF Nanoparticles Immediately after Film Preparation, after 3 Months of Storage at 40 ºC, 75% RH, and after 6 Months of Storage at 40 ºC, 75% RH

3 months	f_1a	17.4	
	f_1b	25.8	
	f_2	43.2	
6 months	f_1a	16.3	3.3
	f_1b	24.6	3.4
	f_2	44.5	84.3
5.0% PEG		Fresh	3 months

A.2 Effect of Film-Forming Polymer Molecular Weight

f_1 and f_2 values for comparison of dissolution profiles are shown in Table A.9.

Table A.9 Similarity (f_2) and Difference (f_1) Factors for Comparison of Dissolution Profiles of HPMC Films Loaded with GF Nanoparticles

E15-Med	f_1	44.0							
	f_1	27.4							
	f_2	33.9							
E15-High	f_1	41.2	4.8						
	f_1	24.9	4.7						
	f_2	35.6	77.4						
E50-Low	f_1	10.1	29.6	26.5					
	f_1	7.6	35.6	32.9					
	f_2	64.0	37.8	39.4					
E50-Med	f_1	10.3	29.0	25.6	3.7				
	f_1	6.9	31.1	28.5	3.3				
	f_2	62.4	39.5	41.4	83.2				
E50-High	f_1	24.8	16.0	12.4	18.4	15.2			
	f_1	14.9	15.5	12.4	14.8	13.7			
	f_2	45.0	54.7	58.2	51.8	54.1			
E4M-Low	f_1	72.9	50.5	51.9	68.8	66.5	58.3		
	f_1	22.3	24.7	26.3	28.0	30.3	29.5		
	f_2	22.7	29.9	28.7	22.6	22.3	26.2		
E4M-Med	f_1	63.8	35.9	37.9	58.9	56.0	45.8	16.6	
	f_1	19.7	17.8	19.5	24.3	25.8	23.5	16.8	
	f_2	25.7	37.0	35.4	26.3	26.3	31.7	53.2	
E4M-High	f_1	59.8	33.9	35.9	56.1	53.3	43.6	18.7	4.2
	f_1	20.2	18.4	20.1	25.3	26.9	24.5	20.7	4.6
	f_2	26.5	37.2	35.5	26.8	26.9	32.2	49.3	78.2
Formulation		E15-Low	E15-Med	E15-High	E50-Low	E50-Med	E50-High	E4M-Low	E4M-Med

A.3 Effect of Drug Loading

f_1 and f_2 values for comparison of dissolution profiles of fresh films are shown in Table A.10. The same for E15 and E4M films after 0, 3, and 6 months of storage at 40 ºC, 75% RH are shown in Table A.11 and Table A.12, respectively.

Table A.10 Similarity (f_2) and Difference (f_1) Factors for Comparison of Dissolution Profiles of Fresh HPMC Films with Different GF Nanoparticle Loadings

	f_1	3.6									
DL2-15	f_1	3.6									
	f_2	81.7									
	f_1	38.1	39.1								
DL3-15	f_1	22.1	23.2								
	f_2	34.7	34.6								
	f_1	70.9	71.4	49.4							
DL4-15	f_1	19.9	20.4	23.9							
	f_2	21.3	21.3	29.2							
	f_1	71.8	72.4	51.5	2.7						
DL5-15	f_1	22.3	22.9	27.5	3.0						
	f_2	20.8	20.8	28.1	86.6						
	f_1	85.3	85.6	75.0	43.3	44.0					
DL6-15	f_1	19.8	20.2	29.9	35.8	32.8					
	f_2	17.3	17.3	19.9	32.0	32.5					
	f_1	51.0	51.9	20.3	21.5	25.7	36.5				
DL1-4M	f_1	21.4	22.2	14.6	32.2	34.8	66.1				
	f_2	28.9	28.8	48.6	38.5	36.7	22.4				
	f_1	82.2	82.5	65.7	20.0	20.5	21.2	51.8			
DL2-4M	f_1	26.1	26.7	35.8	22.6	20.9	29.0	39.1			
	f_2	18.3	18.3	23.1	49.1	50.2	42.9	28.2			
	f_1	89.1	89.3	80.4	52.6	53.3	12.1	72.5	40.3		
DL3-4M	f_1	21.8	22.2	33.8	45.8	41.8	12.8	42.2	31.0		
	f_2	16.4	16.4	18.5	27.9	28.5	62.7	20.4	36.2		
	f_1	88.8	89.0	81.0	54.6	55.3	15.4	73.9	42.6	4.0	
DL4-4M	f_1	19.5	20.0	30.6	42.7	39.1	14.6	38.7	29.5	3.6	
	f_2	16.4	16.4	18.2	27.0	27.6	58.0	20.0	35.0	83.2	
	f_1	92.7	92.8	86.0	60.3	61.5	19.6	79.7	49.0	8.2	5.1
DL5-4M	f_1	21.2	21.7	33.8	49.1	45.3	19.3	43.4	35.4	7.7	5.3
	f_2	15.6	15.6	17.0	25.0	25.5	53.4	18.4	32.5	71.5	79.2
Formulation		DL1 -15	DL2 -15	DL3 -15	DL4 -15	DL5 -15	DL6 -15	DL1 -4M	DL2 -4M	DL3 -4M	DL4 -4M

Table A.11 Similarity (f_2) and Difference (f_1) Factors for Comparison of Dissolution Profiles of HPMC-E15 Films with Different GF Nanoparticle Loadings after 0, 3, and 6 Months of Storage at 40 ºC, 75% RH

Month	DL1-15			DL2-15			DL3-15		
comparisons >	0-3	0-6	3-6	0-3	0-6	3-6	0-3	0-6	3-6
f_1	7.5	15.2	10.3	12.0	18.7	22.7	2.1	9.4	8.5
f_1	8.3	16.2	9.9	10.1	25.0	36.0	2.1	11.4	10.5
f_2	67.0	53.0	62.3	60.2	45.5	37.2	90.9	61.7	63.5
Month	DL4-15			DL5-15			DL6-15		
comparisons >	0-3	0-6	3-6	0-3	0-6	3-6	0-3	0-6	3-6
f_1	10.3	12.9	4.9	10.3	12.9	4.9	10.3	12.9	4.9
f_1	13.3	17.9	5.2	13.3	17.9	5.2	13.3	17.9	5.2
f_2	56.6	51.5	77.9	56.6	51.5	77.9	56.6	51.5	77.9

Table A.12 Similarity (f_2) and Difference (f_1) Factors for Comparison of Dissolution Profiles of HPMC-E4M Films with Different GF Nanoparticle Loadings after 0, 3, and 6 Months of Storage at 40 ºC, 75% RH

Month	DL1-4M			DL2-4M			DL3-4M		
comparisons >	0-3	0-6	3-6	0-3	0-6	3-6	0-3	0-6	3-6
f_1	5.8	21.7	23.5	3.6	25.4	26.1	3.2	29.5	28.1
f_1	5.4	32.0	37.0	3.5	28.5	30.2	3.2	39.1	37.9
f_2	75.4	39.4	36.2	83.5	42.4	41.8	88.3	36.8	38.0
Month	DL4-4M			DL5-4M					
comparisons >	0-3	0-6	3-6	0-3	0-6	3-6			
f_1	2.4	28.5	29.8	13.6	31.1	27.2			
f_1	2.5	54.0	55.0	14.2	61.3	51.4			
f_2	90.2	30.0	29.7	58.5	27.5	31.7			

REFERENCES

Aulton, M.E., Abdul-Razzak, M.H., Hogan, J.E., 1981. The mechanical properties of hydroxypropylmethylcellulose films derived from aqueous systems Part 1: The influence of plasticisers. Drug Dev. Ind. Pharm. 7 (6), 649-668.

Averineni, R.K., Sunderajan, S.G., Mutalik, S., Nayak, U., Shavi, G., Armugam, K., Meka, S.R., Pandey, S., Nayanabhirama, U., 2009. Development of mucoadhesive buccal films for the treatment of oral sub-mucous fibrosis: a preliminary study. Pharm. Dev. Technol. 14 (2), 199-207.

Azad, M., Arteaga, C., Abdelmalek, B., Davé, R., Bilgili, E., 2015. Spray drying of drug-swellable dispersant suspensions for preparation of fast-dissolving, high drug-loaded, surfactant-free nanocomposites. Drug Dev. Ind. Pharm. 41 (10), 1617-1631.

Balakrishnan, A., Rege, B.D., Amidon, G.L., Polli, J.E., 2004. Surfactant-mediated dissolution: Contributions of solubility enhancement and relatively low micelle diffusivity. J. Pharm. Sci. 93 (8), 2064-2075.

Beck, C., Sievens-Figueroa, L., Gärtner, K., Jerez-Rozo, J.I., Romañach, R.J., Bilgili, E., Davé, R.N., 2013. Effects of stabilizers on particle redispersion and dissolution from polymer strip films containing liquid antisolvent precipitated griseofulvin particles. Powder Technol. 236, 37-51.

Bhakay, A., Azad, M., Bilgili, E., Dave, R., 2014a. Redispersible fast dissolving nanocomposite microparticles of poorly water-soluble drugs. Int. J. Pharm. 461 (1-2), 367-379.

Bhakay, A., Azad, M., Vizzotti, E., Dave, R.N., Bilgili, E., 2014b. Enhanced recovery and dissolution of griseofulvin nanoparticles from surfactant-free nanocomposite microparticles incorporating wet-milled swellable dispersants. Drug Dev. Ind. Pharm. 40 (11), 1509-1522.

Bhakay, A., Davé, R., Bilgili, E., 2013. Recovery of BCS class II drugs during aqueous redispersion of core–shell type nanocomposite particles produced via fluidized bed coating. Powder Technol. 236, 221-234.

Bhakay, A., Merwade, M., Bilgili, E., Dave, R.N., 2011. Novel aspects of wet milling for the production of microsuspensions and nanosuspensions of poorly water-soluble drugs. Drug Dev. Ind. Pharm. 37 (8), 963-976.

Bhakay, A., Vizzotti, E., Li, M., Davé, R., Bilgili, E., 2016. Incorporation of fenofibrate nanoparticles prepared by melt emulsification into polymeric films. J. Pharm. Innov. 11 (1), 53-63.

Bilgili, E., Afolabi, A., 2012. A combined microhydrodynamics-polymer adsorption analysis for elucidation of the roles of stabilizers in wet stirred media milling. Int. J. Pharm. 439 (1-2), 193-206.

Biliaderis, C.G., Lazaridou, A., Arvanitoyannis, I., 1999. Glass transition and physical properties of polyol-plasticised pullulan–starch blends at low moisture. Carbohydr. Polym. 40 (1), 29-47.

Boateng, J.S., Matthews, K.H., Auffret, A.D., Humphrey, M.J., Eccleston, G.M., Stevens, H.N., 2012. Comparison of the in vitro release characteristics of mucosal freeze-dried wafers and solvent-cast films containing an insoluble drug. Drug Dev. Ind. Pharm. 38 (1), 47-54.

Bodmeier, R., Paeratakul, O., 1994. Mechanical properties of dry and wet cellulosic and acrylic films prepared from aqueous colloidal polymer dispersions used in the coating of solid dosage forms. Pharm. Res. 11 (6), 882-888.

Borges, A.F., Silva, C., Coelho, J.F.J., Simões, S., 2015a. Oral films: Current status and future perspectives II — Intellectual property, technologies and market needs. J. Control. Release 206, 108-121.

Borges, A.F., Silva, C., Coelho, J.F.J., Simões, S., 2015b. Oral films: Current status and future perspectives: I — Galenical development and quality attributes. J. Control. Release 206, 1-19.

Borgquist, P., Körner, A., Piculell, L., Larsson, A., Axelsson, A., 2006. A model for the drug release from a polymer matrix tablet—effects of swelling and dissolution. J. Control. Release 113 (3), 216-225.

Brackman, J.C., 1991. Sodium dodecyl sulfate-induced enhancement of the viscosity and viscoelasticity of aqueous solutions of poly(ethylene oxide). A rheological study on polymer-micelle interaction. Langmuir 7 (3), 469-472.

Bruce, L.D., McGinity, J.W., 2008. Polymer interactions with drugs and excipients. in: McGinity, J.W., Felton, L.A. (Eds.), Aqueous Polymeric Coatings for Pharmaceutical Dosage Forms, third ed., New York, NY: CRC Press, pp. 369-408.

Cabrera, M.I., Luna, J.A., Grau, R.J.A., 2006. Modeling of dissolution-diffusion controlled drug release from planar polymeric systems with finite dissolution rate and arbitrary drug loading. J. Membr. Sci. 280 (1–2), 693-704.

Cerdeira, A.M., Mazzotti, M., Gander, B., 2010. Miconazole nanosuspensions: Influence of formulation variables on particle size reduction and physical stability. Int. J. Pharm. 396 (1–2), 210-218.

Costa, P., Lobo, J.M.S., 2001. Modeling and comparison of dissolution profiles. Eur. J. Pharm. Sci. 13 (2), 123-133.

Crank, J., 1957. Two methods for the numerical solution of moving-boundary problems in diffusion and heat flow. The Quarterly Journal of Mechanics and Applied Mathematics 10 (2), 220-231.

Dave, R.H., Shah, D.A., Patel, P.G., 2014. Development and evaluation of high loading oral dissolving film of aspirin and acetaminophen. J. Pharm. Sci. Pharmacol. 1 (2), 112-122.

Davé, R.N., Susarla, R., Bilgili, E., Sievens-Figueroa, L., Khusid, B., Muzzio, F., Bhakay, A., 2014. System and method for fabrication of uniform polymer films containing nano and micro particles via continuous drying process. PCT Application No. PCT/US14/30506. Filed March 17, 2014.

de Villiers, M.M., 1996. Influence of agglomeration of cohesive particles on the dissolution behaviour of furosemide powder. Int. J. Pharm. 136 (1–2), 175-179.

Dixit, R.P., Puthli, S.P., 2009. Oral strip technology: Overview and future potential. J. Control. Release 139 (2), 94-107.

Dow, 2002. Methocel cellulose ethers: Technical handbook. The Dow Chemical Company, http://www.dow.com/webapps/lit/litorder.asp?filepath=methocel/pdfs/noreg/192-01062.pdf (accessed on 9/3/2013).

Entwistle, C.A., Rowe, R.C., 1979. Plasticization of cellulose ethers used in the film coating of tablets. J. Pharm. Pharmacol. 31 (1), 269-272.

Frenning, G., 2003. Theoretical investigation of drug release from planar matrix systems: effects of a finite dissolution rate. J. Control. Release 92 (3), 331-339.

Garsuch, V., Breitkreutz, J., 2010. Comparative investigations on different polymers for the preparation of fast-dissolving oral films. J. Pharm. Pharmacol. 62 (4), 539-545.

George, M., Ghosh, I., 2013. Identifying the correlation between drug/stabilizer properties and critical quality attributes (CQAs) of nanosuspension formulation prepared by wet media milling technology. Eur. J. Pharm. Sci. 48 (1–2), 142-152.

Ghebremeskel, A.N., Vemavarapu, C., Lodaya, M., 2007. Use of surfactants as plasticizers in preparing solid dispersions of poorly soluble API: Selection of polymer–surfactant combinations using solubility parameters and testing the processability. Int. J. Pharm. 328 (2), 119-129.

Gibaldi, M., Feldman, S., 1967. Establishment of sink conditions in dissolution rate determinations. Theoretical considerations and application to nondisintegrating dosage forms. J. Pharm. Sci. 56 (10), 1238-1242.

Gómez-Carracedo, A., Alvarez-Lorenzo, C., Gómez-Amoza, J.L., Concheiro, A., 2003. Chemical structure and glass transition temperature of non-ionic cellulose ethers. J. Therm. Anal. Calorim. 73 (2), 587-596.

Gottnek, M., Süvegh, K., Pintye-Hódi, K., Regdon Jr, G., 2013. Effects of excipients on the tensile strength, surface properties and free volume of Klucel® free films of pharmaceutical importance. Radiat. Phys. Chem. 89, 57-63.

Gutiérrez-Rocca, J.C., McGinity, J.W., 1994. Influence of water soluble and insoluble plasticizers on the physical and mechanical properties of acrylic resin copolymers. Int. J. Pharm. 103 (3), 293-301.

Heinz, A., Gordon, K.C., McGoverin, C.M., Rades, T., Strachan, C.J., 2009. Understanding the solid-state forms of fenofibrate – A spectroscopic and computational study. Eur. J. Pharm. Biopharm. 71 (1), 100-108.

Higuchi, T., 1963. Mechanism of sustained-action medication. Theoretical analysis of rate of release of solid drugs dispersed in solid matrices. J. Pharm. Sci. 52 (12), 1145-1149.

Hixson, A.W., Crowell, J.H., 1931. Dependence of reaction velocity upon surface and agitation. Ind. Eng. Chem. 23 (10), 1160-1168.

Hoffmann, E.M., Breitenbach, A., Breitkreutz, J., 2011. Advances in orodispersible films for drug delivery. Expert Opin. Drug Deliv. 8 (3), 299-316.

Honary, S., Orafai, H., 2002. The effect of different plasticizer molecular weights and concentrations on mechanical and thermomechanical properties of free films. Drug Dev. Ind. Pharm. 28 (6), 711-715.

Hu, J., Johnston, K.P., Williams III, R.O., 2004. Nanoparticle engineering processes for enhancing the dissolution rates of poorly water soluble drugs. Drug Dev. Ind. Pharm. 30 (3), 233-245.

Huang, C.L., Kumar, S., Tan, J.J.Z., Boey, F.Y.C., Venkatraman, S.S., Steele, T.W.J., Loo, J.S.C., 2013. Modulating drug release from poly(lactic-co-glycolic acid) thin films through terminal end-groups and molecular weight. Polym. Degradation Stab. 98 (2), 619-626.

Huang, J., Wigent, R.J., Schwartz, J.B., 2008. Drug–polymer interaction and its significance on the physical stability of nifedipine amorphous dispersion in microparticles of an ammonio methacrylate copolymer and ethylcellulose binary blend. J. Pharm. Sci. 97 (1), 251-262.

Hutchings, D., Clarson, S., Sakr, A., 1994. Studies of the mechanical properties of free films prepared using an ethylcellulose pseudolatex coating system. Int. J. Pharm. 104 (3), 203-213.

Hyppölä, R., Husson, I., Sundholm, F., 1996. Evaluation of physical properties of plasticized ethyl cellulose films cast from ethanol solution Part I. Int. J. Pharm. 133 (1–2), 161-170.

Jamzad, S., Fassihi, R., 2006. Role of surfactant and pH on dissolution properties of fenofibrate and glipizide—A technical note. AAPS PharmSciTech 7 (2), E17-E22.

Jinno, J., Oh, D.M., Crison, J.R., Amidon, G.L., 2000. Dissolution of ionizable water-insoluble drugs: The combined effect of pH and surfactant. J. Pharm. Sci. 89 (2), 268-274.

Kakran, M., Sahoo, N.G., Li, L., Judeh, Z., Wang, Y., Chong, K., Loh, L., 2010. Fabrication of drug nanoparticles by evaporative precipitation of nanosuspension. Int. J. Pharm. 383 (1–2), 285-292.

Kararli, T.T., Hurlbut, J.B., Needham, T.E., 1990. Glass–rubber transitions of cellulosic polymers by dynamic mechanical analysis. J. Pharm. Sci. 79 (9), 845-848.

Karavas, E., Georgarakis, E., Sigalas, M.P., Avgoustakis, K., Bikiaris, D., 2007. Investigation of the release mechanism of a sparingly water-soluble drug from solid dispersions in hydrophilic carriers based on physical state of drug, particle size distribution and drug-polymer interactions. Eur. J. Pharm. Biopharm. 66 (3), 334-347.

Keck, C.M., Müller, R.H., 2006. Drug nanocrystals of poorly soluble drugs produced by high pressure homogenisation. Eur. J. Pharm. Biopharm. 62 (1), 3-16.

Kennedy, M.A., Peacock, A.J., Mandelkern, L., 1994. Tensile properties of crystalline polymers: Linear polyethylene. Macromolecules 27 (19), 5297-5310.

Kesisoglou, F., Panmai, S., Wu, Y., 2007. Nanosizing — Oral formulation development and biopharmaceutical evaluation. Adv. Drug Deliv. Rev. 59 (7), 631-644.

Kianfar, F., Chowdhry, B.Z., Antonijevic, M.D., Boateng, J.S., 2011. Novel films for drug delivery via the buccal mucosa using model soluble and insoluble drugs. Drug Dev. Ind. Pharm. 38 (10), 1207-1220.

Kipp, J.E., 2004. The role of solid nanoparticle technology in the parenteral delivery of poorly water-soluble drugs. Int. J. Pharm. 284 (1–2), 109-122.

Knieke, C., Azad, M.A., Davé, R.N., Bilgili, E., 2013. A study of the physical stability of wet media-milled fenofibrate suspensions using dynamic equilibrium curves. Chem. Eng. Res. Des. 91 (7), 1245-1258.

Knieke, C., Azad, M.A., To, D., Bilgili, E., Davé, R.N., 2015. Sub-100 micron fast dissolving nanocomposite drug powders. Powder Technol. 271, 49-60.

Korsmeyer, R.W., Gurny, R., Doelker, E., Buri, P., Peppas, N.A., 1983. Mechanisms of solute release from porous hydrophilic polymers. Int. J. Pharm. 15 (1), 25-35.

Krull, S.M., Ammirata, J., Bawa, S., Li, M., Bilgili, E., Davé, R.N., 2016a. Critical material attributes of strip films loaded with poorly water-soluble drug nanoparticles: II. Impact of polymer molecular weight. J. Pharm. Sci. In press.

Krull, S.M., Li, M., Bilgili, E., Davé, R.N., 2015a. Polymer strip films for delivery of poorly water-soluble drugs. Am. Pharm. Rev. 18 (3), 48-52.

Krull, S.M., Ma, Z., Li, M., Davé, R.N., Bilgili, E., 2016b. Preparation and characterization of fast dissolving pullulan films containing BCS class II drug nanoparticles for bioavailability enhancement. Drug Dev. Ind. Pharm. 42 (7), 1073-1085.

Krull, S.M., Patel, H.V., Li, M., Bilgili, E., Davé, R.N., 2016c. Critical material attributes (CMAs) of strip films loaded with poorly water-soluble drug nanoparticles: I. Impact of plasticizer on film properties and dissolution. Eur. J. Pharm. Sci. 92, 146-155.

Krull, S.M., Susarla, R., Afolabi, A., Li, M., Ying, Y., Iqbal, Z., Bilgili, E., Davé, R.N., 2015b. Polymer strip films as a robust, surfactant-free platform for delivery of BCS Class II drug nanoparticles. Int. J. Pharm. 489 (1–2), 45-57.

Kulicke, W.M., Arendt, O., Berger, M., 1998. Rheological characterization of the dilatant flow behavior of highly substituted hydroxypropylmethyl- cellulose solutions in the presence of sodium lauryl sulfate. Colloid. Polym. Sci. 276 (7), 617-626.

Kumar, G.P., Phani, A.R., Prasad, R.G.S.V., Sanganal, J.S., Manali, N., Gupta, R., Rashmi, N., Prabhakara, G.S., Salins, C.P., Sandeep, K., Raju, D.B., 2014. Polyvinylpyrrolidone oral films of enrofloxacin: Film characterization and drug release. Int. J. Pharm. 471 (1–2), 146-152.

Lai, F., Franceschini, I., Corrias, F., Sala, M.C., Cilurzo, F., Sinico, C., Pini, E., 2015. Maltodextrin fast dissolving films for quercetin nanocrystal delivery. A feasibility study. Carbohydr. Polym. 121, 217-223.

Landau, H.G., 1950. Heat conduction in a melting solid. Q. Appl. Math. 8 (1), 81-94.

Langer, R.S., Peppas, N.A., 1981. Present and future applications of biomaterials in controlled drug delivery systems. Biomaterials 2 (4), 201-214.

Lazaridou, A., Biliaderis, C.G., Kontogiorgos, V., 2003. Molecular weight effects on solution rheology of pullulan and mechanical properties of its films. Carbohydr. Polym. 52 (2), 151-166.

Lee, C., Park, S.K., Min, K.C., Kim, Y., Lee, N.S., 2008. Vibrational analysis and intermolecular hydrogen bonding of azodicarbonamide in the pentamer cluster. Bull. Korean Chem. Soc. 29 (10), 1951-1959.

Li, M., Lopez, N., Bilgili, E., 2016. A study of the impact of polymer–surfactant in drug nanoparticle coated pharmatose composites on dissolution performance. Adv. Powder Technol. 27 (4), 1625-1636.

Lim, H., Hoag, S., 2013. Plasticizer effects on physical–mechanical properties of solvent cast Soluplus® films. AAPS PharmSciTech 14 (3), 903-910.

Lin, S.-Y., Chen, K.-S., Run-Chu, L., 2000. Organic esters of plasticizers affecting the water absorption, adhesive property, glass transition temperature and plasticizer permanence of Eudragit acrylic films. J. Control. Release 68 (3), 343-350.

Lin, S.Y., Lee, C.J., Lin, Y.Y., 1995. Drug-polymer interaction affecting the mechanical properties, adhesion strength and release kinetics of piroxicam-loaded Eudragit E films plasticized with different plasticizers. J. Control. Release 33 (3), 375-381.

Lipinski, C.A., 2002. Poor aqueous solubility-an industry wide problem in ADME screening. Am. Pharm. Rev. 5, 82-85.

Ljungberg, N., Wesslén, B., 2002. The effects of plasticizers on the dynamic mechanical and thermal properties of poly(lactic acid). J. Appl. Polym. Sci. 86 (5), 1227-1234.

Ljungberg, N., Wesslén, B., 2003. Tributyl citrate oligomers as plasticizers for poly (lactic acid): thermo-mechanical film properties and aging. Polymer 44 (25), 7679-7688.

Lourdin, D., Coignard, L., Bizot, H., Colonna, P., 1997. Influence of equilibrium relative humidity and plasticizer concentration on the water content and glass transition of starch materials. Polymer 38 (21), 5401-5406.

Mangwandi, C., Adams, M.J., Hounslow, M.J., Salman, A.D., 2014. Influence of fill factor variation in high shear granulation on the post granulation processes: Compression and tablet properties. Powder Technol. 263, 135-141.

Marucci, M., Andersson, H., Hjärtstam, J., Stevenson, G., Baderstedt, J., Stading, M., Larsson, A., von Corswant, C., 2013. New insights on how to adjust the release profile from coated pellets by varying the molecular weight of ethyl cellulose in the coating film. Int. J. Pharm. 458 (1), 218-223.

Masaro, L., Ousalem, M., Baille, W.E., Lessard, D., Zhu, X.X., 1999. Self-diffusion studies of water and poly(ethylene glycol) in solutions and gels of selected hydrophilic polymers. Macromolecules 32 (13), 4375-4382.

McHugh, T.H., Krochta, J.M., 1994. Sorbitol- vs glycerol-plasticized whey protein edible films: Integrated oxygen permeability and tensile property evaluation. J. Agric. Food Chem. 42 (4), 841-845.

McPhillips, H., Craig, D.Q.M., Royall, P.G., Hill, V.L., 1999. Characterisation of the glass transition of HPMC using modulated temperature differential scanning calorimetry. Int. J. Pharm. 180 (1), 83-90.

Merisko-Liversidge, E., Liversidge, G.G., 2011. Nanosizing for oral and parenteral drug delivery: A perspective on formulating poorly-water soluble compounds using wet media milling technology. Adv. Drug Del. Rev. 63 (6), 427-440.

Merisko-Liversidge, E., Liversidge, G.G., Cooper, E.R., 2003. Nanosizing: a formulation approach for poorly-water-soluble compounds. Eur. J. Pharm. Sci. 18 (2), 113-120.

Mittal, G., Sahana, D.K., Bhardwaj, V., Ravi Kumar, M.N.V., 2007. Estradiol loaded PLGA nanoparticles for oral administration: Effect of polymer molecular weight and copolymer composition on release behavior in vitro and in vivo. J. Control. Release 119 (1), 77-85.

Monteiro, A., Afolabi, A., Bilgili, E., 2013. Continuous production of drug nanoparticle suspensions via wet stirred media milling: A fresh look at the Rehbinder effect. Drug Dev. Ind. Pharm. 39 (2), 266-283.

Mosharraf, M., Nyström, C., 1995. The effect of particle size and shape on the surface specific dissolution rate of microsized practically insoluble drugs. Int. J. Pharm. 122 (1-2), 35-47.

Murdande, S.B., Shah, D.A., Dave, R.H., 2015. Impact of nanosizing on solubility and dissolution rate of poorly soluble pharmaceuticals. J. Pharm. Sci. 104 (6), 2094-2102.

Nair, R., Nyamweya, N., Gönen, S., Martínez-Miranda, L.J., Hoag, S.W., 2001. Influence of various drugs on the glass transition temperature of poly(vinylpyrrolidone): A thermodynamic and spectroscopic investigation. Int. J. Pharm. 225 (1-2), 83-96.

Noyes, A.A., Whitney, W.R., 1897. The rate of solution of solid substances in their own solutions. J. Am. Chem. Soc. 19 (12), 930-934.

Nyamweya, N., Hoag, S.W., 2000. Assessment of polymer-polymer interactions in blends of HPMC and film forming polymers by modulated temperature differential scanning calorimetry. Pharm. Res. 17 (5), 625-631.

Oberle, R.L., Moore, T.J., Krummel, D.A.P., 1995. Evaluation of mucosal damage of surfactants in rat jejunum and colon. J. Pharmacol. Toxicol. Methods 33 (2), 75-81.

Omelczuk, M.O., McGinity, J.W., 1992. The influence of polymer glass transition temperature and molecular weight on drug release from tablets containing poly(DL-lactic acid). Pharm. Res. 9 (1), 26-32.

Pajander, J., Baldursdottir, S., Rantanen, J., Østergaard, J., 2012. Behaviour of HPMC compacts investigated using UV-imaging. Int. J. Pharm. 427 (2), 345-353.

Panda, B., Parihar, A.S., Mallick, S., 2014. Effect of plasticizer on drug crystallinity of hydroxypropyl methylcellulose matrix film. Int. J. Biol. Macromol. 67, 295-302.

Park, H.J., Weller, C.L., Vergano, P.J., Testin, R.F., 1993. Permeability and mechanical properties of cellulose-based edible films. J. Food Sci. 58 (6), 1361-1364.

Peppas, N.A., 1985. Analysis of Fickian and non-Fickian drug release from polymers. Pharm. Acta Helv. 60 (4), 110.

Pillin, I., Montrelay, N., Grohens, Y., 2006. Thermo-mechanical characterization of plasticized PLA: Is the miscibility the only significant factor? Polymer 47 (13), 4676-4682.

Pongjanyakul, T., Puttipipatkhachorn, S., 2007. Alginate-magnesium aluminum silicate films: Effect of plasticizers on film properties, drug permeation and drug release from coated tablets. Int. J. Pharm. 333 (1–2), 34-44.

Prodduturi, S., Manek, R.V., Kolling, W.M., Stodghill, S.P., Repka, M.A., 2005. Solid-state stability and characterization of hot-melt extruded poly (ethylene oxide) films. J. Pharm. Sci. 94 (10), 2232-2245.

Puttipipatkhachorn, S., Nunthanid, J., Yamamoto, K., Peck, G.E., 2001. Drug physical state and drug-polymer interaction on drug release from chitosan matrix films. J. Control. Release 75 (1-2), 143-153.

Qussi, B., Suess, W.G., 2006. The influence of different plasticizers and polymers on the mechanical and thermal properties, porosity and drug permeability of free shellac films. Drug Dev. Ind. Pharm. 32 (4), 403-412.

Ramkissoon-Ganorkar, C., Liu, F., Baudyš, M., Kim, S.W., 1999. Modulating insulin-release profile from pH/thermosensitive polymeric beads through polymer molecular weight. J. Control. Release 59 (3), 287-298.

Repka, M.A., Gerding, T.G., Repka, S.L., McGinity, J.W., 1999. Influence of plasticizers and drugs on the physical-mechanical properties of hydroxypropylcellulose films prepared by hot melt extrusion. Drug Dev. Ind. Pharm. 25 (5), 625-633.

Rodríguez, M., Osés, J., Ziani, K., Maté, J.I., 2006. Combined effect of plasticizers and surfactants on the physical properties of starch based edible films. Food Res. Int. 39 (8), 840-846.

Rowe, R.C., 1986. The effect of the molecular weight of ethyl cellulose on the drug release properties of mixed films of ethyl cellulose and hydroxypropylmethylcellulose. Int. J. Pharm. 29 (1), 27-41.

Sakellariou, P., Rowe, R.C., White, E.F.T., 1986. An evaluation of the interaction and plasticizing efficiency of the polyethylene glycols in ethyl cellulose and hydroxypropyl methylcellulose films using the torsional braid pendulum. Int. J. Pharm. 31 (1), 55-64.

Serajuddin, A.T.M., 1999. Solid dispersion of poorly water-soluble drugs: Early promises, subsequent problems, and recent breakthroughs. J. Pharm. Sci. 88 (10), 1058-1066.

Shen, B.d., Shen, C.y., Yuan, X.d., Bai, J.x., Lv, Q.y., Xu, H., Dai, L., Yu, C., Han, J., Yuan, H.l., 2013. Development and characterization of an orodispersible film containing drug nanoparticles. Eur. J. Pharm. Biopharm. 85 (3, Part B), 1348-1356.

Siepmann, J., Karrout, Y., Gehrke, M., Penz, F.K., Siepmann, F., 2013. Predicting drug release from HPMC/lactose tablets. Int. J. Pharm. 441 (1–2), 826-834.

Siepmann, J., Podual, K., Sriwongjanya, M., Peppas, N.A., Bodmeier, R., 1999. A new model describing the swelling and drug release kinetics from hydroxypropyl methylcellulose tablets. J. Pharm. Sci. 88 (1), 65-72.

Sievens-Figueroa, L., Bhakay, A., Jerez-Rozo, J.I., Pandya, N., Romañach, R.J., Michniak-Kohn, B., Iqbal, Z., Bilgili, E., Davé, R.N., 2012a. Preparation and characterization of hydroxypropyl methyl cellulose films containing stable BCS Class II drug nanoparticles for pharmaceutical applications. Int. J. Pharm. 423 (2), 496-508.

Sievens-Figueroa, L., Pandya, N., Bhakay, A., Keyvan, G., Michniak-Kohn, B., Bilgili, E., Davé, R., 2012b. Using USP I and USP IV for discriminating dissolution rates of nano- and microparticle-loaded pharmaceutical strip-films. AAPS PharmSciTech 13 (4), 1473-1482.

Steiner, D., Finke, J.H., Kwade, A., 2016. Efficient production of nanoparticle-loaded orodispersible films by process integration in a stirred media mill. Int. J. Pharm. 511 (2), 804-813.

Susarla, R., Afolabi, A., Patel, D., Bilgili, E., Davé, R.N., 2015. Novel use of superdisintegrants as viscosity enhancing agents in biocompatible polymer films containing griseofulvin nanoparticles. Powder Technol. 285, 25-33.

Susarla, R., Sievens-Figueroa, L., Bhakay, A., Shen, Y., Jerez-Rozo, J.I., Engen, W., Khusid, B., Bilgili, E., Romañach, R.J., Morris, K.R., Michniak-Kohn, B., Davé, R.N., 2013. Fast drying of biocompatible polymer films loaded with poorly water-soluble drug nano-particles via low temperature forced convection. Int. J. Pharm. 455 (1–2), 93-103.

Thakhiew, W., Devahastin, S., Soponronnarit, S., 2010. Effects of drying methods and plasticizer concentration on some physical and mechanical properties of edible chitosan films. J. Food Eng. 99 (2), 216-224.

Thorat, A.A., Dalvi, S.V., 2012. Liquid antisolvent precipitation and stabilization of nanoparticles of poorly water soluble drugs in aqueous suspensions: Recent developments and future perspective. Chem. Eng. J. 181–182, 1-34.

Trout, B.L., Hatton, T.A., Chang, E., Evans, J.M.B., Mascia, S., Kim, W., Slaughter, R.R., Du, Y., Dhamankar, H.H., Forward, K.M., Layer processing for pharmaceuticals. United States Patent Application No. 13/458222. Filed April 27, 2012.

Van Eerdenbrugh, B., Vermant, J., Martens, J.A., Froyen, L., Van Humbeeck, J., Augustijns, P., Van den Mooter, G., 2009. A screening study of surface stabilization during the production of drug nanocrystals. J. Pharm. Sci. 98 (6), 2091-2103.

Verma, S., Kumar, S., Gokhale, R., Burgess, D.J., 2011. Physical stability of nanosuspensions: Investigation of the role of stabilizers on Ostwald ripening. Int. J. Pharm. 406 (1–2), 145-152.

Verschueren, K., 2001. Handbook of environmental data on organic chemicals. fourth ed., New York, NY: John Wiley & Sons.

Visser, J.C., Woerdenbag, H.J., Crediet, S., Gerrits, E., Lesschen, M.A., Hinrichs, W.L.J., Breitkreutz, J., Frijlink, H.W., 2015. Orodispersible films in individualized pharmacotherapy: The development of a formulation for pharmacy preparations. Int. J. Pharm. 478 (1), 155-163.

Woertz, C., Kleinebudde, P., 2015. Development of orodispersible polymer films containing poorly water soluble active pharmaceutical ingredients with focus on different drug loadings and storage stability. Int. J. Pharm. 493 (1–2), 134-145.

Wong, D., Bodmeier, R., 1996. Flocculation of an aqueous colloidal ethyl cellulose dispersion (Aquacoat®) with a water-soluble polymer, hydroxypropyl methylcellulose. Eur. J. Pharm. Biopharm. 42 (1), 12-15.

Wong, S.M., Kellaway, I.W., Murdan, S., 2006. Enhancement of the dissolution rate and oral absorption of a poorly water soluble drug by formation of surfactant-containing microparticles. Int. J. Pharm. 317 (1), 61-68.

Wu, C., McGinity, J.W., 1999. Non-traditional plasticization of polymeric films. Int. J. Pharm. 177 (1), 15-27.

Wu, N., Wang, L.-S., Tan, D.C.-W., Moochhala, S.M., Yang, Y.-Y., 2005. Mathematical modeling and in vitro study of controlled drug release via a highly swellable and dissoluble polymer matrix: polyethylene oxide with high molecular weights. J. Control. Release 102 (3), 569-581.

Wypych, G., 2004. Handbook of plasticizers, Toronto, Canada: ChemTec Publishing.

Xiang, A., McHugh, A.J., 2011. A generalized diffusion–dissolution model for drug release from rigid polymer membrane matrices. J. Membr. Sci. 366 (1–2), 104-115.

Xie, Y., Li, P., Zhang, J., Wang, H., Qian, H., Yao, W., 2013. Comparative studies by IR, Raman, and surface-enhanced Raman spectroscopy of azodicarbonamide, biurea and semicarbazide hydrochloride. Spectrochim. Acta, Pt. A: Mol. Biomol. Spectrosc. 114, 80-84.

Yalkowsky, S.H., 2003. Handbook of aqueous solubility data, Boca Raton, FL: CRC Press.

Zhang, J., Ying, Y., Pielecha-Safira, B., Bilgili, E., Ramachandran, R., Romañach, R., Davé, R.N., Iqbal, Z., 2014. Raman spectroscopy for in-line and off-line quantification of poorly soluble drugs in strip films. Int. J. Pharm. 475 (1–2), 428-437.

Zhang, L., Long, C., Pan, J., Qian, Y., 2006. A dissolution-diffusion model and quantitative analysis of drug controlled release from biodegradable polymer microspheres. Can. J. Chem. Eng. 84 (5), 558-566.

Zhu, Y., Mehta, K.A., McGinity, J.W., 2006. Influence of plasticizer level on the drug release from sustained release film coated and hot-melt extruded dosage forms. Pharm. Dev. Technol. 11 (3), 285-294.